Energy Transfer in Highly Excited Large Polyatomic Molecules

I. OREF*

Department of Chemistry, Technion—Israel Institute of Technology, Haifa 32000, Israel

D. C. TARDY*

Department of Chemistry, The University of Iowa, Iowa City, Iowa 52242

Received October 20, 1989 (Revised Manuscript Received May 27, 1990)

Contents

I. Introduction

This review discusses intermolecular vibrational energy transfer in gas-phase systems and its relation to rate coefficients of unimolecular and bimolecular reactions; it is limited to highly excited large polyatomic molecules in their ground electronic state. Thus, experimental results on triatomic molecules are excluded. These fundamental reactions are used in studying basic problems in inter- and intramolecular energy transfer and occur as well in laser-induced chemistry, pyrolysis, combustion, and atmospheric studies at high and low temperatures and pressures. Modeling of such complicated systems requires rate coefficients at various temperatures and pressures, and those are dependent on an understanding of energy transfer. Thus, energy transfer in state to state or bulk microcanonical or canonical systems is of current interest in charting out energy evolution in molecules. Both time and effort have been spent in the last 65 years to develop and calculate rate coefficients from basic principles—with higher and higher accuracy—and to probe their relation to energy-transfer efficiency. Until the late 1970s the most reliable energy transfer data for highly excited

0009-2665/90/0790-1407$09.50/0

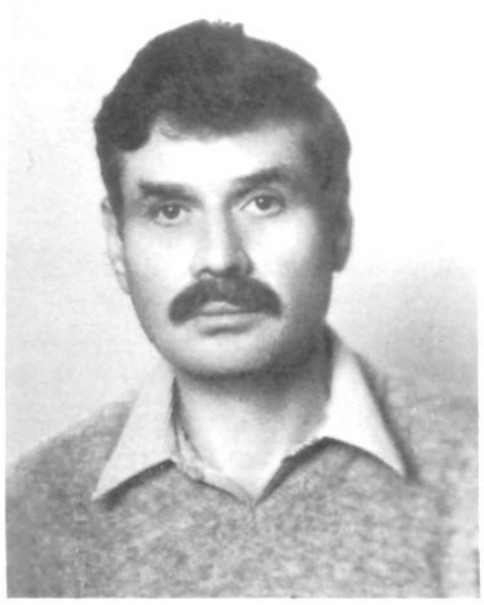

Izhack Oref was born in Tel-Aviv, Israel, in 1936. He obtained his B.Sc. degree in 1962 from the University of Illinois. After spending 1 year with Varian Associates in Palo Alto, CA, he went back to school and received his Ph.D. in 1967 from the University of California at Santa Barbara. He spent 1 year postdoctoring at the University of Washington at Seattle. He joined Gulf General Atomic in La Jolla, CA, and in 1969 joined the Department of Chemistry at the Technion, where he is a member of the faculty. In addition, from 1981 to 1987 he was Science Director of the National Museum of Science and Industry in Israel. His major fields of scientific interests are inter- and intramolecular energy transfer of vibrationally excited molecules and uni- and bimolecular gas-phase reactions.

Dwight C. Tardy was born in San Francisco, CA, in 1940. He obtained a B.A. degree in 1962 from San Diego State University; under the guidance of B. S. Rabinovitch he received the Ph.D. from the University of Washington in 1967. He did postdoctoral work with John C. Polyani at the University of Toronto (1967–69). He joined the University of Iowa in 1969. His research interests include energy transfer and disposal in the gas-phase reactions of vibrationally excited fluorocarbons and alkyl radicals: One of his hobbies is dabbling with computer hardware and software that enhance productivity in his research and quality of life.

polyatomic molecules were obtained mainly from studies of unimolecular reaction rate coefficients in the low-pressure and falloff regions. The major collisional effects are inferred from the solution of the master equation with an assumed collisional transition probability. The energy-transfer information is summarized in two comprehensive reviews (1977) by Tardy and Rabinovitch[1] and Quack and Troe.[2] Energy transfer in small molecules at low levels of excitation was reviewed by Flynn.[3] Here, our understanding of energy transfer is more advanced; energy transfer for moderate-sized molecules in excited electronic states was recently reviewed by Krajnovich, Parmenter, and Catlett.[4] Energy transfer from internally converted molecules was reviewed and analyzed by Hippler and Troe.[5] The purposes of the present review are severalfold: (a) to describe experiments that provide fundamental information; (b) to summarize available energy-transfer results; (c) to illustrate how energy-transfer information is pertinent and applicable to unimolecular reactions or to any system in which molecules must be transported from one energy level to another.

Lindemann (1922) pointed out the importance of collisional energy transfer in the excitation and deexcitation process in unimolecular reactions in a thermal system.

For the first-order unimolecular reaction, A → products

$$k_{uni} = -\frac{1}{[A]}\frac{d[A]}{dt} \tag{1-1}$$

Lindemann's simple, three-step mechanism gave a

$$A + M \rightarrow A^* + M \qquad k_1\text{: activation}$$

$$A^* + M \rightarrow A + M \qquad k_{-1}\text{: deactivation}$$

$$A^* \rightarrow \text{products} \qquad k_2\text{: reaction}$$

predicted pressure-dependent expression for k_{uni} in unimolecular reactions in thermal systems

$$k_{uni} = \frac{k_1}{k_{-1}}\frac{k_2}{1 + \dfrac{k_2}{k_{-1}[M]}} \tag{1-2}$$

where k_1 and k_{-1} are the specific rate constants for excitation and deexcitation of the reactant molecules and k_2 is the unimolecular rate coefficient of the chemical transformation. Hinshelwood (1926) introduced energy dependence into k_1 and Rice and Ramsperger (1927) and Kassel (1928) introduced it into k_2; thus, the RRK theory was born. Marcus and O. K. Rice combined transition-state theory with RRK to give the RRKM theory[6] for which the unimolecular rate coefficient k_2, now denoted $k(E)$, is given by

$$k(E) = L\frac{Q^\ddagger}{Q}\frac{W(E^\ddagger)}{h\,N(E^*)} \tag{1-3}$$

where $W(E^\ddagger)$ is the number of states of the excited molecule in its activated complex configuration and $N(E^*)$ is the density of states of the excited reactant molecule. Q is the adiabatic rotation partition function, and L is the reaction statistical factor.[7,8] Other models such as adiabatic channel and phase space, as well as rotational effects which can be included[9] in the expression for $k(E)$, will not be discussed.

A. Setting Up the Master Equation

For k_{uni} to be calculated properly, account must be taken of the probabilities of transporting a molecule from any total energy state i to any total energy state j. Since for large polyatomic molecules the density of states is very high, the molecular states are grained together into energy levels and a detailed master equation is written whereby the population of each energy level is replenished and depleted explicitly

$$\frac{d[A(E,t)]}{dt} = -\int_0^\infty Z(E)\ [M]\ P(E',E)\ [A(E,t)]\ dE' + \int_0^\infty Z(E')\ [M]\ P(E,E')\ [A(E',t)]\ dE' = k(E)\ [A(E,t)] \quad (1\text{-}4)$$

$$\frac{d[A(E,t)]}{dt} = -\int_0^\infty R(E',E)\ [M]\ [A(E,t)]\ dE' + \int_0^\infty R(E,E')\ [M]\ [A(E',t)]\ dE' - k(E)\ [A(E,t)]$$

where $R(E',E) = P(E',E)\ Z(E)$ is the rate coefficient for energy transfer. Equation 1-4 should be read as follows: the change of the concentration of reactant molecules in energy state E ($d[A(E,t)]/dt$) is equal to the depletion by collision of A in state E to all states E' (first integral), to the replenishment of state E from all states other than E (states E') (second integral), and to the depletion of molecules in E due to reaction (third term). $Z(E)$ [M] is the number of collisions per unit time at E, and $P(E',E)$ is the probability of transferring energy $E' - E$ ($=\Delta E$) in a collision.[1,7,8] In the case of no open reactive channels the last term is dropped. The set of differential equations (eq 1-4) can be solved by solving for the eigenvalues of the normalized transition probabilities and $k(E)$ matrix[15] or by Monte Carlo methods developed by Gillespie[10a] and Barker.[10b]

The time-dependent populations are given by

$$[A(E,t)] = \sum_j a_j(E)\ e^{-k_j t} \quad (1\text{-}5)$$

$a_j(E)$ are the energy-dependent normalization factors, and k_j (rate coefficients) are the negatives of the eigenvalues. Integration over all energy states gives

$$[A(t)] = \int_0^\infty [A(E,t)]\ dE \quad (1\text{-}6)$$

When eq 1-6 is differentiated with respect to t, the overall rate coefficient is obtained.

$$k_{uni} = -\frac{1}{[A(t)]}\frac{d[A(t)]}{dt} \quad (1\text{-}7)$$

From eq 1-7 it is clear that k_{uni} may exhibit time dependence and may not be constant. The progress of the reaction in such a case is simply monitored by observing A(t) at a given t without assigning a specific k_{uni} to the reaction.

At long reaction time and the case where one k_j is much smaller than the rest

$$[A(E,t)] = a(E)\ e^{-kt} \quad (1\text{-}8)$$

Combining eqs 1-6, 1-7, and 1-8, one obtains for k_{uni}

$$k_{uni} = \int_0^\infty \frac{k(E)\ [A(E,t)]\ dE}{[A(t)]} = k \quad (1\text{-}9)$$

k_{uni} is simply the negative of the smallest eigenvalue of the matrix of eq 1-4.

If one defines a quasi steady state

$$\frac{d\left(\frac{[A(E,t)]}{[A(t)]}\right)}{dt} = 0 \quad (1\text{-}10)$$

then by differentiating eq 1-10, rearranging, and using eq 1-7, we obtain

$$\frac{d[A(E,t)]}{dt} = -k_{uni}[A(E,t)] \quad (1\text{-}11)$$

Substituting eq 1-11 into eq 1-4

$$-\int_0^\infty Z(E)\ [M]\ P(E',E)\ [A(E,t)]\ dE' + \int_0^\infty Z(E')\ [M]\ P(E,E')\ [A(E',t)]\ dE' - k(E)\ [A(E,t)] + k_{uni}[A(E,T)] = 0 \quad (1\text{-}12)$$

Integrating eq 1-12 over all energy space yields

$$k_{uni} = \int_{E_0}^\infty \frac{k(E)\ [A(E,t)]\ dE}{[A(t)]} \quad (1\text{-}13)$$

Note that, below E_0, $k(E) = 0$.

The first term in eq 1-12 is equal to $Z(E)$ [M] [$A(E,t)$]; therefore, eq 1-12 can be rearranged to give

$$[A(E,t)] = \frac{Z[M]\int_0^\infty P(E,E')\ [A(E',t)]\ dE'}{Z[M] + k(E) - k_{uni}} \quad (1\text{-}14)$$

where Z is assumed to be independent of E.

For *strong colliders*

$$P(E,E') = B(E) \quad (1\text{-}15)$$

where $B(E)$ is the equilibrium Boltzmann distribution. Then Q_{int} is the partition function for internal degrees

$$B(E) = \frac{N(E)\ e^{-E/RT}}{Q_{int}} \quad (1\text{-}16)$$

of freedom. Introducing eq 1-15 into eq 1-14 and taking $B(E)$ out of the integral

$$\frac{[A(E,t)]}{[A(t)]} = \frac{Z[M]\ B(E)}{Z[M] + k(E) - k_{uni}^{sc}} \quad (1\text{-}17)$$

Multiplying both sides of eq 1-17 by $k(E)$ and integrating over E leads to

$$\int_{E_0}^\infty \frac{k(E)\ [A(E,t)]\ dE}{[A(t)]} = \int_{E_0}^\infty \frac{Z[M]\ B(E)\ k(E)\ dE}{Z[M] + k(E) - k_{uni}^{sc}} \quad (1\text{-}18)$$

Introducing eq 1-13 into eq 1-18, we obtain the final strong-collision expression

$$k_{uni}^{sc} = \int_{E_0}^\infty \frac{Z[M]\ B(E)\ k(E)\ dE}{Z[M] + k(E) - k_{uni}^{sc}} \quad (1\text{-}19)$$

The superscript sc on k_{uni} indicates the strong-collision conditions under which it was obtained.

In the high-pressure limit ($p \to \infty$), eq 1-19 takes the form

$$k_\infty = \int_{E_0}^\infty B(E)\ k(E)\ dE \quad (1\text{-}20)$$

where ∞ indicates high pressure which for some systems may be a few Torr and is independent of $P(E,E')$; i.e. it is valid for both strong or weak collisions. The temperature dependence of k_∞ is frequently given by the simple Arrhenius expression

$$k_\infty = A_\infty e^{-E_{a\infty}/RT} \quad (1\text{-}21)$$

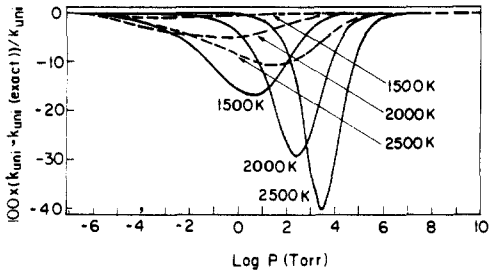

Figure 1. Percent deviation of the exact k_{uni} of quadricyclane from k_{uni} with (- - -) and without (—) k_{uni} in the denominator of eq 1-19 as a function of pressure for various temperatures.

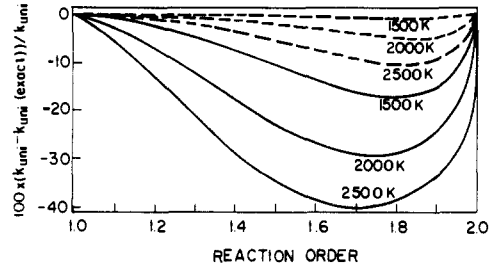

Figure 2. Percent deviation of the exact k_{uni} of quadricyclane from k_{uni} with (- - -) and without (—) k_{uni} in the denominator of eq 1-19 as a function of reaction order for various temperatures.

where A_∞ is the high-pressure frequency factor.

In the low-pressure limit, $p \rightarrow 0$

$$k_0^{sc} = \int_{E_0}^{\infty} \frac{Z[M]\ B(E)\ k(E)\ dE}{k(E) - k_0^{sc}} \qquad (1\text{-}22)$$

In eq 1-21 the equilibrium population is maintained at all times. (Equation 1-19 is sometimes called the RRKM expression, but we reserve the name RRKM for the rate coefficient $k(E)$). At the high-pressure limit, collisions do not play an active role in the reaction and there is no need for a superscript sc on k. At lower pressures, collisions do play a role and a superscript is needed. The subscript 0 indicates k_{uni} at limiting low pressure.

For low temperatures, $k(E) \gg k_0^{sc}$ and eq 1-22 yields the conventional expression

$$k_0^{sc} = \int_{E_0}^{\infty} Z[M]\ B(E)\ dE \qquad (1\text{-}23)$$

The temperature dependence of k_0^{sc} can be given by

$$k_0^{sc} = A_0 e^{-E_{a0}/RT} \qquad (1\text{-}24)$$

where A_0 and E_{a0} are the frequency factor and activation energy at low pressures.

At high temperatures the last term in the denominator of eq 1-19 is not negligible, and even a quasi steady state is not obtained. Montroll and Shuler[11] realized long ago that there is a lower bound value for E_0/k_BT below which steady state is not applicable. Recent calculations[12a] indicate that the contribution of k_{uni}^{sc} in the denominator is negligible when the ratio is >20. This is only a rule of thumb, and for some molecules $E_0/k_BT > 10$ will give good agreement as well.[12b] It should also be pointed out that the reaction need not be in the first-order region, i.e. $k_{uni} = k_\infty$, and there is no easy method to calculate the last term in the denominator. This is summarized in Figure 1 where eq 1-19 is used with and without k_{uni} in the denominator. As expected, the deviations are the largest at high temperatures. In addition, the larger the molecule and the lower the activation energy, the larger the deviation of the *exact* (k_{uni} included) from the *approximate* (k_{uni} removed) expression. The maximum deviation occurs when the reaction order is 1.7–1.9, that is, close to the second-order region. This is depicted in Figure 2.

To summarize, to find k_{uni} for weak collisions, one has to solve a master equation (eq 1-4). To get a master equation, one has to specify the rate coefficients for energy transfer $R(E,E')$; imbedded in them are $Z(E')$, the number of collisions per unit time per unit concentration at energy E' and the transition probability $P(E,E')$ of transferring an amount of energy ΔE (from level E' to level E). Understanding the collision processes characterized by $Z(E)$ and $P(E,E')$ is a prerequisite for an intelligent evaluation of k_{uni}. At low temperatures the quasi-steady-state equation is obtained while at high temperatures no steady state is obtained and a time-independent k_{uni} cannot be defined.

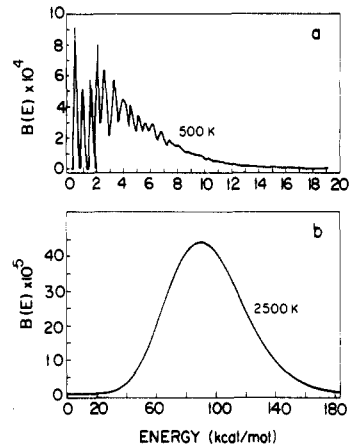

Figure 3. Boltzmann distribution function for cyclobutane vs energy at two temperatures.

B. Details of Solving a Master Equation

Any solution of the master equation is subject to the conservation relations

$$\int_0^{\infty} \frac{r(E',E)}{C(E)}\ dE' = \int_0^{\infty} P(E',E)\ dE' = 1 \qquad (1\text{-}25)$$

$$\int_0^{\infty} [A(E,t)]\ dE = [A(t)] \qquad (1\text{-}26)$$

and to detailed balance

$$[B(E)]\ P(E',E) = [B(E')]\ P(E,E') \qquad (1\text{-}27)$$

For computational purposes $P(E',E)$ has been factored into a shape $r(E',E)$ and normalization factor $C(E)$. The simultaneous imposition of eqs 1-25, 1-26, and 1-27 leads to energy-dependent normalization factors for the probabilities given by the Gilbert and King recursion equation.[13]

$$C(E) = \frac{\int_0^E r(E',E)\ dE'}{1 - \frac{1}{B(E)} \int_E^{\infty} \frac{B(E')\ r(E,E')}{C(E')}\ dE'} \qquad (1\text{-}28)$$

Alternatively, eq 1-25, 1-26, and 1-27 have been intro-

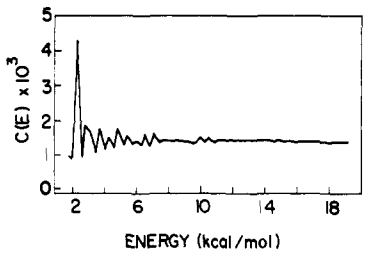

Figure 4. Normalization factors for exponential transition probabilities for cyclobutane dissociation as a function of energy.

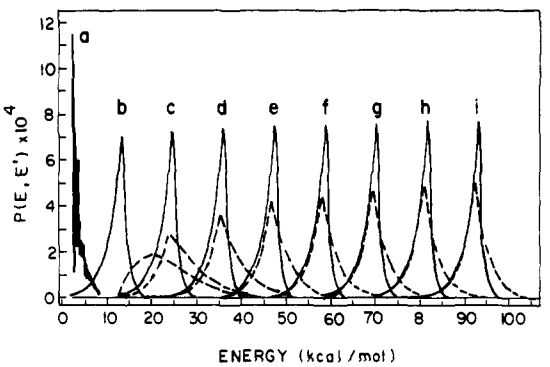

Figure 5. Normalized exponential transition probabilities for cyclobutane dissociation vs energy for 500 K (—) and 2500 K (---). The positions of the letters indicate the energy of the 0–0 transition.

duced explicitly into the master equation, by Tardy and Rabinovitch[14] and by Oref.[15]

The application of eq 1-28 is not trivial. At low energies the density of states is a discrete function, thus causing $B(E)$ to have structure at the low-energy tail of the distribution. This is depicted in Figure 3a where $B(E)$ for cyclobutane at 500 K is shown. The average energy of the molecules is 4.52 kcal/mol. For a given $P(E',E)$ (exponential transition probability, eq 2-14, discussed later) the values of $C(E)$ as a function of E (Figure 4) oscillate due to the quantum structures at low energies.

The form of an exponential transition probability is shown in Figure 5. The shape of the probability function changes as a function of the internal energy. The remarkable change is at the very low energy where the oscillations of $C(E)$ affect $P(E,E')$. In short, at low temperatures and low energy the normalization and detailed balance constraints are anything but trivial. The solution of the master equation has to take these effects in consideration for reactions in which these populations are important. At higher temperatures, $B(E)$ is much smoother (Figure 3b). At even higher temperatures, above 1200 K, application of eq 1-28 demands extreme caution. At lower energies, the denominator approaches zero and $C(E)$ obtains nonphysical values. It can obtain a value 2 orders of magnitude larger than the value of the $C(E)$ preceding it in the recursion equation, or it can even become negative—an unrealistic value. The problem is solved by various mathematical constructs such as letting the population be the equilibrium one below a given value of the energy. At any rate, awareness is required. The normalized exponential transition probability at high temperature as a function of energy is shown in Figure 5, the shape is temperature and energy dependent, and the $\Delta E = 0$ transition is of lower probability at higher temperature than at lower temperature.

The effect of the angular momentum J on the solution of the master equation was discussed by the groups of Forst,[16a] Troe,[16a] and Gilbert.[16b,c] They find that J affects the values of k_{uni} and should be taken into consideration.

II. Probability Models and $\langle \Delta E \rangle$ Quantities

A. Rate of Energy Flow

All kinetic experiments measure a rate of transport. For example, in the case of a unimolecular reaction in the low-pressure (second-order) region, the rate of reaction of product formation is related to the transport of molecules from nonreactive levels to reactive levels. Fundamentally this involves an energy flow (energy/time), which is observed as the rate of formation of products. The rate coefficient for this flow, as given in eq 1-4, has historically been divided into two terms: the collision rate $[Z(E)]$ and the probability of transfer per collision $[P(E',E)]$. It can be seen that for a given rate coefficient a variety of $Z(E)$'s and $P(E',E)$'s are possible: e.g. a high collision rate with a low probability for transfer or a low collision rate with a high probability for transfer. Both will meet the requirement for a given rate coefficient. Thus, it is important that the proper collision rate is used.

The collision or reaction rate coefficient is highly dependent upon the particular experiment: what distribution of initial states of the reactants is prepared and the final states measured. The phenomenological rate coefficient is obtained by a suitable average of the reactive cross section.[17,18] Consider an experiment in which a flux of A molecules with internal energy E_A collides with an M molecule that contains internal energy E_M with a relative velocity v (i.e., relative translational energy, $E_t = 0.5m_Am_M/(m_A + m_B)v^2 = 0.5\mu v^2$), which produces A and M with internal energies E_A' and E_M', respectively.

$$A(E_A) + M(E_M) \rightarrow A(E_A') + M(E_M') \qquad (2\text{-}1)$$

The cross section, $s(E_A', E_M'|E_A, E_M, v)$, is defined as the ratio of the number of product pairs $[A(E_A'), M(E_M')]$ formed per unit time to the initial flux of $A(E_A)$. The rate coefficient, $k(E_A', E_M'|E_A, E_M, v)$, for the energy exchange is calculated from the $s(E_A', E_M'|E_A, E_M, V)$ by the relation

$$k(E_A',E_M'|E_A,E_M,v) = vs(E_A',E_M'|E_A,E_M,v) \qquad (2\text{-}2a)$$

The detailed cross section is not only an indicator of the efficiency for a given "product" but also an indicator with regard to the energy disposition, i.e. whether vibrational energy of A transferred to relative translation (V–T transfer), to rotational modes (V–R), or to vibration of M (V–V). Microscopic reversibility provides the handle for relating V–T to T–V (or other equivalent inverse processes) cross-section or rate coefficient information. As the available details regarding a specific experiment decrease, the cross section must be appropriately averaged. For example, when the internal energy of M is not selected, but has an average ($\langle E_M \rangle$), then the rate coefficient for energy flow is

$$k(E_A'|E_A,\langle E_M\rangle,v) = vs(E_A'|E_A,\langle E_M\rangle,v) = v\int_0^\infty s(E_A'E_M'|E_A,E_M,v)\, f(E_M)\, dE_M \qquad (2\text{-}2b)$$

where $f(E_M)$ is the fraction of M molecules with internal energy E_M. Likewise, if the velocity is not selected but is governed by a Boltzmann temperature T_v, then the reaction rate for

$$A(E_A) + M \rightarrow A(E_A') + M \quad (2\text{-}3)$$

is

$$\text{rate} = k(E_A'|E_A,\langle E_M\rangle,T_v)[A(E_A)][M] \quad (2\text{-}4)$$

and for simplicity E_A can be replaced by E so that

$$k(E_A'|E_A,\langle E_M\rangle,T_v) = \int_0^\infty v s(E'|E,\langle E_M\rangle,v)\, f(v)\, dv \quad (2\text{-}5)$$

The total collision rate is

$$Z(E) = \int_0^\infty k(E'|E,\langle E_M\rangle,T_v)\, dE' \quad (2\text{-}6)$$

For the case where s is a constant equal to $\pi\sigma^2$, the traditional hard-sphere collision rate formula results.

$$Z = Z(E) = \left(\frac{8kT_v}{\pi\mu}\right)^{0.5} \pi\sigma^2 \quad (2\text{-}7)$$

Other relations for the appropriate rate coefficient can be set up depending upon which parameters are to be averaged for a given experimental condition. Although the cross section is impossible to obtain experimentally, it is the ideal quantity to be measured because the rate coefficient can be obtained by the proper averaging over the appropriate distribution function. However, the reverse procedure, that of obtaining the cross section from the rate coefficient, is not unique. Thus, it is important when rate coefficients from different experiments are compared that the experimental parameters are comparable and that the appropriate collision cross section is used if reliable information pertinent to the $P(E',E)$'s are to be obtained. Our discussion in this section is in the following order: probabilities of energy transfer from a single energy level; calculation of the collision rate; macroscopic energy-transfer quantities; energy-transfer quantities from theoretical calculations.

B. Probabilities of Energy Transfer from a Single Energy Level

1. Trajectory Calculations

A new era of computer calculations (which include triatomic molecules not discussed in this review) involving energy transfer is starting. Various energy-transfer models are used in energy-transfer calculations.[18-34] Trajectories for the systems He + HO_2,[35a] He + SO_2,[35b] He + H_2O,[35c] CO_2 + He/Ar,[35d] CS_2 + He,[36] He/Ne/Xe/N_2/H_2 + CH_3NC,[37] CS_2 and SO_2 + He/Ne/Ar/Kr/Xe,[38] Ar + CH_4,[39a] and He + $C_{10}H_8$[40] (azulene) have been reported. These calculations have been performed on potential energy surfaces (PES) using classical mechanics.[20] Canned programs are now available from the Quantum Chemistry Program Exchange.[20c]

In principle, the outcome of a particular collision can be calculated via classical or quantum mechanics. Procedures have been developed to integrate either Hamilton's or Schrodinger's equations so that the trajectory (coordinates and momenta of each atom as a function of time) can be determined. In fact, this has commonly been done for simple atom diatomic systems.[18,19] Even for these simple systems the bottleneck in calculating realistic results is in obtaining an adequate potential energy surface. The same problem exists in inelastic collisions of highly excited polyatomic molecules. (The PES for energy transfer is different from the PES for reactive systems, and both are unknown.)

The second problem in calculating energy-transfer rates by trajectory calculations is obtaining realistic sampling of the initial conditions:[20a,d-f] impact parameter, position and momentum of the atoms (classical conditions), and the quantum states for vibration and rotation. For each atom, six coordinates in phase space are necessary to specify the initial conditions; the volume in phase space increases as E^{3N} where N is the total number of atoms in A and M. The number of initial states, which is proportional to the volume in phase space for the appropriate energy, becomes extremely large for molecules of moderate size and at excitation energies corresponding to reaction threshold. Thus, a selection strategy is needed to reduce the actual number of trajectories for the simulation.

Insight into the fundamental quantities that determine the transfer of energy to various states can be obtained from the formal quantum mechanical equations for the transition probability from the initial (i) to final (f) state. Two results due to Fermi[21] and Born[21] are of particular interest; however, both apply to the limiting case where the energy transferred is smaller than the relative translational energy. For transitions between states of the same energy, Fermi's golden rule is applicable. In this case

$$P(f,i) = \frac{4\pi^2}{h}|V_{f,i}|^2\, N(E_f) \quad (2\text{-}8)$$

i.e., the probability is related to the density of states of the final state and the matrix element connecting the two states. For small perturbations (not always applicable for large energy transfer), the Born approximation shows that the transition probability between the energy states is related to the square of the Fourier transform of the interaction matrix element during the collision.

$$P(E_f,E_i) = \text{constants}\left|\int_0^\infty V_{f,i}(t)\, e^{-i\omega t}\, dt\right|^2 \quad (2\text{-}9)$$

$$V_{f,i}(t) = \Delta E = |E_f - E_i| = \frac{h}{2\pi}\omega$$

Both Fermi's golden rule and the Born approximation illustrate that selection or propensity rules,[22a] i.e., initial and final states that have a high probability for coupling, can be derived in theory: similar "rules" have been successfully used and developed in the field of spectroscopy. The problem that arises in calculating the matrix elements for collisional energy transfer is that the interaction potential is not generally known, as it is for radiation interacting with a dipole in spectroscopy. One important point is that the Born approximation does lead to probabilities for V-T transfer that decrease exponentially as the energy defect between vibration and translation increases:

$$P(E_i,E_j) \approx e^{c|E_j-E_i|} \approx e^{c|E_A-E_A'|} \qquad (2\text{-}10)$$

for the process depicted in eqs 2 and 3. This "exponential gap" dependence has been experimentally observed[22b] in a variety of systems. Another point is that for large amounts of energy transfer the Fourier frequency component of the potential corresponding to $|E_f - E_i|$ must be large. For interactions potentials of the form $1/r^n$, the probability for transfer of large amounts of energy would be most effective for larger n. Impulsive collisions on a repulsive potential meet this requirement; this is also in agreement with the intuitive idea that as the collision time becomes less than the time for a characteristic motion (vibration, rotation), the probability for transfer is enhanced.[21]

2. Simple Models

Due to the large amount of computer time required for classical or quantum trajectory calculations, much effort has been spent on developing an understanding for simple systems. The dependence of energy transfer on general attractive and repulsive portions of the interaction potential have been assessed. The first successful model was that of Schwartz, Slawsky, and Herzfeld[23] (SSH) in which impulsive collisions with an attractive solution for the thermally averaged collision number was derived. The SSH theory is applicable to atom diatomic systems at low levels of excitation. This model was then modified by Tanczos[24] to include polyatomic species at low levels of excitation. The modifications were discussed and corrected by Yardley.[21]

For qualitative purposes it is useful to classify collisions according to the time in which the collision partners are undergoing a significant change in their interaction energy. Two limiting categories are "direct" and "sticky" (complex) collisions. For the "direct" case (single collision encounter with a duration less than a vibrational period)[25] the interaction can involve attractive and/or repulsive terms in the interactive potential while for "sticky" collisions the attractive term must be present to "hold" the collision complex together for a few vibrational cycles. The total energy and total angular momentum must be conserved throughout the trajectory (collision).

For the formation and decomposition of the long-lived "sticky" complex, the internal energy will be statistically distributed.[26,27] The fundamental quantities determining the amount of energy transferred in the statistical model are the density of states for both colliders, the strength of attractive forces, and the total energy of excitation ($E_A + E_B + E_v$) subject to conservation of angular momentum. For this case the microscopic details of the collision are unimportant since the long-lived complex samples "all" of phase space with a random lifetime. In general, the total cross section for energy transfer for the complex case will be comparable to the elastic and inelastic collision cross section; the specific probabilities from initial to final energy states will depend on the number of vibrational modes involved. It is predicted that the amount of energy transferred will increase with the average energy[27b] (Figure 6) and with relative translational energy of the colliding pair[27c] (Figure 7).

As the coupling between collision partners decreases from that for the long-lived "sticky" (statistical) model,

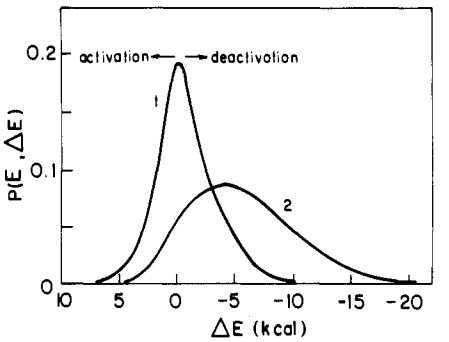

Figure 6. Energy-transfer probability $P(E,\Delta E)$ vs ΔE for C_2H_5CN at 550 K: (1) E = 9.2 kcal/mol (internal energy of C_2H_5CN); (2) E = 38 kcal/mol. In (1) $E \approx \langle E \rangle$ and in (2) $E \gg \langle E \rangle$. Case 2 has much more deactivation than case 1 (reprinted from ref 27b; copyright 1977 Elsevier).

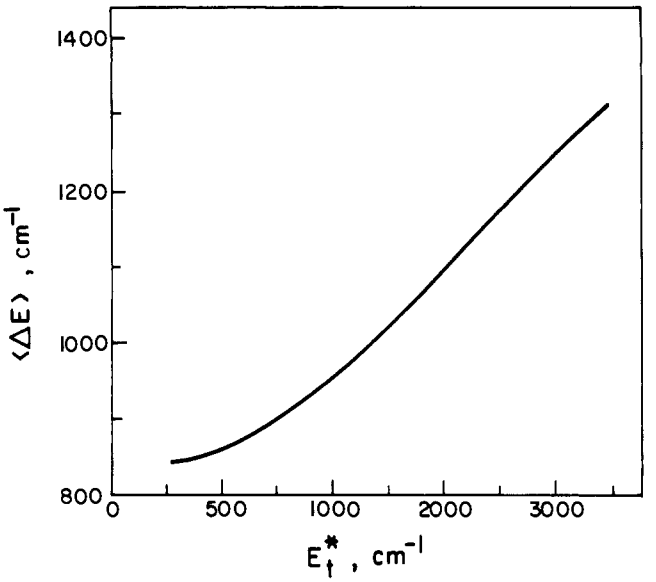

Figure 7. Average energy lost in a $C_5H_9^+$–M collision ($\langle \Delta E \rangle_{d,E}$) at 373 K vs maximum relative translational energy of the colliding pair. Internal excitation of the ion is 38 kcal/mol. The plot applies to both polar and nonpolar M (reprinted from ref 27c; copyright 1979 Elsevier).

due in part to a shorter interaction time, the volume of phase space (equivalent number of oscillators of the substrate) that the deactivator is able to sample is reduced. During the collision between A and M there are relative translational and rotational degrees of freedom that become internal degrees of freedom in the complex; these are the modes that most strongly interact with the internal modes of A so that energy can be efficiently transferred. Various quantitative versions of this model have been presented by Schlag,[28] Lin and Rabinovitch,[29] Bhattacharjee and Forst,[30] Oref,[31] and Troe.[32] In general, these models show the importance of the transitional modes as sinks for the transferred energy; the reduced number of accepting modes decreases the total amount of energy transferred,[29] as shown in Figure 8.

For the limiting case of "direct" collisions, the net interaction is localized to a given pair of atoms and can be either attractive or repulsive. The former has a relatively large cross section that decreases with an increase in relative velocity while the latter has a relatively small cross section that increases with relative velocity.[21] Thus, the temperature dependences for these interactions are opposite to one another; the temperature dependence for the rate constant for the repulsive

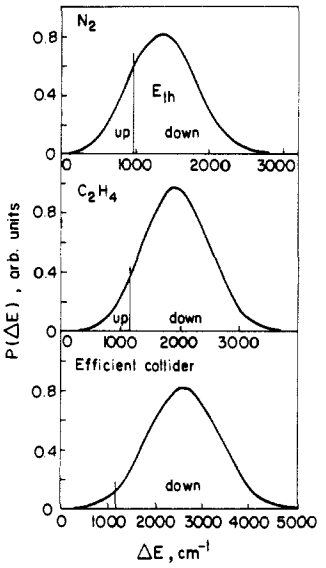

Figure 8. Probability distribution functions from statistical quasi-accommodation model vs ΔE for three colliders (reprinted from ref 29; copyright 1970 American Chemical Society).

potential increases with an increase in temperature. The outcome of the collision is a function not only of the initial conditions for the collision but of the interaction potential. A statistical version of this limit has been given by Light[27a] and modified by Nordholm et al.;[33] for this model

$$\langle \Delta E \rangle = \frac{n_2 + 2}{n_1 + n_2 + 4}(E_1 - \langle E_1 \rangle_T) \qquad (2\text{-}11)$$

where E_1 is the internal energy of the reactant, $\langle E_1 \rangle_T$ is the average equilibrium internal energy of the reactant at temperature T, and n_1 and n_2 are integers directly related to the number of atoms in the reactant and heat bath, respectively. Schranz and Nordholm[34] have modified the ergodic collision theory of Nordholm et al.[33] for impulsive collisions; the duration of the collision is sufficiently short so that the framework of the molecule remains constant. With this assumption only kinetic energy can be transferred. In this case the potential energy is not available and

$$\langle \Delta E \rangle = \frac{n_{K2} + 2}{n_{K1} + n_{K2} + 4}(K_1 - \langle K_1 \rangle_T) \qquad (2\text{-}12)$$

where K_1 is the kinetic energy of the reactant, $\langle K_1 \rangle_T$ is the average kinetic energy, and n_{K1} and n_{K2} are the number of momentum degrees of freedom of reactant and heat bath, respectively (see Table I). This model is adequate for large polyatomic deactivators.

All of the above simplified models can easily be used to calculate the probability for the energy transfer. Unfortunately, the calculated average energies transferred are either too high or, due in part to the uncertainty of the interaction potential, there are empirical constants that can be adjusted to fit the experiment. Sceats[38] has recently developed an atom–atom encounter model that shows good agreement with experiment and calculation for the deactivation of SO_2 and CS_2 by inert gases.

The histograms of the energy transfer from trajectory studies[35a,40] indicate the possibility of a double exponential for both the down ($E' < E$) and up ($E' > E$) branch of $P(E', E)$ and a large 0–0 probability. The

TABLE I. n Quantities for Statistical Model[a]

	substrate		deactivator	
	n_1	n_{K1}	n_2	n_{K2}
monoatomic			1	1
diatomic	2	1	5	4
linear polyatomic	$6M_1 - 10$	$3M_1 - 5$	$6M_2 - 7$	$3M_2 - 2$
nonlinear polyatomic	$6M_1 - 11$	$3M_1 - 5$	$6M_2 - 8$	$3M_2 - 2$

[a] M_1 and M_2 are the number of atoms in the substrate and deactivator, respectively. Subscripts 1 and 2 indicate substrate and bath, respectively. K indicates impulsive model; only kinetic energy is involved.

former may be real or a result of inadequate sampling or of the particular PES used. However, new experiments by the groups of Oref[41-43] and Luther[44,45] indicate that this observation is real. Diagnostic trajectory studies on fabricated PES's in which systematic variations can be introduced should be performed as was done by Polanyi for the A + BC → AB + C reactive system.[46]

Potential problems in the classical trajectory studies are participation of zero-point energy and the large number of elastic collisions. The first problem has been discussed by Hase and Miller[39b] and Bowman et al.;[39c] as of this time no definitive answer has been reached although empirical constraints have been put forward. The problem of a large probability for a zero energy transferred [$P(E,E)\,dE \approx 1$] relates to not knowing the proper cutoff for the impact parameter: large impact parameters in which there is no interaction during the "collision" will produce a 0–0 contribution. The proper cutoff of the impact parameter rests on knowledge of a correct collision cross section. At least three different approaches have been used or suggested to obtain "correct" cross sections: (i) The best fit double-exponential function is obtained without using the 0–0 trajectories.[35] (ii) Trajectories are ignored in which the energy transferred is less than that predicted by the uncertainty principle[47] or the numerical accuracy of the calculation. (iii) The rate of energy transfer, not the probability per collision,[36,48] is considered so that the arbitrariness of a cutoff impact parameter is not necessary. Another potential problem of a different sort is the mixing of electronic and vibrational levels now being investigated by Toselli and Barker. The redistributed successive collision method developed by Bruehl and Schatz[36] addresses the angular momentum distribution problem correctly.

Trajectory calculations for azulene–Ar and methane–Ar show that energy transfer is taking place in a time frame of ~0.5 ps longer than "direct" collisions; the large change in energy is due to repulsive interaction, and the duration is related to the attractive potential. Plots of internal energy vs time indicate a random-walk behavior in internal energy space with the constraints of a minimum (0) and maximum ($E_A + E_M + E_v = E_{tot}$) energy.

C. Calculation of the Collision Rate

As discussed above, calculation of the collision number with the correct collision cross section is critical to determine the correct transition probabilities. The problem of choosing incorrect cross sections has also appeared in calculating relative collisional efficiencies[1] β.

Rabinovitch and co-workers measured collisional efficiencies based on a per pressure basis for the thermal isomerization of methyl[49,50] and ethyl[51] isocyanides in the second-order region. After factoring out the effect of the reduced mass of the colliders, they were able to show that the increment in the collision cross section was constant for a given structural increment: i.e., s increased by a constant Δs for every CH_2 group added to a hydrocarbon homologous series. This experimental method provides a unique manner to determine collision cross sections in reactive systems. Unfortunately there are a limited number of systems where data of the necessary precision have been obtained.

More recently, Durant and Kaufman[52] presented a method in which the total collision cross sections could be calculated from the interaction potential. When these cross sections were used to calculate the efficiency for the quenching of NO_2 (A^2B_2) fluorescence, the relative efficiencies for 13 deactivators were within 25% of the mean value of 0.154 as compared to Lennard-Jones parameters in which the relative efficiencies varied by more than 400%. Although, in theory, this technique is generally applicable if the interaction potential is known, it does involve calculating the cross section by evaluating the phase shifts of the scattered waves for a given relative velocity and orbital angular momentum (impact parameter). The advantage is that once $s(v)$ is computed, then $s(T)$ is easily calculated by averaging it over the appropriate velocity distribution function. For systems that do not have a spherically symmetric interaction potential, additional averaging over the geometry of the collision is required.

For systems that do not have strong dipole–dipole interactions, the collision cross section is typically calculated from the square of the Lennard-Jones s times the reduced collision integral[53] $\Omega^{(2,2)}$. The Lennard-Jones parameters for the AM collision pair are determined by $\sigma_{AM} = (\sigma_A + \sigma_B)/2$ and $\epsilon_{AM} = (\epsilon_A\epsilon_M)^{0.5}$. Tables of σ and ϵ are available[53] as are prescriptions to synthesize these parameters for molecules that have not been experimentally determined;[53d] a specific prescription may not produce collision rates with the proper temperature dependence or that can be quantitatively compared with other prescriptions. The Stockmayer potential[53a] has been used when two polar partners are involved. A comparison of reported energy-transfer quantities from different research groups calls for extra caution. For example, Gilbert's group[54] have analyzed the $\langle\Delta E\rangle_{all}$ values reported for the relaxation of azulene in nitrogen from the laboratories of Barker[55,56] and Troe.[57] The Lennard-Jones collision numbers used by these research groups differ by a factor (Barker/Troe)[54] of 1.27 and 1.30 at 300 and 630 K, respectively; while their ratio of $\Omega^{(2,2)}$, which was calculated from different prescriptions, differed by only 3%. The reported values for $\langle\Delta E\rangle_{all}$(Barker)/$\langle\Delta E\rangle_{all}$(Troe) were 1.43 and 1.29 for this temperature range, which is apparently within good agreement. However, when Barker's $\langle\Delta E\rangle_{all}$'s are rescaled to Troe's collision parameters, a 30% increase in the discrepancy results.[54]

Thus, it is important that the technique and parameters used in calculating the collision number are reported along with the derived transition probability information.

D. Macroscopic Energy-Transfer Quantities: Moments of the Probability Function

The transition probability model can be used to calculate various moments of the distribution function (average energy-transferred quantities per collision); in many experiments the details of $P(E',E)$ are not required so in fact these are the desired quantities. The equations defining the averages are given in eq 2-13 where $f(E,t)$ is the normalized population distribution function.

$$\langle\Delta E\rangle_{d,E} = \frac{\int_0^E (E'-E)\,P(E',E)\,dE'}{\int_0^E P(E',E)\,dE'} \quad \text{for } E' < E \quad (2\text{-}13)$$

$$\langle\Delta E\rangle_{up,E} = \frac{\int_E^\infty (E'-E)\,P(E',E)\,dE'}{\int_E^\infty P(E',E)\,dE'} \quad \text{for } E' > E$$

$$\langle\Delta E\rangle_{all,E} = \int_0^\infty (E'-E)\,P(E',E)\,dE'$$

$$\langle p\rangle_{up,E} = \int_E^\infty P(E',E)\,dE' \text{ for } E' > E$$

$$\langle p\rangle_{d,E} = \int_0^E P(E',E)\,dE' \text{ for } E' < E$$

$$\langle E\rangle_t = \int_0^\infty E\,f(E,t)\,dE$$

$$\langle\Delta E\rangle_t = \int_0^\infty \langle\Delta E\rangle_{all,E}\,f(E,t)\,dE$$

$$\int_0^\infty f(E,t)\,dE = 1; \quad \int_0^\infty P(E',E)\,dE' = 1$$

When more than one originating energy level is involved, then $\langle\Delta E\rangle_E$ must be calculated for each E. The probabilities are no longer independent; the condition of detailed balance (eq 1-27) must be satisfied in addition to the normalization constraint (eqs 1-25 and 1-26). The detailed balance condition relates the "down" probability from energy level E to E' to the "up" probability from energy level E' to E. When $P(E',E)$ is an element of a matrix (row, column notation), then normalization corresponds to the sum of the elements in any column being unity while detailed balance relates elements that are symmetrically located across the diagonal (the transpose of one another). When the same form of down probabilities is assumed for all energies, then detailed balance relates the "up" and "down" probabilities originating from single nondegenerate energy levels, i.e., the element of a column in the matrix.

Penner and Forst[58a] have pointed out that the bulk average energy transferred $\langle\langle\Delta E\rangle\rangle$ is another quantity that must be defined and used for certain experiments. The physical experiments (sometimes called direct) as opposed to chemical methods monitor the average energy of *all* of the molecules (i.e., all energy levels) as a function of time. It is easily shown that the average energy of the ensemble $\langle E\rangle$ changes by $\langle\langle\Delta E\rangle\rangle$ after one collision. The bulk averate $\langle\langle\Delta E\rangle\rangle_{t\to\infty}$ goes to zero when the normalized population distribution $f(E,t)$ (=

$[A(E,t)]/[A(t)]$) approaches the equilibrium distribution of populations. (This does not apply to physical methods such as MPI discussed later.)

The three commonly used forms for $P(E',E)$ with $E' < E$ are the exponential[14]

$$P(E',E) \equiv e^{-(E-E')/\langle\Delta E\rangle_{d,E}} \quad (2\text{-}14)$$

the Gaussian[14]

$$P(E',E) \equiv e^{-(E-E')^2/\langle\Delta E\rangle_{d,E}^2} \quad (2\text{-}15)$$

and the stepladder[14]

$$P(E',E) = \text{constant when } |E'-E| = \langle\Delta E\rangle_{d,E} \quad (2\text{-}16)$$

$$P(E',E) = 0 \text{ otherwise}$$

models. One simplification often used is to assume that $\langle\Delta E\rangle_{d,E}$ is independent of E and is given simply by $\langle\Delta E\rangle_d$; energy-dependent $\langle\Delta E\rangle_d$ can be implemented easily into an equal-grained system for the exponential and Gaussian models, but unequal energy level spacing must be used for the stepladder model. Independent of which model is used, as energy dependence of $\langle\Delta E\rangle_{up}$ is automatically built in by the detailed balance constraint involving both the ratio of the density of states, which is a function of the energy level and the step size, and the Boltzmann factor, which is a function of the step size and temperature. This is necessary since for an ensemble of molecules with energies below the $\langle E\rangle$ "up" transitions must dominate while for an ensemble of molecules with energies above $\langle E\rangle$ "down" transitions must dominate; at some energy the "up" transitions are balanced by the "down" transitions. Thus, it is expected that $\langle\Delta E\rangle_{all,E}$ will be strongly dependent on energy and temperature and will undergo a sign change; for high-energy levels at low temperature it will be negative while for low-energy levels at high temperature it will be positive, and as can be seen from Figure 9 and from the expression for strong colliders:

$$\langle\Delta E\rangle_{all,E} = \langle E\rangle - E \quad (2\text{-}17)$$

This can be proven easily for strong collisions by starting from the basic definition

$$\langle\Delta E\rangle_{all,E} = \int_0^\infty (E'-E)\,P(E',E)\,dE' \quad (2\text{-}18)$$

where $P(E',E)$ is normalized to unity.

For strong collisions

$$P(E',E) = B(E') \quad (2\text{-}19)$$

Introducing eq 2-19 into eq 2-18 and integrating, one obtains eq 2-17.

For other transition probability models

$$\langle\Delta E\rangle_{all} = \int_0^\infty E'\,P(E',E)\,dE' - E = \bar{E} - E \quad (2\text{-}20)$$

where $\bar{E}$ denotes a special average different from $\langle E\rangle$. The relation between $\langle\Delta E\rangle_d$ and $\langle\Delta E\rangle_{up}$ is not simple and is given by eq 2-13.

Of all of the $\langle\Delta E\rangle$ quantities, $\langle\Delta E\rangle_d$ and $\langle\Delta E\rangle_{all}$ have been used the most often. Unfortunately, they have often been used interchangeably and without a designated subscript which has added to the confusion. These quantities can be related by analytical expressions for a specified form of $P(E',E)$.[1,2,55,59,60] It has been argued that $\langle\Delta E\rangle_d$ is a more useful representation since it does not contain the limited range imposed on $\langle\Delta E\rangle_{all}$ by subtracting the up and down average energies transferred and the added temperature dependence mandated to $\langle\Delta E\rangle_{all}$ by detailed balance.[1,61] (Often only one of these averages is directly related to a specific experiment.)

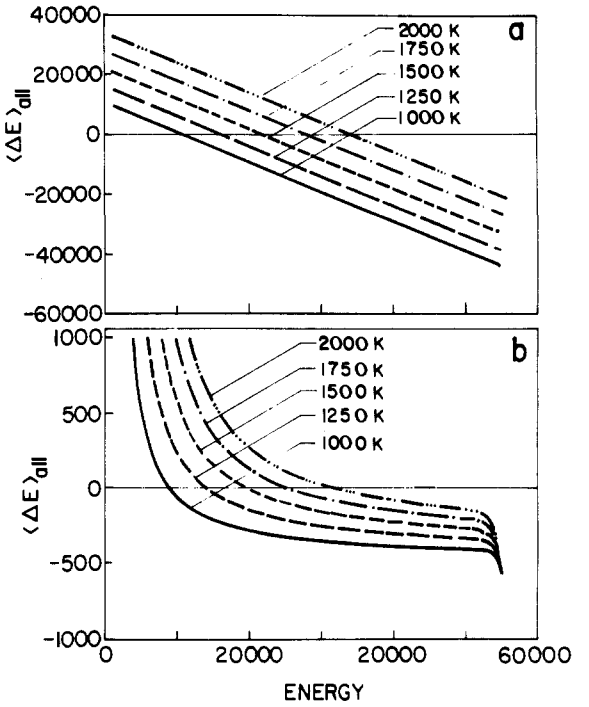

Figure 9. $(\Delta E)_{all}$ vs E: (a) for strong colliders for cyclohexene at 1000, 1250, 1500, 1750, and 2000 K; (b) for exponential weak colliders ($\langle\Delta E\rangle_d$ = 600 cm^{-1}) for cyclohexene at 1000, 1250, 1500, 1750, and 2000 K.

The average energy transferred per second can be calculated by the following expression:

$$\frac{d\langle\Delta E\rangle}{dt} = \int_0^\infty (E'-E)\,Z(E)\,P(E',E)\,dE' \quad (2\text{-}21)$$

If $Z(E)$ is not dependent on E, then this reduces to the quantities given above for the average energy transferred per collision.

If the initial population distribution is monoenergetic, then after the first collision $\langle\langle\Delta E\rangle\rangle = \langle\Delta E\rangle_{all,E}$ is linearly dependent on E, then after the first collision $\langle E\rangle_t$ will decay exponentially; if it is independent of E, then $\langle E\rangle$ will exhibit a linear decay. (See discussion in section VII.A.)

E. Energy-Transfer Quantities from Theoretical Calculations

In addition to the models discussed in section II.B.2 there are two more methodologies in which a $\langle\Delta E\rangle$ quantity can be obtained from calculations: (i) trajectory calculations that determine $P(E',E)$ and (ii) calibrated biased random walk. Experimental methods are discussed in the next section.

1. Trajectory Calculations

Trajectory studies can lead to a dynamical picture of the energy-transfer process and the important parameters determining the $P(E',E)$'s. There have been a number of studies of the deactivation of a triatomic molecule by an inert gas.[35] Two important studies involving more complex molecules (with 5 and 18 atoms) are the deactivation by argon of methane[39] and azul-

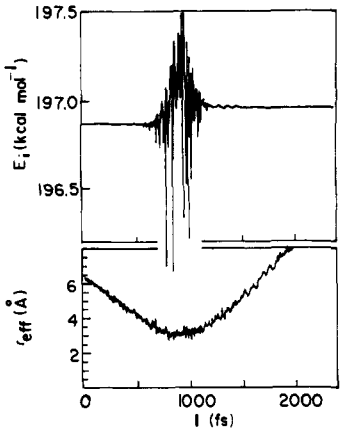

Figure 10. Internal energy and effective separation vs time for a trajectory simulating an azulene–Ar collision (rotational energy E_r = 1.0 kT, T = 630 K) (reprinted from ref 40; copyright, 1986 AIP).

ene.[40] The methane[39] study in which the methane had 103 kcal/mol of vibrational–rotational energy and 5 kcal/mol of relative translational energy (comparable to the experimental conditions of thermal unimolecular decomposition of methane) shows that a long-lived complex is not involved as there is only one inner turning point for the relative motion between the collision pair. However, the collision pair interacts for 0.1–0.2 ps; during this time there is strong coupling between the vibrational–rotational motion of methane and the transition modes. There is time scale overlap between this model and a complex formation model since the two collision partners stick together long enough (>0.1 ps) to allow for some intramolecular energy redistribution between the two partners. For 10 trajectories, $\langle \Delta E \rangle_d \approx -1$ kcal/mol; the authors claim that this is a fortuitous agreement with the experimental value.

The azulene[40] system with an excitation of approximately 100 kcal/mol above the zero-point energy (95 kcal/mol) revealed similar dynamics to that of methane. The internal energy of azulene exhibits rapid and wildly varying oscillations as it temporarly traps the argon atom. The argon atom wanders over the periphery of the azulene molecule, each miniencounter causes the internal energy of azulene to change phase. This description is illustrated in Figure 10. The apparent random behavior is the foundation for the biased random-walk model.[40]

Trajectory studies[62] for the recombination efficiency of ion–molecule reactions indicate that the structures of both collision partners are important. It is expected that more detailed understanding of energy transfer will result as future calculations become available. The important problems to solve are finding a realistic PES, proper sampling of the available phase space, and the availability of large amounts of computer time.

2. Biased Random Walk

Lim and Gilbert[40] have developed a model for calculating $\langle \Delta E \rangle$ quantities from the results of a few trajectories or from readily available experimental data. In this model, during the collision time the energy transfer is considered a random walk in the internal energy space of A + M with the constraints on the total energy and microscopic reversibility. Each collision has "many" samples of the impact parameters and phases of the oscillators. Equations are developed that characterize the diffusion of energy in terms of an energy diffusion constant and the duration of the collision. A single quantity, S, which can be calculated from as few as 10–50 trajectories, is used to calculate $\langle \Delta E \rangle_d$ or $\langle \Delta E \rangle_{all}$. Alternatively, S can be estimated from

$$S = 0.1H\frac{E}{n_{vib}}(\nu_{avg}\sigma_{LJ})^{0.5}\left(\frac{8k_B}{\pi\mu}\right)^{-0.25} \quad (2\text{-}22)$$

where n_{vib} is the number of oscillators, E is the excitation energy, ν_{avg} is the average vibrational frequency of A defined by

$$\nu_{avg} = \frac{\sum_i^{n_{vib}} \nu_i}{n_{vib}} \quad (2\text{-}23)$$

σ_{LJ} is the Lennard-Jones diameter, and H is a correction factor (of the order of 1.0) determined by fitting $\langle \Delta E \rangle_d$ from 13 different experimental systems. With use of statistical analysis, H was determined to be a function of the polarizability, dispersion of the vibrational frequencies of A, temperature, reduced mass, and $E/(n_{vib}\nu_{avg})$. The value of S is then used to calculate $\langle \Delta E \rangle_d$ by

$$\langle \Delta E \rangle_d = 2S(w\ \mathrm{erfc}(-w) + \pi^{-0.5}\frac{e^{-w^2}}{\mathrm{erfc}(-w)} \quad (2\text{-}24)$$

where erfc is the complementary error function and

$$w \equiv -0.5S\frac{\mathrm{d}\ \ln f(E)}{\mathrm{d}E} \quad (2\text{-}25)$$

with $f(E) = N(E)\exp(-E/k_BT)$. Presently, this model is limited to monatomic deactivators. [Added in proof: A new version was recently published; see ref 40c.]

This algorithm for calculating $\langle \Delta E \rangle_d$ is within 40% of the experimental values for the systems Lim and Gilbert considered when H is arbitrarily set to 1 and is within 24% of the expected value when the correction term is included. This latter uncertainty is within the normal errors associated with reported experimental $\langle \Delta E \rangle$ quantities. Hence, this method is recommended to calculate $\langle \Delta E \rangle_d$ when experimental data are not available. Alternatively, it can be used to modify an experimentally determined $\langle \Delta E \rangle_d$ from one deactivator to another, from one temperature to another, or from one excitation energy to another.

III. A Pragmatic Approach: Easier Calculations

It is clear from the previous section that a solution of the master equation is the only way to obtain reliable results for weak collisions. However, it is also clear that a great deal of time and effort must be invested in order to obtain reliable results. Therefore, in cases where k_{uni} is not needed with great accuracy or the calculational facilities are not available, other pragmatic approaches can be taken. We now discuss some of the approaches.

A. Collisional Efficiency

Imbedded in eq 1-19 is the fact that there are many states that contribute to reaction and each channel

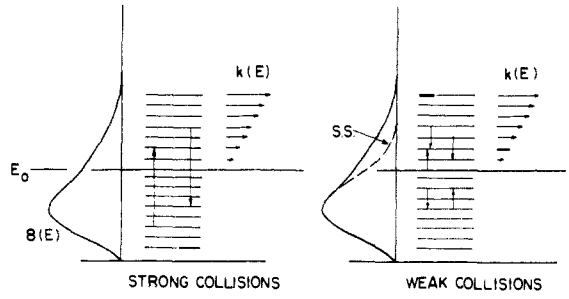

Figure 11. Equilibrium and steady-state distributions for strong and weak colliders.

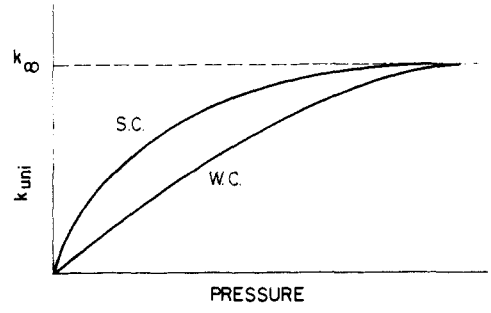

Figure 12. Schematic plot of k_{uni} vs pressure for weak and strong colliders (not to scale).

(state) has a characteristic rate coefficient $k(E)$. The derivation of eq 1-19 contains the explicit assumption that each collision is "strong" (SC) or efficient enough such that a steady-state distribution below E_0 is maintained at all times, thus; the collision frequency (Z[M]) is a true representative of the collisional deactivation process. However, if collisions are not efficient in transporting molecules up and down the energy ladder, the equilibrium Boltzmann distribution will not be maintained. This is depicted in Figure 11. In the SC case, molecules can be transported from levels well below E_0 to replenish the levels depleted by reaction with rate coefficients $k(E)$. In the inefficient collisions case, or "weak collisions" (WC), the depleted levels above E_0 are not replenished at high enough rate and the population distribution differs from the equilibrium one and at a low and moderate temperatures will reach a steady state. The experimental manifestation of weak collisions is to provide k_{uni} a different pressure dependence than in the strong collision case. This is shown schematically (not to scale) in Figure 12.

One pragmatic approach often taken is to modify eq 1-19.

$$k_{uni} = \beta_0 \int_{E_0}^{\infty} \frac{Z[M]\, B(E)dE}{\beta_0 Z[M] + k(E)} \qquad (3\text{-}1)$$

Here, $\beta_0 Z$[M] replaces Z[M] in eq 1-19, and k_{uni} is ignored in the denominator. The scaling term β_0 is a collisional efficiency. The product $\beta_0 Z$[M] is a "reduced" or effective collisional frequency. β_0 is defined as

$$\beta_0 = k_0^{wc}/k_0^{sc} \qquad (3\text{-}2)$$

where k_0^{wc} and k_0^{sc} are the low-pressure second-order weak-collider and strong-collider rate coefficients, respectively. It is clear that simply using eq 3-2 in eq 3-1 is wrong. First, β_0 (independent of pressure) is applicable only in the low-pressure limit and therefore cannot be used in eq 3-1 over the whole pressure range. Second, all that β_0 does to Z[M] is to shift the k_{uni}^{sc} vs [M] curve without changing its curvature. This is contrary to experimental findings[63] and calculations where the curvature of a weak collider differs from that of a strong collider. Third, eq 3-1 is applicable only in the low-temperature range. At higher temperatures, detailed eigenvalue solutions should be used.

B. Analytical Solution of the Master Equation: Example for Exponential Transition Probability

It is possible, in the low-temperature range, to obtain approximate analytical solutions of the master equation for a few cases of transition probabilities. Snider[60] has given expressions for β for four transition probability models: exponential, separable power, drop-off, and stepladder. We discuss the exponential model in detail.

In the following the derivation and underlying approximations for an analytical solution for β as a function of pressure for the exponential model are given. We follow Keck and Carrier,[64,65] Troe,[66a] and others. Consider the expression

$$F_e = \frac{\int_{E_0}^{\infty} N(E)\, e^{-E/RT}\, dE}{RT\, N(E_0)\, e^{-E_0/RT}} \qquad (3\text{-}3)$$

At low temperatures and at high energies around E_0, the Boltzmann distribution in the numerator of eq 3-3 is governed by the exponential tail. It is possible therefore to approximate $N(E)$ in eq 3-3 in the low-temperature range by an exponential form $N(E) = e^{ME}$. Substituting $N(E)$ in eq 3-3 and integrating, one obtains for M

$$M = \frac{1}{RT}\frac{F_e - 1}{F_e} \qquad (3\text{-}4)$$

Now the exponential transition probability model was defined by eq 2-14 and is defined here in greater detail

$$P(E',E) = Ce^{-(E-E')/\alpha} \quad E' < E \quad \text{down collisions} \qquad (3\text{-}5)$$

$$P(E',E) = Ce^{-(E'-E)/\gamma} \quad E' > E \quad \text{up collisions}$$

where E and E' denote the reactant energy levels before and after the collision.

Assuming that strong collisions apply, $[A(E,t)]$ in eq 1-27 can be replaced by the equilibrium population $B(E)$. Introducing eq 3-4 into the density of states part of $B(E)$ and introducing eq 3-5 into eq 1-27, one obtains for "up" collisions

$$\gamma = \frac{\alpha F_e RT}{\alpha + F_e RT} \qquad (3\text{-}6)$$

γ is independent of the initial energy; therefore, eq 1-25 can be used, and one obtains the normalization factor of the transition probability to be

$$C = \frac{1}{\alpha} + \frac{1}{\gamma} \qquad (3\text{-}7)$$

The average energy down for this model is

$$\langle \Delta E \rangle_d = \frac{\int_0^E (E - E')e^{-(E-E')/\alpha}\, dE'}{\int_0^E e^{-(E-E')/\alpha}\, dE'} = -\alpha \qquad (3\text{-}8)$$

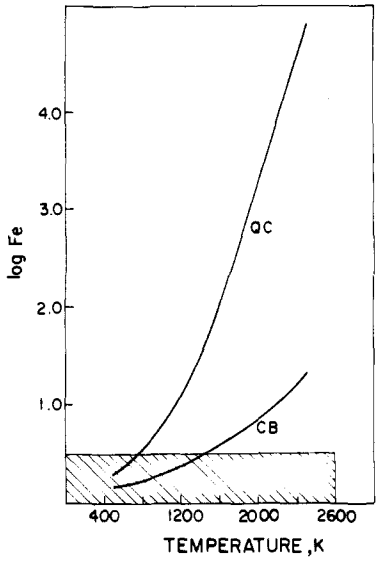

Figure 13. log F_e from eq 3-3 vs temperature for quadricyclane (QC) and cyclobutane (CB). The shaded area indicates the region in which F_e can be used.

Note that the normalization in eq 3-8 is done such that the denominator includes only the down collision part of $P(E',E)$. The overall average energy transferred $\langle\Delta E\rangle_{all}$ for all collisions is found by

$$\langle\Delta E\rangle_{all} = \int_{-\infty}^{\infty}(E' - E)\, P(E',E)\, dE' = \gamma - \alpha \qquad (3\text{-}9)$$

Combining eqs 3-6 and 3-9, one obtains

$$\langle\Delta E\rangle_{all} = -\frac{\alpha^2}{\alpha + F_e RT} \qquad (3\text{-}10)$$

Analysis of eq 3-9 (and eq 3-10) shows that always $\langle\Delta E\rangle_{all} < 0$. This situation is nonphysical for high temperatures where the prevailing energy flow is upward and $\langle\Delta E\rangle_{all}$ should change sign. Equation 3-10 breaks down for the case that the approximation of $N(E)$ by an exponential is not applicable and F_e is meaningless. The dependence of F_e on the temperature for quadricyclane and cyclobutane is given in Figure 13. The first molecule is large with low E_0 and the second is small with high E_0. The dashed part indicates the region in which F_e is useful, i.e., $F_e < 3$. For quadricyclane the useful temperature region is below 800 K, while for cyclobutane it is below 1400 K. Caution should be exercised and F_e should not be used in a temperature region in which it does not apply.

The expression for F_e, eq 3-3, primarily developed for parameterizing thermal unimolecular reactions in the second-order region, takes into account the energy dependence of the density of states; in this case the competition between "up" and "down" transitions is not present. Other approximations relating $\langle\Delta E\rangle_{all}$ and $\langle\Delta E\rangle_d$ have been developed by Barker and Golden[55] (BG) and by Tardy and Rabinovitch[59] (TR). Both groups have developed equations for $\langle\Delta E\rangle_{all}$ in terms of $\langle\Delta E\rangle_d$ that exhibit both a sign change and energy dependence for $\langle\Delta E\rangle_{all}$, a behavior expected in physical systems; this is done by considering the ratio of the density of states that occurs in the detailed balance constraint and thus takes into account both the "up" and "down" transition probabilities. BG have used the Whitten–Rabinovitch approximation for the density of states while TR invoked a "fitted classical approximation". Both produce results comparable to the exact solution; the BG formulation is somewhat easier to implement than that of TR; however, the exact solution can be readily computed.

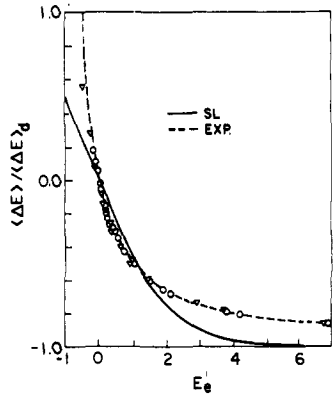

Figure 14. Plots of $\langle\Delta E\rangle_{all}/\langle\Delta E\rangle_d$ vs E_e' (=$\langle\Delta E\rangle_d/RT^{TR}$) for SL (solid line) and EXP (broken line) models with nitryl chloride (○), methyl isocyanide (○), cyclopropane (▽), and cycloheptatriene (△) with step sizes of 100, 200, 400, 800, and 1600 cm^{-1} each at 250, 500, 1000, 2000, and 4000 K (reprinted from ref 59b; copyright 1986 American Chemical Society).

TABLE II. Calculated Values of $\langle\Delta E\rangle_{all}/\langle\Delta E\rangle_d$ for the Exponential Transition Probability Model

system	$\langle\Delta E\rangle_d$, cm^{-1}	T, K	exact	Troe	BG	TR
CH_3NC	100	250	−0.343	−0.345	−0.345	−0.344
		500	−0.191	−0.193	−0.192	−0.192
		1000	−0.084	−0.088	−0.086	−0.086
		1500	−0.042	−0.047	−0.044	−0.044
		2000	−0.020	−0.027	−0.022	−0.022
	1600	250	−0.883	−0.894	−0.894	−0.883
		500	−0.786	−0.793	−0.792	−0.787
		1000	−0.598	−0.606	−0.601	−0.599
		1500	−0.428	−0.443	−0.424	−0.423
		2000	−0.274	−0.308	−0.261	−0.261
cyclohepta-triene	100	250	−0.319	−0.325	−0.325	−0.324
		500	−0.154	−0.163	−0.162	−0.161
		1000	−0.037	−0.050	−0.047	−0.047
		1500	0.009	−0.012	−0.001	−0.001
		2000	0.034	−0.001	0.023	0.023
	1600	250	−0.873	−0.885	−0.885	−0.875
		500	−0.743	−0.756	−0.755	−0.751
		1000	−0.405	−0.458	−0.440	−0.439
		1500	0.037	−0.161	−0.017	−0.017
		2000	0.578	−0.020	0.579	0.578

In lieu of the exact or approximate calculations, TR[59b] have generated a quasi-universal curve (Figure 14) by parameterizing $\langle\Delta E\rangle_{all}/\langle\Delta E\rangle_d$ in terms of a reduced energy transferred, E'_e (=$\langle\Delta E\rangle_d/RT_e$), for both exponential and stepladder transition probability models. In this case an effective temperature, T_e, is defined in terms of an inversion temperature, T_I (at which $\langle\Delta E\rangle_{all} = 0$): $T_e = T/(1 - T/T_I)$. The inversion temperature can be calculated by the methods of BG or TR. For low temperatures and moderately small molecules $T_e = T$ and $F_e = 1$ so the approximations become equivalent and equal to the exact solution. The relative merit of each approximation is illustrated in Table II for a small and large molecule, CH_3NC and cycloheptatriene (CHT), respectively, as a function of $\langle\Delta E\rangle_d$ and temperature. As can be seen there is agreement between all models and the exact calculations at temperatures below 1500 K. Above 1500 K and for a large molecule (CHT) the agreement is less satisfying, with BG and TR faring better than Troe (T).

C. β as a Function of $\langle \Delta E \rangle$

The functional dependence of the collisional efficiency on ΔE is given by Troe[66a,67]

$$\frac{\beta_0}{1-\beta_0^{0.5}} = \frac{-\langle \Delta E \rangle_{all}}{F_e RT} \tag{3-11}$$

and by Tardy and Rabinovitch[1] (for very weak collisions)

$$\beta_0 = \frac{\langle \Delta E \rangle_{all}^2}{(RT)^2 I_{TR}} \tag{3-12}$$

where I_{TR} is a correction factor given in ref 1.

An alternative method for calculating the falloff curve of a weak collider is that described by Tardy and Rabinovitch[1] in which the appropriate collisional efficiencies are used to transform the strong-collider falloff curve. TR have shown by performing master equation calculations for N_2O, NO_2Cl, CH_3NC, C_3H_6 (cyclopropane), and C_5H_{10} (dimethylcyclopropane) from 273 to 1000 K in the second-order region that β_0 is a quasi-universal function of the reduced energy, E', defined as

$$E' = \frac{\langle \Delta E \rangle_d}{\langle E^+ \rangle} \tag{3-13}$$

where $\langle E^+ \rangle$ is the average energy of molecules in excess of E_0

$$\langle E^+ \rangle = \frac{\int_{E_0}^{\infty} (E - E_0)\, B(E)\, dE}{\int_{E_0}^{\infty} B(E)\, dE} \tag{3-14}$$

and can be approximated by

$$\langle E^+ \rangle = 1.1 + \frac{sRT}{E_0} + \ldots \tag{3-15}$$

where s is the classical equivalent number of oscillators. This dependence of β_0 on E' is illustrated in Figure 7 of ref 1; the dependence on the specific probability model (stepladder, poisson or exponential) is also illustrated. Falloff curves for methyl isocyanide and cyclopropane from 353 to 728 K were also computed, and β ($=k^{wc}/k^{sc}$) was calculated; the resulting plots of $\beta(E')_{order}$ vs E' (Figure 8 in ref 1) for different reaction orders show a similar behavior to what was observed for the second-order region except, as to be expected, that for a given E', i.e., a specified $\langle \Delta E \rangle_d$, $\beta(E')_{order}$ increases with a decrease in reaction order.

In order to calculate a weak-collider rate coefficient for a given reaction, the prescription is as follows:

1. A rate coefficient is calculated from either a strong-collision expression or one of the parametric equations (see 4, below) of Oref,[68] Gardiner,[69] or Troe,[67,70] for the collision frequency of the weak collider (calculated from the pressure with an assumed collision cross section for the substrate deactivator combination).

2. $\langle \Delta E \rangle_d$ is estimated for the appropriate substrate deactivator at the temperature in question from tables. When direct information is not available, similar chemical systems are used to make an educated guess; even then unknown errors may be present.

3. With use of the strong-collider calculation or from experiments, values for $\langle E^+ \rangle$ (from the equation given above) and the reaction order are estimated. Alternatively, $\langle E^+ \rangle$ can be estimated by using the average energy of all molecules $\langle E \rangle$ calculated from molecular properties, the threshold energy E_0, and the activation energy in the second-order region E_{a0}.

$$\langle E^+ \rangle = E_{a0} + \langle E \rangle - E_0 \tag{3-16}$$

The reaction order Φ is estimated from the equation

$$\Phi = 1 + \frac{d(\log k)}{d(\log \omega)} \tag{3-17}$$

where ω is the collisional frequency. $\beta(E')_\Phi$ is obtained from these quantities and the universal plot (Figure 8 of ref 1).

4. Finally, $k^{wc} = \beta(E')_\Phi k^{sc}$.

Forst[71] gives an expression for β

$$\beta \approx \frac{\langle \Delta E^2 \rangle_{ss}}{2kT^2 C_v} \tag{3-18}$$

where ss is for the steady-state population distribution (i.e. a function of falloff) and C_v is constant-volume heat capacity. β decreases with temperature for moderately weak collisions. This is found experimentally.[1,72-74]

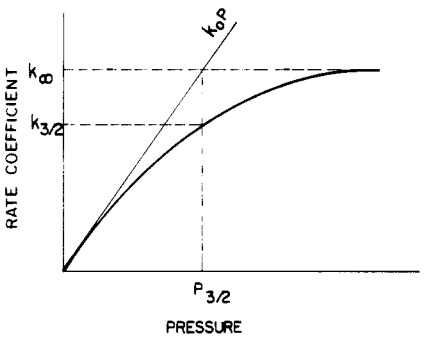

Figure 15. Rate coefficient vs pressure. $P_{3/2}$ denotes the pressure at which the reaction order is $^3/_2$ and at which the lines k_0P and k_∞ intersect.

IV. Calculations of Rate Coefficients in Strong and Weak Collision Systems Using Parametric Equations

Calculations of rate coefficients involve an assumption of a transition probability model, calculations of $k(E)$ (or $k(E,J)$) from RRKM or other theories, and a solution of a master equation—a procedure too time consuming for those who are involved in large-scale modeling of combustion or air pollution processes. For them, rate coefficients are only part of input parameters into large-scale rate matrices from which reaction schemes are drawn. Therefore, parametric equations giving the rate coefficient as a function of pressure for weak colliders are helpful. Three equations due to Troe,[66,67] Gardiner,[69] and Oref[68] exist. They have common features that will be discussed first, and the specifics of each model will follow. Figure 15 shows the dependence of the rate coefficient on pressure, P. The intersection point $k_0P_{3/2} = k_\infty$ occurs at reaction order[68] $^3/_2$. k_0 is the low-pressure and k_∞ the high-pressure rate coefficient with appropriate units. Troe preserved the Lindemann strong-collision expression

$$\frac{k}{k_\infty} = \frac{\frac{k_0 P}{k_\infty}}{\frac{k_0 P}{k_\infty} + 1} F \tag{4-1}$$

and modified it by a broadening factor F, which takes care of the deviation of the experimental curve from the Lindemann strong-collision curve as in Figure 8. F is a product of two parameters: a strong collision F_c^{sc} and a weak collision one F_c^{wc} related to the collisional efficiency β and evaluated at $P_{3/2}$. F_c^{sc}, the strong-collision center-broadening factor, takes care of the fact that real systems are multilevel as compared with Lindemann's one-level system. F_c^{wc} takes care of the fact that the curvature depends on $\langle \Delta E \rangle$ of the collision. F is an empirical function of the F_c's and pressure and temperature. Ten parameters[75] are needed in total for this and other parametric models listed below to specify k at any pressure, temperature, and collision efficiency. Some of these parameters have limitations on their regions of validity. F_c^{sc} calculated by an empirical equation deviates from exact strong collision F_c^{sc}, with a maximum deviation of 25% for ethane, butane, hexane, and octane fission.[75]

An empirical function that well represents falloff behavior is Gardiner's expression[69]

$$\frac{1}{k} = \left[\left(\frac{1}{k_0 P}\right)^a + \left(\frac{1}{k_\infty}\right)^a\right]^{1/a} \qquad (4\text{-}2)$$

based on a Minkowski metric form.[76] The parameter a is given by an empirical expression related to $P_{3/2}$ and is a function of temperature and heat capacity of the molecule. A comparison is made with the work of Larson et al.,[75] and the agreement seems to be good. The effect of weak collisions on the rate coefficient via the suggested formalism is presently being explored.[69b]

Another expression that is less empirical and is rooted in basic physical understanding is the J equation due to Oref.[68]

$$k = \frac{-(k_\infty + k_0 P) + [(k_\infty + K_0 P)^2 + 4(J_{3/2} - 1)k_\infty k_0 P]^{0.5}}{2(J_{3/2} - 1)} \qquad (4\text{-}3)$$

$J_{3/2}$ is given by the expression

$$J_{3/2} = \left[\frac{k_\infty}{k_{3/2}} - 1\right]^2 \qquad (4\text{-}4)$$

where $k_{3/2}$ is evaluated from eq 4-3 at $P_{3/2}$. The meaning of J at $P_{3/2}$ is given by the expression

$$J_{3/2}^{1/2} = \left\langle \frac{k(E)}{\omega} \right\rangle^T \qquad (4\text{-}5)$$

where ω is the collision frequency and T indicates that the average is over Tolman's distribution of reacting molecules.

$$T = \frac{B(E)\, k(E)}{k(E) + \omega} \qquad (4\text{-}6)$$

The temperature dependence of $J_{3/2}$ is given by the expression

$$J_{3/2} = \left[\frac{c e^{-E/RT}}{T^m} - 1\right]^2 \qquad (4\text{-}7)$$

where c, E, and m are constants specific to a given system. This equation, rooted in theory,[68] is good up to $\langle E \rangle / E_0 \approx 0.5$ where E_0 is the threshold energy for decomposition. An expression that yields good agreement with master equation calculations is of a Gaussian form

$$J_{3/2} = e^{A(T/1000) - T_1) + B} \qquad (4\text{-}8)$$

where A, B, and T_1 are constants defining the function. k from the J equation was evaluated over a wide range of pressures and temperatures for a variety of strong and weak colliders. The molecules studied were quadricyclane, cyclobutene, cyclobutane, cyclopropene, chlorodeuterioethane, and bromoethane colliding with strong collider and with He, Ar, and C_6H_6 as bath molecules with $\langle \Delta E \rangle_d$ = 250, 500, and 1200 cm^{-1}, respectively. The pressure range covered was 10^{-4}–10^{10} Torr, and the temperature range was up to 2500 K depending on E_0. In all cases studied, the deviations between k^{sc}(RRKM) and $k(J)$ above the $P_{3/2}$ were a few percent. The ten parameters which determine the whole system can be calculated from k^{sc}. Figure 16 compares exact master equation calculations with results from the J equation (eq 4-3) for cyclobutane fission. Figure 17 shows the percent deviation of k (eq 4-3) from k^{sc}(RRKM) as a function of pressure.

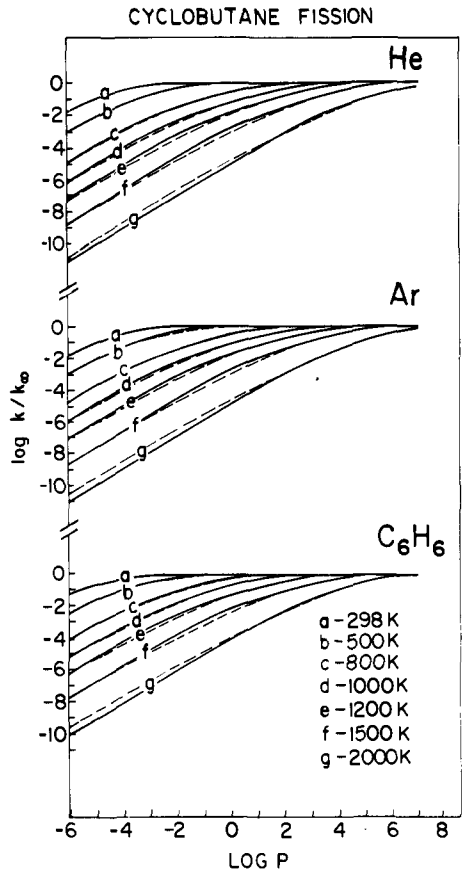

Figure 16. log (k/k_∞) vs log P (Torr) for cyclobutane fission with He, Ar, and benzene as colliders: full line, k calculated with the J equation; dashed line, exact RRKM calculations. In places where there is only one line, the results of the two calculations overlap (reprinted from ref 68b; copyright 1990 American Chemical Society).

The basic idea behind parametric equations is the fact that the parameters used in evaluating k are drawn from the limiting rate coefficient values, k_0 and k_∞, and the shape factors of the various models obtained from either RRKM calculations or experiments. The utility

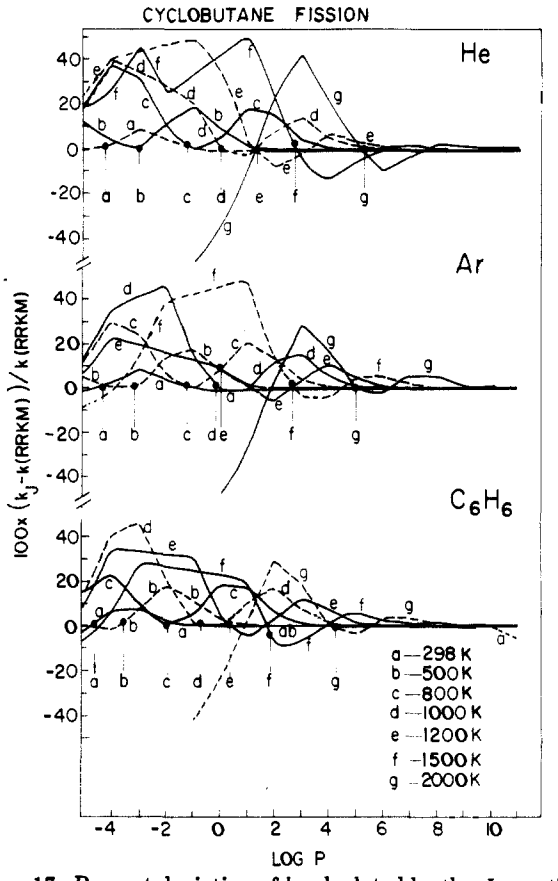

Figure 17. Percent deviation of k calculated by the J equation from k(RRKM) vs log P (Torr) for cyclobutane fission in He, Ar, and benzene as inert colliders. The dots indicate the $P_{3/2}$ point at each temperature.

of such models lies in the fact that once a complete RRKM calculation is done and the parameters are evaluated at a few temperatures, the value of k can be found at any temperature or pressure without each time resorting to a complete set of master equation calculations.

V. From Experiment to Energy-Transfer Quantities

Before specific experiments are described, a general discussion pertaining to experimental requirements is presented. In deconvoluting an energy-transfer experiment, the question of uniqueness must be considered when the system of equations is solved, since the number of experimental observables is much less than the number of variables in the master equation; i.e., the system is underdetermined. If energy, spatial, or temporal variables are not specified and/or not limited in range, the resulting energy-transfer information will include a high degree of averaging, which may also prevent direct comparison with other experiments. Thus, specific information relating the dependence of the energy-transfer model on excitation energy, temperature, and complexity of A and M (vibrational frequency patterns, mass, geometry, intermolecular interaction, etc.) will not be available.

So that limitations of the data can be reasonably assessed, excited molecule preparation, number of collisions experienced by the prepared molecule (exposure), and product observation/analysis as they appear in energy-transfer experiments must be understood. A simple model is presented here to illustrate the importance of these steps and how they interact. In the case of intermolecular energy transfer, information on the step

$$A(E) + M(E_2) \rightarrow A(E') + M(E'_2) \qquad (5\text{-}1)$$

is required; in this case the primes designate the final energies and the subscript 2 corresponds to the deactivator (M). The prepared (initial) concentration distribution of A ($[A(E_p,r_p,t_p)]$) is dependent on the specific experiment; in this case the subscript p corresponds to the prepared substrate with energy E at position r in the reactor at time t (if relevant). The prepared energies distribution of E_p may be wide, as in a thermal system, or relatively narrow, as in the case of single-photon excitation experiments. In a similar manner the preparation time, t_p, can span the range from a near δ function input, e.g., a pulsed laser, to a wide temporal distribution in which A is continually formed, i.e., by a collisional process. In some experiments discussed later where mass transport (such as VLPP) and/or collection efficiencies (IRF or UVA) are important, the inhomogeneities in the spatial distribution of the prepared substrate must be included; i.e., the distribution function for r_p must be specified.

The concentration distribution function ($[A(E',r',t)]$) for A at a specified energy E', time t, and position r' is obtained by solving the master equation with the appropriate prepared populations. In order to determine the time evolution of M, i.e., $[M(E'_2,r',t)]$, additional differential equations involving energy transfer (both activation and deactivation) and transport must be included.

The final step in simulating the experiment requires a transfer function $T(E_{obs},r_{obs},t_{obs},E',r',t)$, which converts the concentrations specified by E', r', and t to the experimentally observed signal S at the observed energy, position, and time, E_{obs}, r_{obs}, and t_{obs}, respectively. Energy, spatial, and temporal dependence is obtained for the particular experiment by appropriate integration limits for

$$S(E_{obs},r_{obs},t_{obs}) = \int\int\int T(E_{obs},r_{obs},t_{obs},E',r',t') [A(E',r',t')]\, dE'\, dR'\, dt' \qquad (5\text{-}2)$$

In any experiment the signal may be due directly to $A(E')$ or $M(E'_2)$ or indirectly to a chemical reaction, photon emission, or absorption.

From these equations it is justified to state that the ideal experiment demands energy, spatial (possibly), and temporal resolution for both the reagent and the observed product. In reality, an evaluation of the quality of a particular experiment is difficult to make since there is a strong interaction between these variables. This is particularly true since most experimental techniques at this time have at least one of the above deficiencies.

A. Time Resolution: Preparation and Exposure

Much detail is lost (or equivalently more assumptions are made in the analysis) if the time resolution of t_p and t_{obs} is relaxed. The interplay of the collisional process, i.e., the probability matrix **P** (the matrix used in setting up the master equation), t, and t_p is complex, although limiting cases can be considered; for the examples given

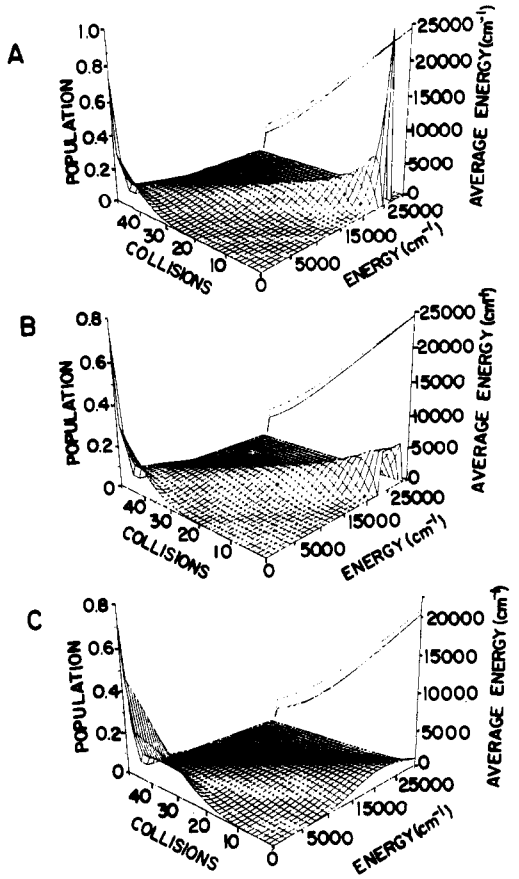

Figure 18. Relaxation of cyclohexene with exponential weak-collider model ($\langle\Delta E\rangle_d$ = 500 cm^{-1}). Population as a function of energy and number of collisions with inputs: (a) delta function at 25 000 cm^{-1}; (b) box function between 22 000 and 28 000 cm^{-1}; (c) Boltzmann distribution at 1500 K ($\langle E\rangle$ = 22 000 cm^{-1}). The average energy, $\langle E\rangle$ (solid line), and $\langle E^2\rangle^{0.5}$ (dashed line) are also shown as a function of the number of collisions.

below, NZ is the number of collisions that the substrate undergoes after time t.

For single-collision experiments in which NZ = 1 (molecular beam, jet, etc.), the probability of transporting the substrate from initial (unprimed quantities) to final (primed quantities) energy and position at time t reduces to the probability matrix. For the case of specific energy selection of A, the transition probabilities are just the elements in the appropriate column in the **P** matrix and there is a simple correspondence between A(E',r',t') and A(E,r,t) as shown in Figure 18a. However, as the number of initially populated energy levels in A increases, the origin of the states generating a specific E' becomes fuzzy (Figure 18b). In the limit of a complete equilibrium population distribution at the ambient temperature T, then

$$[A(E',r',t)] = [A(E,r,t)] = [A(r,t)]\,B(E) \quad (5\text{-}3)$$

where [A(r,t)] is the total concentration of A at r at time t. $B(E)$ is the Boltzmann population distribution function, and there will be no new information generated by the experiment (Figure 18c).

As the number of collisions increases, i.e., an increase in NZ or equivalently in exposure time, the details of the path producing the shuffled states becomes more spread out since there are numerous ways in populating a specific final energy state, E' (Figure 18a). This becomes even more complicated if there is a distribution of preparation times t_p, since energy states populated later in the preparation stage will undergo fewer collisions than those formed at the beginning. In the limit for single-collision experiments, t_p becomes unimportant; i.e., experiments in which there is a continuous input of prepared substrate molecules over the duration of the experiment will contain an equivalent amount of information.

B. Observation

If the time constant for the observation is small compared to collision times, then the signal will follow the instantaneous time dependence of the population. However, for single-collision experiments the observation time is not relevant. For multicollision exposures, as the time constant for observation increases, accumulation takes place until the signal gives the integral of the population, i.e., the product yield. For purposes of analysis it is usually assumed for a multicollision experiment in which the observation time is long relative to the preparation and exposure times that a steady state persists for the duration of the exposure; this is the typical case for studies of thermal unimolecular reactions. For high-temperature systems, such as shock tubes, induction times (i.e., preparation time) may be a significant part of the exposure time and this assumption would not be valid.[77]

C. Energy Resolution

In general, as in the case of temporal resolution, there is no advantage in observing the products with an energy resolution greater than that of the reagent preparation. As the preparation and/or exposure time increases, the energy distribution provides less information about the energy-transfer process and the demands on energy resolution are reduced. Energy resolution of thermal systems is not commonly obtained and is not warranted; however, a bulk average energy is sometimes used.

D. Obtaining the Transfer Function

The complete transfer function is often not known; however, some parts may be known or estimated. In some experiments the time constant of the detector and associated electronics can be determined along with the spectral bandwidth. The relative collection efficiency of emitted photons as a function of the emitter's position in the reaction cell is another factor that can be determined; this is crucial for systems exhibiting inhomogeneities in the spatial distribution. In general, the observed signal will also be a summation over many energy states; since in general the dependence of the transfer function on energy is not known a priori, a calibration curve is often used. For example, in thermal systems the experimentally determined high-pressure rate constant can be used to obtain the transfer function ($=k(E)$) since the populations are Boltzmann and the RRKM model is assumed.[18]

The importance of the correct form for the transfer function and its dependence on the shape of the distribution of populations can be realized by considering a simple system in which the position of the substrate in the reactor and time constants of the detector system can be ignored. Thus, the dependence of the transfer function on energy can be replaced by a power series

expansion in the energy E in which case the observed

$$T(E_{obs},r_{obs},t_{obs},E,r,t) = \sum_{i=0}^{\infty} a_i' E^i \quad (5\text{-}4)$$

signal given by

$$S(E_{obs},r_{obs},t_{obs}) = \int\int\int \sum_i a_i' E^i [A(E,r,t)]\, dE\, dr\, dt \quad (5\text{-}5)$$

reduces to

$$S(E_{obs},r_{obs},t_{obs}) = \int\int \sum_i a_i' \int E^i [A(r,t)]\, f(E)\, dE\, dr\, dt \quad (5\text{-}6)$$

$$S(E_{obs},r_{obs},t_{obs}) = \int\int \sum_i a_i' \langle E^i \rangle [A(r,t)]\, dr\, dt$$

where $f(E)$ is the normalized population distribution defined in eq 2-13 and the last equation was the result of substituting the definition of the generalized moment

$$\langle E^i \rangle = \int E^i f(E)\, dE \quad (5\text{-}7)$$

into the previous equation. S obtains the final form

$$S(E_{obs},r_{obs},t_{obs}) = \sum_i a_i \langle E^i \rangle \quad (5\text{-}8)$$

$$a_i = \int\int a_i' [A(r,t)]\, dr\, dt$$

That is to say, in the general case, the observed signal is determined by the moments of the population distribution. In the special case that $T(E_{obs},r_{obs},t_{obs},E',r',t)$ is linearly dependent on E', i.e., $a_0 + a_1E'$ ($a_i = 0$ for $i > 1$) as is nearly true for IRF experiments, the observed signal will be determined only by the average energy of the population distribution, i.e., distribution functions with different shapes (for example, a δ function and Boltzmann distribution) but with the same average energy will produce the same observed signal; this does not hold when nonlinear terms are included, in which case different distributions with different average energies may not give the same observed signal. For sufficiently small changes in the population distribution, the observed signal should be linear with $\langle E \rangle$ (this linear dependence is a special case); for small enough changes in the average energy this would also be the case. However, any nonlinearities in the transfer function are amplified when the distributions are not closely related. Specifically, during the relaxing process the population spreads out and higher moments of E are becoming larger with increasing Z; if the transfer function is a function of these moments, they must be included in the appropriate integrals to prevent unwanted distortions that develop when population distributions are compared at early and late observation times.

The problem of determining the transfer function, i.e., calibration, involves the same problems. For example, the signal as a function of temperature in a system with a Boltzmann population distribution (in which the populations for translational, rotational, and vibrational energy states are governed by a single temperature) is determined solely by $\langle E \rangle$. Similar population distributions can be compared, any nonlinearity in the transfer function will tend to cancel, and differences in the observed signal will be attributed to different average energies. Thus, the observed signal in the relaxation of a Boltzmann distribution at T_2 and T_1 would show a strong correlation to the curve generated by a series of temperatures in this range. However, in a microcanonical system, such as formed by laser excitation experiments, the initial population is very narrow (a room-temperature Boltzmann distribution offset by the energy of the absorbed photon); this initial distribution will finally relax to a Boltzmann population distribution at the ambient temperature. Clearly the initial distribution in these experiments differs markedly from the Boltzmann distribution used in the calibration, i.e., $\langle E^2 \rangle - \langle E \rangle^2 \approx 0$, while for the Boltzmann distribution it is C_vRT^2. The microcanonical and canonical systems are compared by taking the internal energy of the formed molecules to be equal to the average energy $\langle E \rangle$ of the latter.[86b,89a] Another factor that is difficult to evaluate is due to the nonequilibrium between the translational, rotational, and vibrational degrees of freedom in the experiment, which is absent in the calibration. In multiphoton excitation (MPE) experiments a bimodal distribution may be formed and should be taken into consideration.

VI. Experiments

This section describes experiments that use single or multiphoton excitation, collisional or chemical activation, and various detection techniques. A variety of the latter can be used with a given excitation method, and many excitation sources can be used with a given detection technique.

A. Energy Transfer from Molecules Excited Vibrationally by Internal Conversion from High Electronic Levels

An efficient way of obtaining vibrationally excited molecules with a very narrow internal distribution of energy in the ground electronic state is to electronically excite a molecule to a high electronic level followed by internal conversion to the ground electronic state. For example, azulene[56,57,78,79,81-85] has the origin of S_1 at 40.0 kcal/mol and of S_2 at 80.0 kcal/mol; thus, excitation can be obtained in the range 300–700 nm, easily accessible to visible and near-UV lasers. Internal conversion occurs rapidly in picoseconds from S_1 and in nanoseconds from[56] S_2. The hot molecule so formed can then undergo an energy-degrading collision (or in some cases reaction). To monitor the process, a specific physical property, which is a function of the internal energy content of the molecule, is followed. Barker et al.[56,78-82] followed the IR emission from the CH stretching vibration of azulene. Troe et al.[57,83,84,86-93] have followed the excitation decay of a series of molecules by UV absorption. Flynn et al.[85] have followed the vibration to vibration energy transfer from excited azulene to CO_2 by diode laser absorption spectroscopy. Oref et al.[41,42] have studied suprastrong collision by collisionally induced sensitization. The internal conversion method of excitation has provided important energy-transfer information, and each of the methods will be discussed separately.

1. Infrared Fluorescence (IRF)

Infrared fluorescence was used by Barker et al.[78,79,81,82] to study energy transfer, the average energy transferred per collision $\langle \Delta E \rangle_{all}$, and its dependence on the internal energy of the hot azulene molecule. The experimental

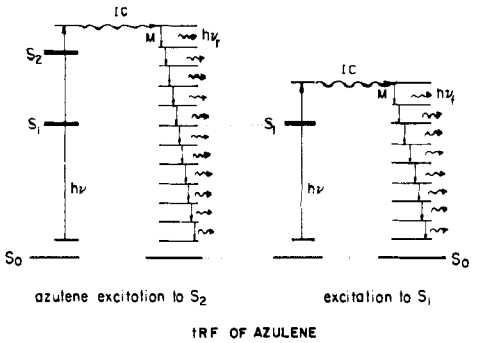

Figure 19. Level diagram of infrared emission (IRF) experiment. The cascade in the energy ladder follows IR emission of the CH stretch or combination bands in azulene.

setup consisted of a cell containing a mixture of azulene and an inert gas irradiated by a UV or visible laser. The emission was detected by a photovoltaic detector. The intensity of the laser was monitored by a photoacoustic detector. A calibration curve based on fundamental principles was constructed to give IRF as a function of the initial excitation of the molecule. The IRF theory of Durana and McDonald[94] and Rossi and Barker[78] assumes the applicability of the fundamental expression for a single oscillator emission and that the internal energy is statistically distributed in the molecule[25] and verified the expressions for low and high energies. Thus, the average number of molecules with v quanta in the emitting mode is

$$A_v = A_{ex}\frac{N_{s-1}(E - vh\nu)}{N_s(E)} \tag{6-1}$$

where $N_{s-1}(E - vh\nu)$ is the density of states of all modes except the emitting mode, $N_s(E)$ is the density of states of the excited molecule, and A_{ex} is the total number of excited molecules. Internal energy redistribution takes place on a picosecond time scale[25] and IRF on a microsecond time scale[56] so the statistical assumption is more than reasonable. The total IRF is given by

$$I(E) = \frac{A_{ex}}{N_s(E)}\sum_{i=1}^{\text{modes}} h\nu_i A_i^{1,0}\sum_{v_i=1}^{v,\max} v_i N_{s-1}(E - v_j h\nu_i) \tag{6-2}$$

where $A_i^{1,0}$ is the Einstein coefficient for the $\Delta v = -1$ spontaneous emission. A plot of $I(E)$ vs E provides the calibration curve from which E can be found at any given $I(E)$.[56]

The principle of the measurement is as follows: When a hot azulene molecule collides, it loses some energy and the intensity of the IRF decreases; i.e., the emission probes the average vibrational energy in the way that a thermometer probes the average translational temperature. The collision partner gains a small quantity of energy, <8.6 kcal/mol (Figure 19); it is assumed that its contribution to the observed IRF is negligible. In the case where the bath molecule emits in the same spectral region as the hot azulene, as is the case for CO_2, a double-exponential intensity profile is observed and the azulene emission is deconvoluted. Thus, the IRF intensity profile as a function of time provides information on $\langle\Delta E\rangle_{all}$. To extract the latter, three methods are used:[56,78-82] (1) In a master equation simulation,[55,95] a collision transition probability (exponential or reverse exponential) and a linear dependence of $\langle\Delta E\rangle_d$ on energy are assumed and the IRF time profile is matched. (2) In decay analysis, IRF intensity is converted directly into internal energy, producing an energy decay vs time curve. The decay curve is fitted by a third-order polynomial and differentiated to obtain $\langle\Delta E(t)\rangle_{all}$ ($=\langle E\rangle_0 - \langle E(t)\rangle$) and $\langle\Delta E(E)\rangle_{all}$ from the equation

$$\frac{d\langle E\rangle}{dt} = Z_{LJ}[A_{AZ}]\langle\Delta E(t)\rangle_{all} \tag{6-3}$$

where Z_{LJ} is the Lennard-Jones collision number and $[A_{AZ}]$ is the concentration of azulene molecules. (3) In a rate constant analysis method[82] the rate constant for the neat system is defined by $k = (\tau[A_{AZ}])^{-1}$ where τ is the exponential decay time constant. k together with Z_{LJ} and the IRF calibration curve are used to find $\langle\Delta E\rangle_{all}$ at the initial value of internal energy

$$\langle\Delta E\rangle_{all} = -\frac{k}{Z_{LJ}}\left[I\frac{dE}{dI}\right]_0 \tag{6-4}$$

The factor in brackets is evaluated from the calibration curve.

Of the three methods, the last one is the least accurate and has recently been modified by Shi and Barker.[82] Fitting the calibration curve to more than one empirical expression showed that $\langle\Delta E\rangle_{all}$ strongly depends on the type of calibration curve used; deviation from the theoretical curve will affect $\langle\Delta E\rangle$ strongly.[82] Therefore, in the analysis of the data, the theoretical calibration is used.

Results of IRF indicate that $\langle\Delta E\rangle_{all}$ is a nearly linear function of the internal energy content of the excited molecule. The curve is slightly concave down—the curvature is within experimental error or might be due to detailed balance.[82] Shi and Barker[82] give a table of 17 mono-, di-, and polyatomic colliders and the corresponding values of $\langle\Delta E\rangle_{all}$. The linear dependence of $\langle\Delta E\rangle_{all}$ on E contradicts the results obtained by UV absorption (UVA) studies at high temperatures (see later discussion). The temperature dependence of $\langle\Delta E\rangle_d$ in IRF experiments varies from $T^{0.6}$ for azulene–N_2 to being independent for the neat azulene gas.[55,95]

2. Vibrational Energy Transfer from Azulene to CO_2

Barker[56] has followed the population of CO_2 subsequent to a deactivating collision of internally converted azulene. The IRF from azulene is observed at 3.3 and 4.3 μm. The former is emission from the C–H stretch, and the latter is from combination bands and a broadened CH stretch. CO_2 emits at 4.3 μm and when added to the hot azulene system a biexponential decay was observed. The fast component was due to hot azulene emission and the slow one to CO_2 emission. A cold CO_2 gas filter in front of the detector absorbed 60% of the radiation, indicating that 40% was in modes other than the v_3 mode, which emits at 4.3 μm. The total number of excited CO_2 molecules was found to be only 1.5% of the number of excited azulene molecules.

A particularly interesting experiment is vibrational energy transfer from highly excited (E = 88.6–117.2 kcal/mol) azulene obtained from internal conversion to the vibrational modes of CO_2.[56,85] After collision of CO_2 with the hot azulene, Flynn et al.[85] probed the population of the vibrational levels of CO_2 by diode laser absorption spectroscopy. The data are compared to a model that assumes a collision complex,[27b,29,31,33,34,96,97]

azulene–CO_2, and uses a statistical model to calculate the amount and distribution of the energy transferred during a collision. The statistical probability of transferring a given amount of vibrational and translational energy to the CO_2 when the total energy of the system E is fixed is given by

$$P(E,n,n_v) = N_{AZ}(E - \epsilon)\ W_{CO_2}(\epsilon_v)\ (\epsilon - \epsilon_v)^{3/2}\frac{d\epsilon}{Q} \qquad (6\text{-}5)$$

$N_{AZ}(E - \epsilon)$ is the density of states of the excited azulene at energy E, $W_{CO_2}(\epsilon_v)$ is the number of vibrational states of CO_2 with energy ϵ_v, and $(\epsilon - \epsilon_v)^{3/2}$ is related to the relative translational energy. Q is the normalization factor such that

$$Q = \int_{n=0}^{E}\sum_{n=0}^{n} N(E,\epsilon,\epsilon_v) \qquad (6\text{-}6)$$

It is found that approximately 25% of the initial azulene energy is converted into vibrational energy in the CO_2, that the rate constants for removal of energy from azulene by CO_2 are in reasonable agreement with those found by Barker in IRF and Troe in UVA experiments, and that the CO_2 bending mode (667 cm^{-1}) population is much greater than is the antisymmetric stretching mode (2340 cm^{-1}). This might be due to a combination of reasons. Azulene does not have vibrational modes in the range between 1000 and 3000 cm^{-1} and has many below 1000 cm^{-1} that might undergo[85] a resonance energy transfer to the low-frequency bending mode of CO_2. In addition, $\langle\Delta E\rangle_{all}$ as found by Barker[56] and Troe[84] is 1.0–1.4 kcal/mol, closer to the bending mode frequency. Unlike the case of small molecules with low levels of excitation where resonance energy transfer takes place, large molecules with high levels of excitation in the quasi-continuum provide a complicated energy-transfer system where V–V′ and V–T/R take place simultaneously.

The results obtained by Flynn et al. are consistent with those of Barker et al. since the latter measured the population in the asymmetric stretch of CO_2 where the population is ~1% of the population in the bending mode observed by Flynn et al. When proper weighing is done, the results of both experiments agree within experimental errors.

3. Ultraviolet Absorption (UVA)

An additional method of observing energy transfer from excited molecules is by ultraviolet absorption.[86-93] It was recently reviewed by Hippler and Troe,[5] and only a summary description will be given here. They have performed extensive energy-transfer studies from internally converted cycloheptatriene (CHT),[87] substituted CHT,[86] toluene,[86,87] CS_2,[89] and azulene[57,83,84,98] (as well as on infrared multiphoton excited CF_3I[99]). Nakashima, Yoshihara, Ichimura, and Mori[100-102] have studied internally converted benzene and hexafluorobenzene. In the former method the CHT isomerizes to form an internally excited toluene. The basic principles of UVA are as follows, with toluene serving as an example. Toluene was heated over a wide temperature range and its UVA recorded. It was found that at 223 nm the extinction coefficient of the excited toluene is linearly dependent on its internal energy over a wide range of energies; i.e., the transfer function is sensitive to the first moment of E. Thus, a correlation exists between internal energy and UVA. A laser pulse initiates the excitation, and the decay of the internal excitation due to collisional energy transfer to the bath is followed by an interrogation light at 223 nm. The energy–time profile is analyzed by the expression

$$\langle E(t)\rangle \simeq \langle E(0)\rangle + \langle\Delta E\rangle_{all}Z_{LJ}[M]t \qquad (6\text{-}7)$$

As can be seen, the slope of the energy vs time line is the product $\langle\Delta E\rangle_{all}Z_{LJ}$ and the uncertainty in $\langle\Delta E\rangle_{all}$ is in part due to the fact that the collisional frequency is not known. Over 60 different bath gases were investigated, and their $\langle\Delta E\rangle_{all}$'s are tabulated; temperature dependences were also reported.

The results follow the general trend that the more atoms in the deactivator the larger $\langle\Delta E\rangle_{all}$, but there is a discrepancy between the magnitudes of $\langle\Delta E\rangle_{all}$ from studies of unimolecular reactions and the UVA technique.

The UVA technique was applied to azulene as well, and the $\langle\Delta E\rangle_{all}$ values of many inert bath gases were reported.[57,84] The values of $\langle\Delta E\rangle_{all}$ so obtained agree reasonably well with those reported by IRF by Barker et al.[82] with deviations of up to a factor of 2 for some exceptional cases. The energy dependence of $\langle\Delta E\rangle_{all}$ is linear in the low-energy range and becomes very weakly dependent on E for the values above[57,83,84,98] 57.2 kcal/mol. This is in disagreement with the work of Barker et al.[82] who find an almost linear dependence up to high energies. Both groups are aware of the sensitivity of the results to the form of the calibration curves used in the process of calculating $\langle\Delta E\rangle_{all}$. An experimental problem in the IRF and UVA methods is local heating following the laser pulse. Hippler, Troe, and Wendelken[86] indicate that under the condition of their experiment (10 mJ of energy absorbed by CHT, 25% of CHT excited, and 25 Torr of He) there is a temperature rise from 295 to 360 K. The change in temperature might be even larger for different experimental conditions. However, since $\langle\Delta E\rangle_{all}$ is determined to be a weak function of temperature, this may not be important. In addition, experiments were done at low levels of excitations, which cause a very small increase in temperature without noticeable differences in the experimental results.

Other internal conversion followed by UVA systems are benzene and hexafluorobenzene studied by Nakashima, Yoshihara, and others.[100-102] In their studies, the parent molecule was excited by an excimer laser at 193 nm to the S_3 level and intermolecular energy transfer was observed following internal converson to S_0. A linear dependence of $\langle\Delta E\rangle_{all}$ on E was assumed for the benzene and energy dependence or independence fit the hexafluorobenzene data. A variety of bath gases were used and the corresponding $\langle\Delta E\rangle_{all}$ obtained.

4. Sampling the Collision Transition Probability Function: Suprastrong Collisions by Collisional Activation

In the experiments discussed so far, the energy-transfer quantities evaluated in the various experiments are $\langle\Delta E\rangle_d$ and $\langle\Delta E\rangle_{all}$. These quantities, which are only parameters of a transition probability function, can fit a set of data with more than one model. That is to say, the shape of the distribution is not sampled during the experiment, only the moments of the distribution. Oref, Steel, and others[41,42] have explored a method by which

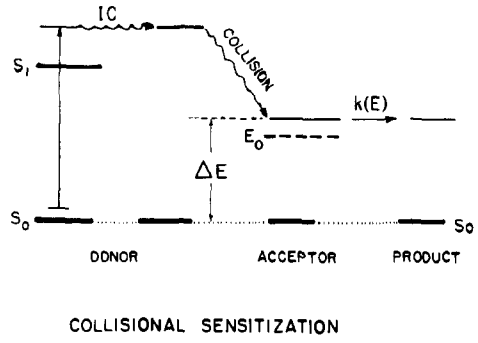

Figure 20. Level diagram of thermal sensitization experiment. The donor collides with an acceptor, transferring an amount of energy $\Delta E > E_0$. The acceptor decomposes or is deactivated.

ΔE (and not the average quantities) of very strong collisions can be found experimentally. The level diagram of the experiment is shown in Figure 20. Two systems were studied: azulene–quadricyclane and hexafluorobenzene–cyclobutene. The azulene–quadricyclane will be discussed in detail. Azulene is excited to its S_2 electronic state and internally converts to the ground electronic state. The highly vibrationally excited azulene is allowed to collide with quadricyclane at a low pressure of ~5 mTorr. The latter does not interfere with the azulene absorption but when excited isomerizes with a low activation energy of ~33 kcal/mol to norbornadiene. A single azulene deactivating collision with $\Delta E > 33$ kcal/mol can cause isomerization of the excited quadricyclane, which competes with its collisional deactivation. Actually few levels above E_0 can be excited by the energy-transfer process; however, the probability of transferring large quantities of energy in one collision is small and declines strongly with energy. This offsets the increase of $k(E)$ with energy. In practice, therefore, ΔE represents a very narrow range of energies close to E_0.

A kinetic scheme of the process allows isolation of the only unknown parameter, the probability of transferring a $\Delta E > 33$ kcal/mol, which was found for the present case to be $\sim 10^{-3}$. The pair hexafluorobenzene–cyclobutene with $E_0 \approx 33$ kcal/mol for the latter gave a similar value of $P(E',E)$. The azulene–norbornadiene system, with $E_0 \approx 52$ kcal/mol, and the hexafluorobenzene–cyclopropane system, with $E_0 \approx 65$ kcal/mol, did not show any isomerization products, which attests to very low values of $P(E',E)$ when $E' - E > 50$–60 kcal/mol (Figure 21). It should be realized that $\langle \Delta E \rangle_d$ for a suprastrong collision is not as large as the value of ΔE. For example, for the case of hexafluorobenzene and cyclobutene for all $E' \geq 33$ kcal/mol, $P(E',E) = 3 \times 10^{-3}$ mol/kcal. For an exponential model, 3×10^{-3} mol/kcal = $\exp(-33/\langle \Delta E \rangle_d)/\langle \Delta E \rangle_d$ so $\langle \Delta E \rangle_d = 9.2$ kcal/mol. That is to say, a relatively low value of $\langle \Delta E \rangle_d$ does not preclude a small number of very strong collisions with $\Delta E_d > 33$ kcal/mol. Results from internally converted hot ground-state molecules studied by UVA gave the following values for $\langle \Delta E \rangle_{all}$. Neat hexafluorobenzene excited at 300 and 350 nm gave $\langle \Delta E \rangle_{all} = -3.5$ kcal/mol while neat benzene gave[100-102] $\langle \Delta E \rangle_{all} = -5.9$ and -4.7 kcal/mol for the neat and isopentane as a bath molecule. Toluene and cycloheptatriene[86] gave lower values of -2 to -2.5 kcal/mol. Azulene studied by IRF gave -3.8 and -3.1 kcal/mol for the neat and *n*-butane as collider. All the values of $\langle \Delta E \rangle_{all}$ can be converted to $\langle \Delta E \rangle_d$ by the use of eq 3-10 with $Fe \approx$ 1; relatively small errors are incurred at room temperature. The values of $\langle \Delta E \rangle_d$ thus obtained are larger in magnitude than the values of $\langle \Delta E \rangle_{all}$. Chemical activation results[1] gave higher values of ~10 kcal/mol for deactivation of cyclopropane. It should be pointed out that the experimental value of $P(E',E)$ depends on σ_{LJ} and can vary somewhat. The value of $\langle \Delta E \rangle_d$ found in collisional activation experiments can be the value of a second exponential in a biexponential $P(E',E)$ (see next section).

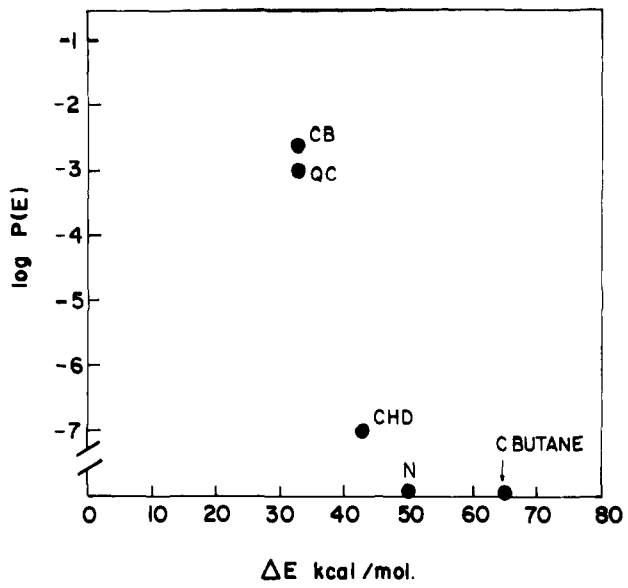

Figure 21. Collision probability as a function of ΔE from thermal sensitization.

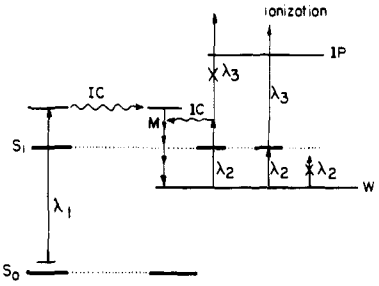

Figure 22. Multiphoton ionization detection of hot molecules. λ_1 excites the molecule to a high electronic level. Internal conversion (IC) occurs followed by a collisional cascade. λ_2 carries the deactivated molecule to an excited electronic state. If the transfer is exactly to $v = 0$ state, then λ_3 will ionize the molecule. If not, the molecule will internally convert before having a chance to ionize.

5. *Sampling the Collision Transition Probability Function: Detection by Multiphoton Ionization (MPI)*

Detection by the multiphoton ionization method used by Luther et al.[44,45] allows for a sensitive probing of the collision process. The principle of the method is depicted in Figure 22. A photon with wavelength λ_1 excites a molecule that undergoes internal conversion. The ground-state vibrationally hot molecule is allowed to collide with a bath molecule M and cascade down the energy ladder. After a time interval Δt, a two-color two-photon process is initiated. Molecules that arrived at energy level w (called window) are excited precisely to the ground rovibronic level of S_1 by a photon of wavelength λ_2 and then ionized by a second color, λ_3. Molecules that passed w down the ladder will not be excited, and molecules that have not yet arrived at w

will be excited by λ_2 to high rovibronic levels of S_1 and internally convert to the ground state. The success of the method depends on the rapid turn off of internal conversion at the zero-point level of S_1. In this way, by measuring Δt and the ionization current, a temporal profile can be established from which information on $\langle \Delta E \rangle_{all}$ and its dependence on E can be obtained by comparing the experimental results to ones calculated with various models of the dependence of $\langle \Delta E \rangle_{all}$ on E. It was found that $\langle \Delta E \rangle_{all}$ depends on E^a where $a > 1$ for very low energies and $a = 1$ at moderate energies and it levels off for $E > 42.9$ kcal/mol with $a \approx 0$.

The MPI results were obtained for excited toluene and methylcycloheptatriene. An additional feature was observed in the intensity–time profiles, which was assigned to suprastrong collisions. This feature was observed only when the bath molecules were cycloheptatriene and was absent when Ar was used as a bath molecule supporting this interpretation. These findings are in agreement with classical trajectory calculations for smaller molecules.[35,36]

The results were interpreted by assuming a biexponential transition probability

$$P(E',E) = a_1 e^{-(E-E')/a} + a_2 e^{-(E-E')/b} \qquad (6\text{-}8)$$

The first term represents the "normal" exponential decay model and the second the contribution of the supracollisions. a_1 and a_2 are the weighing factors that take care of the proportional contribution of the two type of collisions. It should be pointed out that the biexponential function is a mathematical construct representing an unknown probability distribution function with a long large ΔE tail. The MPI method enables the direct observation of the dependence on E not only of $\langle \Delta E \rangle_{all}$ but also $\langle \Delta E^2 \rangle_{all}$, giving directly the width of the distribution.

B. Energy Transfer from Molecules Excited by Infrared Multiphoton Excitation (IRMPE)

In this technique a CO_2 laser is used to multiphoton pump a molecule to a high internal energy level in the ground electronic state. The technique is applicable to many molecules containing C–F bonds. The interpretation of energy transfer and kinetic results requires complicated and careful analysis of the experimental data. Pulse line shapes, temporal and spatial evolution of the temperature profile during the pulse, laser power and fluence, and reaction rate coefficients must all be known in order to model the population energy distribution and the rate of energy transfer. IRMPE as an excitation source was used with various detection methods, UVA[99] and IRF[80] discussed before and TROA,[106] TDTL,[110] and HgT[111] discussed below.

1. Ultraviolet Absorption (IRMPE-UVA)

CF_3I, an intermediate-size molecule, was excited by infrared multiphoton excitation and the UVA recorded as a function of pressure of bath gases.[99] It is found that for large bath molecules $\langle \Delta E \rangle_{all}$ is proportional to $\langle E \rangle$ while for Ar, an inert collider, the dependence of $\langle \Delta E \rangle_{all}$ is $\langle E \rangle^a$ where $a > 1$ at lower energies and approaches unity at higher energies. At high energies of 42.9–57.2 kcal/mol the values of $\langle \Delta E \rangle_{all}$ approach limiting values of 0.20 kcal/mol for argon, 0.91 kcal/mol for propane, and 2.5 kcal/mol for octane.

2. Infrared Fluorescence (IRMPE-IRF)

CHF_2CH_2F was investigated by Barker et al.[80a] using IRF as the detection method. The molecule was irradiated at various laser fluences and argon pressures and the evolution of the energy content of the molecule studies.[80b,c] The experimental results were interpreted by a master equation simulation that included the absorption, emission, and deactivation processes. For the exponential transition probability model it was found that $\langle \Delta E \rangle_d$ (cm^{-1}) = (200 ± 20) + (0.005 ± 0.002)E, where E is the internal energy of the molecule. No temperature dependence of $\langle \Delta E \rangle_d$ was observed in the range 400–1000 K.

3. Pressure and Density Detection

Two analytical techniques that rely on the change of pressure or density are time-resolved optoacoustics (TROA) and time-dependent thermal lensing (TDTL). A pulsed source prepares a molecule in highly excited vibrational states in the ground electronic state. During relaxation, the vibrational energy is redistributed among the vibrational, translational, and rotational degrees of freedom. The increase in temperature produces a pressure wave that propagates to regions of lower pressure; accompanying the pressure wave is a change in the local density. These density and pressure changes are determined by solving the appropriate continuity, energy, and momentum conservation equations; various approximations can be made depending on the relative importance of energy transfer, diffusion, viscosity, and thermal conductivity. Barker[103a] and Jacobs[103b] have presented a unified theory that includes energy transfer, thermal conductivity, diffusion, and acoustic effects; for a detailed and comprehensive discussion of TDTL and TROA experiments and theory see a recent review by Barker.[104]

3.1. Time-Resolved Optoacoustics. The theory for time-resolved optoacoustic measurements was developed by Bailey et al.[105] and the experimental technique implemented by Gordon et al.[106] It is based on the formation of the initial acoustic wave, which is produced when the internal energy is released to the translational modes. This is to be contrasted to the resonance optoacoustic method in which the pressure wave is modulated by natural frequencies of the cell in a steady-state system.[107]

The vibrationally excited species is formed by a pulsed laser with a preparation time t_p, substantially shorter than the V–T relaxation process. The excitation laser (beam diameter 0.5 cm) propagates along the axis of a cylindrical cell (30 cm in length with a diameter of 30 cm) while the acoustic transducer, a fast-responding microphone, is placed halfway between the center and the inner wall of the cell and halfway between the ends.

The acoustic wave propagates in the radial direction with a velocity related to the temperature of the bath gas and is comprised of condensation (compression) and rarefraction (expansion) components; the amplitudes of these components are I_+ and I_-, respectively. A dimensionless quantity ϵ is defined as

$$\epsilon = t_s/t_r = r/ct_r \qquad (6\text{-}9)$$

where t_s is the time for the acoustic wave to propagate the radius of the excitation volume ($=r/c$, where c is the

velocity of the acoustic wave and r is the radius of the initially excited volume) and t_r, the relaxation time for V–T transfer, is found to be a universal function of I_-/I_+ for a given excitation intensity profile. Either single or multiphoton excitation sources can be used. The latter suffers from the fact that although the average internal energy per molecule in the irradiated volume is known, the internal energy distribution is not. Analysis for multiphoton excitation sources is somewhat simplified if a square-wave (top hat) intensity profile is used; i.e., a uniform distribution of energy is present in the radial direction.

The shape of the acoustic wave can be calculated by solving the gas dynamic equations for mass, energy, and momentum transfer.[103] For the case that the temperature, pressure, or density change is less than 10%, these coupled nonlinear equations can be linearized and solved by the Fourier transform or Green's function or Bessel function expansion approach.[103]

Gordon et al.[108] have shown that if the energy relaxation follows the phenomenological equation

$$dE(t)/dt = -kE^n \qquad (6\text{-}10)$$

then the lifetime t_r (determined from E given above) is given by

$$t_r = E_0^{1-n}/k \qquad (6\text{-}11)$$

where E_0 is the initial excitation energy and k is defined by eq 6-10. Thus, from the dependence of t_r on excitation energy n can be determined.

The technique has been established[108b] for SF_6, COS, and C_6F_5H. The advantage of this technique is that a calibration curve is not necessary; the sonic velocity and excitation radius are determined from the width of the acoustic wave; the time it takes for the wave to reach the microphone and the distance the microphone is from the excited volume.

Gordon et al.[106] have reported that for SF_6 (formed by multiphoton excitation with $\langle E \rangle$ in the range from 11.4 to 54.3 kcal/mol) + Ar that $\langle \Delta E \rangle_{all}/\langle E \rangle$ is 4.1×10^{-4}; a factor of 5 smaller than what is observed for SiF_4 and a factor of 10 smaller than what is observed for azulene + Ar. Thus, at 54.3 kcal/mol $\langle \Delta E \rangle_{all}$ is 0.024 kcal/mol, a surprisingly small value.

More recently Braun et al.[109] have presented a technique for analyzing TROA data so that the derived information is obtained from the full acoustic wave not from just I_- and I_+. In this technique the observed time-dependent acoustic signal is deconvoluted from the observed signal to directly give the relaxation function; typically an exponential decay is found. The relaxation function can then be fitted to obtain the rate law and coefficient. The requirements on laser beam profile are less restrictive with use of this analysis than is required when the I_-/I_+ ratio is used.

3.2. Time-Dependent Thermal Lensing. For this type of experiment, use is made of the fact that a material exhibiting a density gradient will behave as an optical lens when light is transmitted through it. In the case of a Gaussian excitation source the central section of the excitation volume will contain a larger amount of energy per unit volume than peripheral sections. Thus, during the energy relaxation, the gas density at the center will be less and a diverging lens is formed; i.e., the beam of a probe laser coaxial with the excitation laser will diverge. If a pinhole, smaller than the diameter of the probe laser, is mounted in front of a detector, then a decrease in intensity will be observed; the opposite effect will be observed if cooling takes place in the central section. It is extremely important that the intensity profile of the excitation beam is known and constant during the experiment and the optical train is stable with minimal diffraction effects.

For relaxation processes with high efficiency, low pressures must be used so the relaxation is comparable to the acoustic transit time. For these low-pressure conditions, diffusion and thermal conductivity become important and the full unified theory must be used. The Barker group[110] has studied the deactivation of highly excited azulene (87 mTorr excited with 600-nm photons) in krypton (1.00 Torr) at 370 K; the observed relaxation time was $\sim 10^{-5}$ s, which is comparable to that observed by following the decay of the azulene energy by IRF. Even though the krypton is in excess, it was concluded that azulene–azulene collisional energy transfer plays an important role in the relaxation, probably via V–V transfer. Thus, $\langle \Delta E \rangle_d$ values for krypton cannot be obtained until this relative contribution to the relaxation can be quantitatively assessed.

4. Mercury Tracer (HgT)

Braun et al.[111] have developed a real-time technique for measuring V–T transfer. A mixture of substrate, deactivator, and a small amount of mercury vapor is prepared. The substrate, which is excited by a pulsed laser (single or multiphoton absorption with $\langle E \rangle < 18.3$ kcal/mol), then undergoes vibrational relaxation via collisions with the deactivator. The localized translational temperature of the bath and the Hg in it will increase. The temperature increase is probed by observing the change in the absorption of Hg at 254 nm where Lorentz and Doppler broadening affect the absorption coefficient. A calibration curve is obtained by monitoring the absorption as a function of temperature in a thermostated cell. Since the absorption also depends on the density of Hg, it is imperative that the Hg concentration remains constant and is known. Approximately 5 μs after an initiating pulse, an acoustic wave propagates in the radial direction so that the Hg concentration changes; thus, to minimize correction terms, it is important to restrict data to this time region. The acoustic wave can be greatly reduced by irradiating the total volume of the cell. These secondary waves can appear in IRF and UVA experiments.

The relaxation time is determined from the intensity profile as is the final equilibrium temperature. The average excitation energy is calculated from the temperature change; $\langle \Delta E \rangle_{all}$ is computed from the observed time constant and the Lennard-Jones collision number. The technique has been benchmarked with SF_6; the relaxation times are consistent with those obtained by TROA.[112] For nonmonatomic deactivators V–V and V–R processes must also be considered. For C_6F_5H self-deactivation, $\langle \Delta E \rangle_{all}/\langle E \rangle$ was determined[111] to be 0.0133, independent of $\langle E \rangle$ fom 0.54 to 18.4 kcal/mol.

More recently Braun et al.[113] have followed both V–V and V–T processes by merging the HgT and UVA techniques. In the "barebones" prototype system, vibrationally excited SF_6 (formed by MPE) transfers its energy to the deactivator (an aromatic hydrocarbon that

absorbs UV radiation). The takeup of vibrational energy from SF_6 by translation is probed by Hg absorption at 254 nm while the increase in vibrational energy of the deactivator is probed by its absorption coefficient.

Braun et al.[114] have also studied the coupling of the vibration, rotation, and translation modes of substrate and deactivator. The coupling was determined by measuring the time constant for V to T relaxation as a function of dilution for a mixture of C_6F_5H and argon (using multiphoton excitation with $\langle E \rangle$ in the 1.57–15.7 kcal/mol range); $\langle \Delta E \rangle_{all}/\langle E \rangle$ was ~0.0125, also in agreement with other studies.[112] If an equilibrium between the translation and rotation modes is established, then the observed rate coefficient would obey the linear relation $k_{obs} = X(\text{deactivator})k(\text{deactivator}) + X(\text{substrate})k(\text{substrate})$, where k is the second-order rate coefficient and X is the mole fraction. The experiments exhibit a nonlinearity in a plot of k_{obs} vs mole fraction. This is interpreted by Braun et al.[114] as if there is a near-equilibrium between the vibrational and rotational modes and that the transfer between translation and rotation or vibration is slow. This bottleneck interpretation calls for further substantiation by other experimental methods.

C. Collisional Activation in Equilibrium Systems

The oldest method and the one that provided the earlier data and the bulk of the kinetic information is collisional activation. At a given temperature the molecule possesses a given average internal and translational energy. A molecule can be excited above a threshold energy by a collision with another molecule. This collisional process is operative in all gas–gas and gas–surface systems. The basic processes manifest themselves in the master equation description discussed at length in previous sections. In later text we discuss recent applications of this excitation method.

1. Thermal Unimolecular Reactions

Studies of thermal unimolecular reactions have provided the early bulk of the input to the energy-transfer database. Comprehensive reviews[1,2] were published in 1977, and only a brief and general discussion will be presented here together with later work. For these systems the preparation and exposure time is the duration of the experiment, while the analysis involves detection of the total yield of reaction products. As discussed in the Introduction the main requirement is to monitor the reaction in the second order (ideally) or falloff region where collisional energy transfer is decoupled from the intramolecular energy transfer. It is the rate-limiting step. Thus, for a meaningful thermal experiment the chemistry must be clean, the kinetics well determined, and the collision cross section known.

Only a few systems have met the above requirements, the isomerization of methyl isocyanide[1] being one of them. Techniques to probe the population distribution, which provides details on the transition probabilities, have been used: dilution studies in the falloff and second-order region.[63] These studies have verified that each collision removes a small amount of energy and that large amounts of energy are not removed with a small collision cross section.

It was suggested by Chow and Wilson[115] in the early 1960s that observation of multichannel unimolecular reaction would provide more details of the population distribution. This was successfully achieved for chemical activation systems somewhat later.[116] But it was not until the early 1980s that Rabinovitch and coworkers[117] were able to obtain reliable energy-transfer data on multichannel thermal systems. The idea behind these studies is that the product yield from a particular reaction channel directly probes the population above the critical threshold for that reaction; in theory, by having a large number of reactions with various threshold energies the population distribution would be determined. In some multichannel systems relative comparison is made such that the demands on the specific details such as collision cross section, model for k(E), and the thermochemistry are not as restricted.[117]

The cancellations occurring by studying competitive processes are best illustrated in the following way. As shown in the Introduction, the rate coefficient for a thermal unimolecular reaction is given by

$$k_\infty = \int_{E_0}^{\infty} \frac{B(E)\ k(E)\ \omega\ dE}{\omega + k(E)} \tag{6-12}$$

where ω is the collision frequency, which is related to the experimental pressure by

$$\omega = \pi\sigma^2 \left[\frac{8kT}{\pi\mu}\right]^{0.5} \frac{PN_{Av}}{RT} \tag{6-13}$$

$\sigma^2 = \Omega^{(2,2)}d^2$, where $\Omega^{(2,2)}$ is the collision integral,[53a] d is the hard-sphere radius, $B(E)$ is the normalized Boltzmann population distribution function, and N_{Av} is Avogadro's number. In the limit as $\omega \to 0$

$$k_0 = \omega \int_{E_0}^{\infty} B(E)\ dE \propto \sigma^2 P \tag{6-14}$$

Thus, as expected, the observed rate constant at low pressure is linear with pressure with a proportionality constant related to the collision cross section. For a multichannel reaction eq 6-12 becomes

$$k_\omega{}^i = \int_{E_0{}^i}^{\infty} B(E) \frac{k^i(E)\ \omega\ dE}{\omega + k(E)} \tag{6-15}$$

The ratio of rate coefficients for two channels, m and n, is

$$\frac{k_\omega{}^m}{k_\omega{}^n} = \frac{\int_{E_0{}^m}^{\infty} B(E) \dfrac{k^m(E)\ dE}{\omega + k(E)}}{\int_{E_0{}^n}^{\infty} B(E) \dfrac{k^n(E)\ dE}{\omega + k(E)}} \tag{6-16}$$

To be noted is the cancellation of ω in the numerator of the integrands; also, the error in the rate coefficient ratio produced by an incorrect cross section appearing in the denominator of the integrands is greatly reduced due to compensating effects in the ratio. In the low-pressure limit, eq 6-16 reduces to

$$\frac{k_0{}^m}{k_0{}^n} = \frac{\int_{E_0{}^m}^{\infty} B(E) \dfrac{k^m(E)}{k(E)}\ dE}{\int_{E_0{}^n}^{\infty} B(E) \dfrac{k^n(E)}{k(E)}\ dE} \tag{6-17}$$

In this case the lower limit of integration depends on the threshold energy for the designated reaction chan-

nel. It is now evident that this limiting ratio does not depend on pressure or the collision cross section. The high-pressure limit for single and multichannel reactions k_ω is insensitive to pressure. In the falloff pressure range k_ω is a complex function of pressure, going from a P^0 to a P^1 dependence as the pressure is lowered. The ratio $k_\omega{}^m/k_\omega{}^n$ is independent of pressure for both limiting regimes.

For weak colliders, as discussed in the Introduction, the appropriate master equation must be solved for the steady-state populations, $A^{ss}(E)$; for $E > E_0$ these populations are linearly dependent on pressure in the low-pressure limit and independent of pressure in the high-pressure limit. The rate coefficients and ratio are

$$k_\omega = \frac{\int_{E_0}^{\infty} k(E)\ [A^{ss}(E)]\ dE}{\int_0^{\infty} [A^{ss}(E)]\ dE} \qquad (6\text{-}18)$$

$$\frac{k_\omega{}^m}{k_\omega{}^n} = \frac{\int_{E_0{}^m}^{\infty} k^m(E)\ [A^{ss}(E)]\ dE}{\int_{E_0{}^n}^{\infty} k^n(E)\ [A^{ss}(E)]\ dE} \qquad (6\text{-}19)$$

As for the strong-collider case, this ratio is relatively insensitive to minor changes in the cross section. Thus, in the high-pressure limit no information is obtained about energy transfer. However, both k_ω and $k_\omega{}^m/k_\omega{}^n$ provide energy-transfer information as the pressure is reduced; the optimum pressure is that for the second-order region. It is important that for weak-collider modeling a properly weighted probability (**P**) matrix is used[1] as there are nonlinear dilution effects even though a linear combination of weak and strong colliders is used. The primary example of a multichannel reaction (three channels) is the isomerization of isotopically substituted cyclopropane-*1*-t_1,*2*,*2*-d_2[72,118] with helium, krypton, and carbon dioxide as deactivators. The different thresholds are provided by the primary isotope effect for T, D, and H atom transfer. There are eight distinct structural isomers of propene produced; however, some of these are combined so that only three paths are used:

(a) H migration

$CH_3CT{=}CD_2$ $CD_2HCT{=}CH_2$

$CH_2TCH{=}CD_2$ $CD_2HCH{=}CHT$

(b) D migration

$CH_2DCD{=}CHT$ $CHDTCD{=}CH_2$

(c) T migration

$CH_2TCH{=}CD_2$ $CD_2TCH{=}CH_2$

For this system the reaction is clean, the thermochemistry is established, and the second-order region is approached ($k/k_\infty = 0.01$). Questions relating to the dependence of $\langle\Delta E\rangle_d$ and the collision efficiency β on temperature and energy have been addressed. They[72] observe that $\langle\Delta E\rangle_d$ for He depends on $T^{-1.3}$ in the 823–1123 K region; i.e., the step size decreases with temperature from 0.92 to 0.60 kcal/mol. This is an outcome of the fact that the transition modes energy is $2RT$ and the average energy of cyclopropane in excess of E_0 is only RT. If the total energy $E_0 + 3RT$ is now divided on a purely statistical basis, then $\langle\Delta E\rangle_{all} = (E_0 + RT) - n_R(E_0 + 3RT)/(n_R + 3)$ and $\langle\Delta E\rangle$ will decrease with temperature (n_R is the number of modes of the reactant). This temperature dependence is consistent with an attractive interaction and/or a quasi-accommodation (long-lived complex) model for energy transfer; see discussion on statistical models for energy transfer. At higher temperatures the onset of a leveling off in $\langle\Delta E\rangle_d$ was observed. The expected temperature dependence of β, which depends on the function $(\langle\Delta E\rangle_d/\langle E^+\rangle)^2$, is $T^{-5.6}$ since $\langle E^+\rangle$ (the average energy of molecules in excess of the critical energy) is linear with T and $\langle\Delta E\rangle_d$ depends on $T^{-1.8}$. This calculated dependence of β was also observed experimentally.[118] This strong temperature dependence of β illustrates the problems with extrapolating low-temperature unimolecular reaction data to high temperatures for weak colliders if the exact exponent for T is not known.

2. Shock Tube Experiments

Shock tube studies of unimolecular reactions can provide energy-transfer information at high temperatures.[119–121] Details of the preparation step (a rapid increase in the vibrational energy of the substrate via T–V transfer) in terms of energy transfer are not known, although it is assumed that the population distribution retains an equilibrium distribution corresponding to the final temperature up to a level where depletion effects due to reaction are important. Observations are made either in real time by optical absorption or emission spectroscopy or laser schlieren techniques or by measuring distribution of product yields at the end of a run. Chemical complexities, such as change in mechanism and secondary reactions, become important so the observations must contain enough specificity to unravel the energy-transfer steps. Due to the high pressure required for these studies, the reaction for reasonably complex polyatomic molecules is often not in the second-order region so the sensitivity of the results to energy-transfer parameters is decreased.

Kiefer and Shah[122] (KS) have studied the decomposition of cyclohexene using the laser schlieren technique in the 1200–2000 K region with krypton as the heat bath. Their interpretation was that $\langle\Delta E\rangle_{all}$ was constant and equal to −0.21 kcal/mol over this temperature range; this requires that $\langle\Delta E\rangle_d$ increases from 1.6 to 4.6 kcal/mol. KS suggested that this increase was due to an increase of the average energy with temperature. However Tardy and Rabinovitch[123] showed that the average energy of reacting molecules increases only moderately (~18 kcal/mol compared to the average energy of all molecules which increases by ~56 kcal/mol) since the increase predicted by KS is offset by the decrease in energy caused by the increase of reaction order with increasing temperature; i.e., at a given pressure the reaction approaches the second-order region with increasing temperature. TR also showed that when the correct relation for $\langle\Delta E\rangle_{all}$ and $\langle\Delta E\rangle_d$, which exhibits a dependence on average energy, is used, $\langle\Delta E\rangle_d$ increases to 2.3 kcal/mol. However, it now appears that KS conclusions were due to the use of an inadequate high-temperature relationship between $\langle\Delta E\rangle_{all}$ and $\langle\Delta E\rangle_d$ and equations that have numerical problems at high temperatures. The experimental data are best fit

with $\langle \Delta E \rangle_d$ constant and equal to ~1.6 kcal/mol; this is in agreement with master equations calculations performed by Tardy[124] and Shi and Barker.[125] The weak- and strong-collider calculations[123-125] support the proposition that simple predictive formulations for unimolecular reactions (eqs 3-10, 3-11, 3-12, 3-18, 4-1, 4-2, and 4-9) should be used cautiously when used at high temperatures for moderately large reagents. At this time a master equation solution is suggested; a self-contained computer program written by Gilbert and Smith[126,127] is readily available.

The preparation time of the high-temperature molecules involves knowledge of the transition probabilities for both low levels of excitation (small steps with low probability) and higher levels (larger steps with high probability); a bottleneck limiting the transport of energy can be present at some intermediate energy. A simple transition probability model was used by Malins and Tardy[77] to calculate the induction time for the excitation of cyclopropane; the time was linear with pressure, increasing with final temperature and a weak function of $\langle \Delta E \rangle_d$. Recently, master equation calculations using Monte Carlo methods performed by Barker et al.[125] for the thermal decomposition of cyclohexene indicate an induction time that is comparable to that measured by KS; their calculations also show a dependence of the induction time on $\langle \Delta E \rangle_d$.

The energy-transfer mechanism affects the interpretation of shock tube results. At high temperatures the measured rate coefficient may be in the pressure falloff region where the reaction order is not known. Therefore, the A factors and activation energies reported are not the high-pressure values. The degree of falloff depends on the efficiency of the collider, i.e., on $\langle \Delta E \rangle_d$. This problem has always complicated the interpretation of shock tube experiments.

3. Very Low Pressure Pyrolysis (VLPP)

VLPP was developed in the early 1970s primarily to obtain thermokinetic information;[128] in its simplified form, molecules enter a thermostated reaction vessel and have a mean residence time determined by the size of an exit orifice (a steady state is established). The vibrational energy of the reagent is increased via collisions with the walls of the reactor; gas–gas collisions are unimportant. Another method of studying energy transfer at the walls is by using the variable-encounter method (VEM) developed by Rabinovitch and coworkers[129-133] and discussed later. Gilbert, King, and others[134] (GK), in a complex combination of modeling and experiments, have developed the pressure-dependent VLPP technique to obtain intermolecular energy-transfer information by comparing gas–wall and gas–gas collisions. The highest pressure is limited by the mean free path being less than the dimension of the exit orifice. At the very low pressure the reagent only undergoes gas–wall collisions; the rate constant is determined from the wall efficiency, the fraction of the reactants reacted, and the residence time. Reagents with known rate coefficients have been used to determine the gas–wall collision efficiency.

Two very difficult problems to contend with are knowing the degree of falloff for the specific experimental conditions and the gas–wall collision efficiency. This is analogous to a dilution study (a mixture of two different colliders) in a homogeneous system where the falloff, degree of dilution, collision cross sections, and $\langle \Delta E \rangle_d$ for each collider must be known; in homogeneous studies at least three of these quantities are generally known from independent measurements. In VLPP studies, the degree of falloff is often estimated from RRKM calculations and the absolute gas–wall collision efficiency is difficult to determine.

In addition to the above-mentioned problems the possibility of heterogeneous reactions must be considered along with knowledge of the diffusion coefficient due to the spatial inhomogeneity. However, some of these problems are reduced by studying multichannel systems. Nonetheless, one of the primary sources of potential errors in the method is that the effect of added gas, i.e., to monitor the effect of gas–gas collisions, is small relative to gas–wall activation; if the extent of falloff is not exactly known, then different behaviors will be observed. Additionally, extensive modeling must be used, which requires solution of the integrodifferential reaction–diffusion master equation where both energy and spatial dependencies are required and the gas–wall collision efficiency must be known. In spite of these difficulties in determining a homogeneous event in a background of heterogeneous events, this method has attempted to answer some of the important questions pertaining to homogeneous energy transfer.

GK findings[135] indicate that the efficiency for gas–wall collisions in the two-channel thermal decomposition of bromoethane decreases with an increase in temperature (1000–1200 K) while that for $\langle \Delta E \rangle_d$ for gas–gas collisions remains constant, within experimental error, over the same range. They found evidence that $P(E',E)$ for $E' < E$ falls off faster than for an exponential model. The decomposition of chloro- and bromoethanes, which have similar dipole moments and thermochemistry with bromoethane having a higher density of states, indicates that $\langle \Delta E \rangle_d$ for chloroethane is 1.6 kcal/mol compared to 0.7 kcal/mol for bromoethane; this is supportive of a statistical model in which more energy will be removed from the molecule with the lowest density of states. A similar result was obtained when deuterated and undeuterated isopropyl bromide[136] and *tert*-butyl chloride[137] systems were compared. In this case the deuterated species has the higher density of states and the lower $\langle \Delta E \rangle_d$. Ethylene-$d_0$ and -d_4 were also used as deactivators; the deuterated ethylene removes less energy than the undeuterated ethylene when the reagent is undeuterated isopropyl bromide while for the deuterated reagent the effect is reversed. There is no theory that accounts for these observations; in fact, isotope effects for energy transfer have not been observed in other systems.[1]

The possibility of a resonance-enhanced energy transfer has been presented by the GK groups.[138] In this case, the reactions studied were the competitive decompositions of 1,1,2,2-tetrafluorocyclobutane (TFCB) and 1-chloro-2,2,3,3-tetrafluorocyclobutane (CTFCB); the latter molecule has a ring deformation mode at 738 cm^{-1} while the comparable mode for TFCB is 667 cm^{-1}. It is observed that CO_2 removes 4.98 kcal/mol from TFCB and 1.20 kcal/mol from CTFCB; similarly, C_2H_4 removes 2.75 and 2.63 kcal/mol from TFCB and CTFCB, respectively. The comparable results for C_2H_4 indicate an internal consistency in the experimental

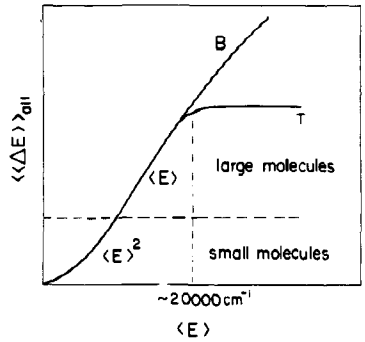

Figure 23. $(\langle\Delta E\rangle)_{all}$ as a function of average internal energy. B indicates Barker et al. T indicates Troe et al. See text for details.

results; the large difference observed for CO_2 in these two systems is associated with the resonance between the 667 cm^{-1} (bending mode) of CO_2 and the ring deformation of TFCB. It was suggested that further enhancement may be due to the Fermi resonance in the CO_2 so that ladder climbing will be enhanced by overtones of 667 cm^{-1}.

4. Supracollisions in Jets

A collision-induced dissociation of 1,4-cyclohexadiene (CHD) by vibrationally hot 1,3,5-trimethyl-1,1,3,5,5-pentaphenyltrisiloxane (TTP) was studied in a jet by Pashutski and Oref.[43] TTP ($C_{33}H_{34}O_2Si_3$) was heated in a lower oven to temperatures of 468–498 K, setting the vapor pressure of TTP to 20–190 mTorr. The temperature, and thus the internal energy, was determined by the upper oven in the range 603–831 K. The hot gas of TTP molecules was allowed to collide with 1,4-cyclohexadiene, which has a threshold energy for dissociation of 42.5 kcal/mol. CHD molecules that acquired energy >42.5 kcal/mol decomposed to benzene and H_2. These were detected by a quadrupole mass spectrometer. The basic principle of the experiment is similar to the internal conversion experiments of Oref and Steel[41,42] discussed before. The TTP is a large molecule with 210 degrees of freedom, and at the temperatures of the jet the average internal energy ranges between 72 kcal/mol at 603 K to 132 kcal/mol at 831 K. A collision of CHD with this hot large "wall"-like molecule has a finite chance of transferring ΔE larger than ~43 kcal/mol. It was found that $P(\Delta E = 45) \approx 5 \times 10^{-7}$. That is to say, one fruitful collision in 2×10^6 collisions. The average energy transferred per down collision from the exponential model is a = 3.2 kcal/mol, and the theoretical probability for $\Delta E > 45$ kcal/mol is $P(\Delta E) = \exp(-45/3.2)/3.2 = 2.4 \times 10^{-7}$. The value of a agrees with conventional wisdom that $0.1 < a < 10$ kcal/mol for such systems. That is to say, even though the average energy transferred per down collision is small, there is a finite probability of suprastrong collisions.

D. Chemical and Photochemical Activation (CA)

When a new substrate entity is formed by a chemical reaction, the method is classified as a chemical activation technique; another common technique is photochemical excitation in which the substrate is converted to a new entity; several examples of the latter have been described earlier and a few other interesting cases are considered here. Both techniques were extensively re-

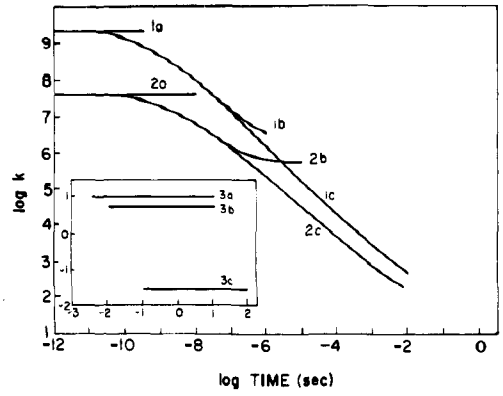

Figure 24. log k vs log reaction time. Ten normal modes in substrate and bath, E_0 = 30 kcal/mol. (1) T = 2500 K: (a) 10^7 Torr, (b) 1 Torr, (c) 10^{-4} Torr. (2) T = 1500 K: (a) 10^7 Torr, (b) 1 Torr, (c) 10^{-4} Torr. (3) T = 600 K: (a) 10^4 Torr, (b) 1 Torr, (c) 10^{-4} Torr.

viewed earlier by Tardy and Rabinovitch[1] and Quack and Troe.[2] The experiments consist of forming an excited substrate with a known excitation distribution function that can undergo a unimolecular reaction. Ideally, the distribution would be monoenergetic; however, in practice it is the convolution of the ambient thermal population distribution of the precursors with the process that performs the activation (the bandwidth of the excitation source and the associated Franck–Condon factors or the formation rate coefficients). At each energy level there is a competition between collision (energy transfer) and reaction; due mainly to the energy dependence of the unimolecular process, this competition is also energy dependent. On completion of the energy cascade and reaction the observed products result from reaction (D) or stabilization (S); experiments support the idea that weak colliders involve small $\langle\Delta E\rangle_d$ for each collision. Most of these experiments are of the steady-state variety in which total and relative product yields are measured as a function of pressure and/or excitation energy and/or temperature.

The benefits of competitive studies in external activation systems are easily seen by considering the equations for a strong collider that relate the apparent rate coefficient k_ω with the experimental observations (namely S and D)

$$k_\omega^i = \omega\frac{[D]}{[S]} = \omega\frac{\int_{E_0}^{\infty} f(E)\,\dfrac{k^i(E)\,dE}{\omega + k(E)}}{\int_{E_0}^{\infty} f(E)\,\dfrac{\omega\,dE}{\omega + k(E)}} \qquad (6\text{-}20)$$

where $k(E)$ is the sum over $k^i(E)$, E_0 is the lowest critical threshold, and $f(E)$ is the normalized population of reagents formed by the activation process. In this case k_ω takes on two limiting pressure values

$$k_0 = \frac{\int_{E_0}^{\infty} f(E)\,dE}{\int_{E_0}^{\infty} \dfrac{f(E)\,dE}{k(E)}} = \frac{1}{\left\langle \dfrac{1}{k(E)} \right\rangle_f} \qquad (6\text{-}21)$$

$$k_\infty = \frac{\int_{E_0}^{\infty} k(E)\,f(E)\,dE}{\int_{E_0}^{\infty} f(E)\,dE} = \langle k(E)\rangle_f \qquad (6\text{-}22)$$

TABLE III. Compilation of Energy-Transfer Experiments

	excitation[a]	detection[b]	excited molecule	bath molecule	$\langle\Delta E\rangle_d$ dependence on energy $\langle\Delta E\rangle = E^n$ and energies, cm^{-1}	$\langle\Delta E\rangle_d$ dependence on temp (T^{γ})	ref
1	IC	IRF	azulene	azulene, He, Ne, Ar, Kr, Xe, H_2, D_2, N_2, O_2, CO, CO_2, H_2O, NH_3, CH_4, C_4H_{10}, SF_6	n = 1; 17 500, 30 600	γ = 0.6	82
2	IC	IRF	azulene	CO_2, IR emission	17 500, 30 600		56
3	IC	IR abs	azulene, azulene-D_8	CO_2	30 600, 31 500, 41 000		85
4	IC	UVA	azulene	He, Ne, Ar, Kr, Xe, H_2, CO, N_2, CO_2, H_2O, NH_3, SF_6, CH_3OH, CH_4, C_3H_8, C_4H_{10}, C_5H_{12}, C_8H_{18}, $C_{10}H_{22}$, CF_4, C_2F_6, C_3F_8, C_7F_{16}	17 500, 30 600	$\gamma \approx 0.6$	84, 57
5	IC	UVA	toluene (by IC of CHT)	He, Ar, Kr, Xe, N_2, CO, CO_2, N_2O, SF_6, CH_4, C_3H_8, C_6H_{14}, C_7H_{16}, C_8H_{18}, CF_4, C_3F_8, C_7F_{16}, C_7H_8	52 000, 40 000	γ = 0.3	86b, 87
6	IC	UVA	benzene	Ar, N_2, O_2, C_3H_8, benzene, C_5H_{12}	n = 1; 53 000		100
7	IC	UVA	hexafluorobenzene	Ar, O_2, N_2, C_6F_6	n = 0, 1; 53 400		101, 102
8	IRMPE	UVA	CF_3I	Ar, C_3H_8, C_8H_{18}	$n \approx {}^3/_2$–1; 15 000–20 000		99
9	IRMPE	IRF	F_2HCCH_2F	Ar	n = 1; 1000–27 000	indep 400–1000 K	80a
10	IC	thermal sensitizn	azulene	quadricyclane	30 600		41
11	IC	thermal sensitizn	hexafluorobenzene	cyclobutene	38 600		42
12	thermal	jet	TTP	cyclohexadiene	25 300–46 300		43
13	IC	MPI	toluene	CHT, Ar, MeCHT, heptane	52 000		44
14	IC	MPI	xylene	CHT, Ar, MeCHT, heptane	52 000		45
15	IRMPE	TROA	SF_6	Ar	1000		106a
16	IRMPE	TROA	ethyl acetate	Ar	1000		106a
17	IC	TROA	azulene	Ar	1000		106a
18	IRMPE	TROA	SF_6	Ar	n = 1; 4000–19 000		106b
19	IRMPE	TROA	SF_6	Ar	4000–19 000		108
20	IRMPE	TROA	C_6F_5H	Ar	2650–14 000		108
21	IRMPE	TROA	SF_6	Ar	3000–19 000		112a
22	IRMPE	HgT	SF_6	Ar	550–5500		112a
23	IRMPE	HgT	C_6F_5H	Ar	n = 1; 550–5500		112a
24	IRMPE	TROA	C_6F_5H	Ar	n = 1; 265–1400		112a
25	IRMPE	HgT	SF_6	SF_6	n = 1.5–1; 320–5000		112b
26	IRMPE	HgT	C_6F_5H	C_6F_5H	175–6500		111
27	IRMPE	HgT	C_6F_5H	Ar	560–5500		114
28	IC	TDTL	azulene	Kr	16 700		104
29	IRMPE	HgT + UVA	SF_6	C_6H_6, $C_6H_5CH_3$, C_6F_6, C_6H_5F	n = 1; >4000		113
30	shock tube	laser schlieren	cyclohexene	Kr	c		122, 125
31	thermal	GC	cyclopropane-t,d_2	He	c	γ = 1.8	118
32	thermal	GC	cyclopropane-t,d_2	Kr, CO_2	c	γ = 5.6	72
33	photo	GC	$H_2C{=}CH_2$	He, CF_4, CO_2, C_2H_5Br	28 000		150
34	CA	GC	cyclohexadiene	SF_6, CO_2, N_2, He	26 000		147
35	CA	GC	cyclobutane-t	He, Ne, Ar, Kr, Xe	42 100		151
36	photo	GC	EtCHT	self	35 000–43 200		144
37	CA	GC	methylcyclobutane	self	36 800		141
38	CA	GC	ethylcyclobutane	self	36 800		142
39	CA	GC	methylcyclopropane	self	35 800		143
40	CA	GC	ethylcyclopropane	He, Ar, CO_2, CF_4, C_2F_6	35 800		143
41	CA	GC	tetrafluorocyclopropane	He, Ar, CO_2, CF_4, C_2F_6	30 600		146
42	photo	GC	CCl_3CH_3	self, CF_4	30 800		148
43	CA	GC	CH_3CF_3	He, Ne, Ar, Kr, Xe, H_2, O_2, N_2, CO_2, CH_4, CH_3Cl, CF_4, SF_6, C_2F_6, C_4F_8, C_6F_{14}, C_8F_{18}	35 800	very small	139
44	CA	GC	CH_2FCH_2F	He, N_2, CO_2, SF_6, CH_2ClF,	32 400		145a
45	CA	GC	CH_3CH_2F	$(CH_2F)_2CO$	31 900		145a
46	CA	GC	$H_2C{=}CHCl$	He, Ar, N_2, CO_2	30 400		149
47	VLPP	MS	H_2DCCH_2Cl	He, Ne, Kr	c	slight	134b
48	VLPP	MS	CD_3CH_2Cl	CO_2	c		134c
49	VLPP	MS	HCD_2CD_2Br	Ne, CO_2, C_2H_4, C_6H_6	c		135
50	VLPP	MS	CH_3CO_2Et	He, Ar, Ne, Kr, C_2H_4	c		134d
51	VLPP	MS	$CH_3CHBrCH_3$	Ne, Xe, C_2H_4, C_2D_4	c		136
52	VLPP	MS	$CD_3CDBrCD_3$	Ne, Xe, C_2H_4, C_2D_4	c		136
53	VLPP	MS	C_4H_9Cl	Kr, N_2, CO_2, C_2H_4	c		137
54	VLPP	MS	C_4D_9Cl	Kr, N_2, CO_2, C_2H_4	c		137
55	VLPP	MS	chlorocyclobutane	C_2H_4	c		134e

TABLE III (Continued)

	excitation[a]	detection[b]	excited molecule	bath molecule	$\langle\Delta E\rangle_d$ dependence on energy $\langle\Delta E\rangle = E^n$ and energies, cm^{-1}	$\langle\Delta E\rangle_d$ dependence on temp (T^{γ})	ref
56	VLPP	MS	tetrafluorocyclobutane	CO_2, C_2H_4	c		138b
57	VLPP	MS	tetrafluorochlorocyclobutane	CO_2, C_2H_4, Ne, CH_4, CF_4, CH_2CF_2	c		138a

[a] Legend for excitation method: IC, internal conversion; IRMPE, infrared multiphoton excitation; CA, chemical activation; VLPP; very low pressure pyrolysis. [b] Legend for detection method: IRF, infrared fluorescence; UVA, ultraviolet absorption; MPI, multiphoton ionization; TROA, time-resolved optoacoustic; HgT, mercury tracer; TDTL, time-dependent thermal lensing; GC, gas chromatography; MS, mass spectrometry. [c] Average energy of the thermal system at the temperature of the experiment.

where the $\langle\ \rangle_f$ expressions are averages over the $f(E)$ distribution function. The ratio of rate coefficients ($=D^m/D^n$) for strong colliders is given by

$$\frac{k_\omega{}^m}{k_\omega{}^n} = \frac{\int_{E_0{}^m}^{\infty} f(E)\,\frac{k^m(E)\,dE}{\omega + k(E)}}{\int_{E_0{}^n}^{\infty} f(E)\,\frac{k^n(E)\,dE}{\omega + k(E)}} \tag{6-23}$$

which for the limiting pressures reduce to

$$\frac{k_0{}^m}{k_0{}^n} = \frac{\int_{E_0{}^m}^{\infty} f(E)\,\frac{k^m(E)\,dE}{k(E)}}{\int_{E_0{}^n}^{\infty} f(E)\,\frac{k^n(E)\,dE}{k(E)}} \tag{6-24}$$

$$\frac{k_\infty{}^m}{k_\infty{}^n} = \frac{\int_{E_0{}^m}^{\infty} f(E)\,k^m(E)\,dE}{\int_{E_0{}^n}^{\infty} f(E)\,k^n(E)\,dE} \tag{6-25}$$

For weak colliders, the rate coefficients and ratios are calculated from the steady-state populations $[A^{SS}(E)]$ calculated from the master equation

$$k_\omega{}^i = \frac{\int_{E_0{}^i}^{\infty} k^i(E)\,[A^{SS}(E)]\,dE}{\int_0^{\infty} [A^{SS}(E)]\,dE} \tag{6-26}$$

$$\frac{k_\omega{}^m}{k_\omega{}^n} = \frac{\int_{E_0{}^m}^{\infty} k^m(E)\,[A^{SS}(E)]\,dE}{\int_{E_0{}^n}^{\infty} k^n(E)\,[A^{SS}(E)]\,dE} \tag{6-27}$$

As in the thermal activation case, the rate coefficient ratio is nearly independent of collision cross section.

In the low-pressure limit, S ≪ D, the shape of the S/D vs pressure curve is a strong function of $P(E',E)$ and the collision cross section since the small amounts of S depend on the details of the cascade; however, the ratio, D^m/D^n is insensitive to the pressure since $D^{tot} \approx 1$ (total amount of decomposition); i.e., any decomposition resulting from energy loss is negligible; and consequently the ratio is the same as that for a strong collider. In the high-pressure limit, where D ≪ S, the ratio D^m/D^n will contain information about the stabilization since the stepwise deactivation will result in an enhanced probability for reaction, i.e., an increase in D^m, while k^m will provide less information about energy transfer than if it were determined at low pressure. Thus, if the collision cross section is known, then low-pressure S/D measurements are the preferred choice while if the cross section is not known, then competitive studies from moderate to high pressure are recommended.

For presentation purposes we have divided the discussion into two sections: *simple* reactions, if the formation of excited molecules is via a single process and the energy distribution function is known, and *complex* reactions, if the energy distribution function of the excited molecule is unknown. It should be reemphasized that for these systems the chemistry and thermochemistry must be well-known. As in thermal systems, errors in multichannel studies are usually less than for single-channel systems in which the absolute cross sections and rate coefficients and their energy dependence must be adequately and independently determined. The method of analyzing the data from these experiments to obtain $\langle\Delta E\rangle_d$ is extremely important as noted by Marcoux and Setser,[139] who studied activation of CH_3CF_3; although the experimental data were comparable, Root et al.[140] assigned smaller $\langle\Delta E\rangle_d$ for CH_3CF_3 than Marcoux and Setser.[139]

1. Simple Reactions

McCluskey and Carr have studied the collisional stabilization of methylcyclobutane,[141] ethylcyclobutane,[142] and the homologous series of alkylcyclopropanes[143] (cyclopropane, methylcyclopropane, ethylcyclopropane) formed by the addition of methylene to the appropriate cyclobutane[141,142] or olefin;[143] the initial excitation energy of 100–110 kcal/mol was ~40 kcal/mol in excess of the critical energy for reaction. The S/D vs pressure plots indicated a multistep collisional deactivation; $\langle\Delta E\rangle_d$ values for a stepladder model were determined by matching the experimental data with computer simulations. The average step size for energy removal was found to decrease as the number of atoms in the substrate increases from approximately 10 kcal/mol for cyclopropane to ~3 kcal/mol for ethylcyclobutane. Their conclusion is that a quasi-statistical model for energy transfer fits the data; however, it should be pointed out that the size of the deactivator is also changing in these experiments. Studies using the same deactivator, such as an inert gas, for these chemically activated species would provide discriminating information on the validity of the statistical model. Also of interest is the similarity of the step size for the deactivation of photoactivated cycloheptatriene and ethylcyclopropane and methylcyclobutane.

TABLE IV. $\langle\Delta E\rangle_{all}$ of Azulene at Various Internal Energies

Reference 82, T = 298 K

bath molecule	$-\langle\Delta E\rangle_{all}$ at excitation energy 16700 cm^{-1} [a]	$-\langle\Delta E\rangle_{all}$ at excitation energy 29700 cm^{-1} [b]
azulene	783 ± 18	1262 ± 28
He	33 ± 4	73 ± 10
Ne	68 ± 5	130 ± 22
Ar	108 ± 7	190 ± 5
Kr	117 ± 8	171 ± 8
Xe	93 ± 6	187 ± 12
H_2	124 ± 21	175 ± 9
D_2	101 ± 11	136 ± 7
N_2	108 ± 8	261 ± 46
O_2	119 ± 8	271 ± 16
CO	137 ± 6	332 ± 15
CO_2	250 ± 40	463 ± 15
H_2O	247 ± 26	647 ± 79
NH_3	231 ± 21	729 ± 50
CH_4	157 ± 7	397 ± 39
n-C_4H_{10}	641 ± 66	1093 ± 33
SF_6	319 ± 25	543 ± 17

Reference 57, T = 300 K

int E, cm^{-1}	$-\langle\Delta E\rangle_{all}$ at excitation energy 17000 cm^{-1}: 5000	15000
He	40	80
Ne	60	130
Ar	70	170
Kr	60	160
Xe	50	170
H_2	60	100
CO	90	230
N_2	85	180
O_2	60	170
N_2O	110	320
CO_2	110	360
SF_6	145	560
H_2O	120	440
NH_3	120	300
CH_3OH	70	520
C_2H_6	160	430
C_3H_8	210	610
n-C_8H_{18}	290	860
CF_4	100	310
C_2F_6	150	400
C_3F_8	200	430
n-C_8F_{18}	590	1020

Reference 57, T = 300 K

bath molecule	$-\langle\Delta E\rangle_{all}$ at excitation energy 30000 cm^{-1}: 15000	29670
He	80	80
Ne	170	180
Ar	190	210
Kr	210	230
Xe	220	230
H_2	120	150
CO	280	320
N_2	180	200
CO_2	320	360
SF_6	610	750
H_2O	320	480
NH_3	230	350
CH_3OH	500	680
CH_4	310	370
C_3H_8	670	760
C_4H_{10}	980	1010
C_5H_{12}	960	1050
n-C_8H_{18}	1050	1170
$C_{10}H_{22}$	1410	1420
CF_4	360	440
C_2F_6	500	560
C_3F_8	530	570
C_7F_{16}	1200	1250

[a] Energy lowered due to energy decay to 13943 cm^{-1}. [b] Energy lowered due to energy decay to 24073 cm^{-1}.

Chung and Carr[144] have determined the energy dependence of collisional self-deactivation of ethylcycloheptatriene. With use of a stepladder model, the master equation was solved; $\langle\Delta E\rangle_{all}$ increases from 0.9 to 3.35 kcal/mol as the excitation energy increase from 100 to 123 kcal/mol. The agreement of $\langle\Delta E\rangle_{all}$ with UVA results of Troe et al.[86] at 115 kcal/mol is good. However, this energy dependence is in disagreement with earlier UVA experiments where energy dependence was absent and with other experiments where a weaker energy dependence was observed.

Setser et al.[139,145a] have studied the deactivation of vibrationally excited fluorinated ethanes (ethyl fluoride[145a] (MFE), 1,2-difluoroethane[145a] (DFE), 1,1,1-trifluoroethane[139] (TFE)); the excitation energy (~91 kcal/mol) is the result of the association of fluoro-substituted methyl radicals at 300 K. The efficiency for deactivation by helium, from the exponential model ($\langle\Delta E\rangle_d$ = 1.0 kcal/mol), was comparable in all three systems; for N_2 and CO_2 ($\langle\Delta E\rangle_d$ = 1.5 and 2.0 kcal/mol, respectively) it was marginally lower than what is reported for the dichloroethane system[145b] while that for SF_6 (5 kcal/mol) is the same in all these systems. The TFE system was studied at 195 and 300 K; a small temperature dependence, nearly within the limits of experimental error on $\langle\Delta E\rangle_d$, was observed. At this time it is not understood why $\langle\Delta E\rangle_d$ is smaller in the TFE system than what has been tabulated[1] for other systems (1,2-dichloroethane, cyclopropane, alkyl radicals) and why $\langle\Delta E\rangle_d$ for the inert gases is constant at 1.0 kcal/mol, i.e., does not increase with mass as typical for other systems. These observations are not in agreement with a statistical model for energy transfer.

The results from Setser et al.[139,145] for deactivation by argon can be compared with those of Barker et al.[80] for 1,1,2-trifluoroethane using the multiphoton excitation technique and observing the IRF; Barker observes $\langle\Delta E\rangle_d$ = 0.9 kcal/mol compared with Setser's value of 1.0 kcal/mol.

Arbilla et al.[146] produced tetrafluorocyclopropane with an average energy of ~87 kcal/mol by the association of CH_2 and C_2F_4 at 300 K; collisional deactivation was studied for five bath gases. For He and Ar the data were fit with an exponential model with $\langle\Delta E\rangle_d$ = 2.1 and 4 kcal/mol, respectively. These values for $\langle\Delta E\rangle_d$ are higher than those reported above or for other systems;[1] if these values are different from others, then the results further illustrate that there are still many parameters in energy transfer that are not understood.

Orchard and Ramsden[147] formed vibrationally excited 1,4-cyclohexadiene by the thermal isomerization of *cis,anti,cis*-tricyclo[3.1.0.0]hexane (TCH) at 528 K; CHD can undergo either H_2 elimination or collisional stabilization with TCH or added quenchers (SF_6, CO_2, N_2, He). The results were modeled by a stepladder model with only down steps allowed and using the linear region (no turnup) in the S/D vs pressure plots. Due to these approximations and the relatively high temperature of the study [there is a broad range of thermal energies (~10 kcal/mol)], the results should not be taken quantitatively; i.e., relative trends but not absolute values for $\langle\Delta E\rangle_d$ can be accepted. They report that on going from He, to N_2, to CO_2, to SF_6 and TCH that $\langle\Delta E\rangle_d$ increases from 0.5 to 1 to 1.2 to 1.7 kcal/mol, respectively. These values are lower than other chemical activation experiments; however, the problems cited above may account for this difference.

TABLE V. $\langle\Delta E\rangle_{all}$ for Toluene and Cycloheptatriene at Various Temperatures and Internal Energies

Toluene (Reference 86b)

bath molecule	$-\langle\Delta E\rangle_{all}$ temp, K	$-\langle\Delta E\rangle_{all}$ excitation energy 52 000 cm^{-1}	bath molecule	$-\langle\Delta E\rangle_{all}$ temp, K	$-\langle\Delta E\rangle_{all}$ excitation energy 52 000 cm^{-1}
He	300	75	CF_4	300	320
Ne	300	84		872	300
Ar	300	130	C_2F_6	300	370
	865	130	C_3F_8	300	480
Kr	300	130		860	420
	865	160	C_4F_{10}	300	590
Xe	300	140	C_5F_{12}	300	680
	865	150	C_6F_{14}	300	770
H_2	300	92	C_7F_{16}	300	840
D_2	300	100		852	480
CO	300	160	C_8F_{18}	300	930
N_2	300	130	$CBrF_3$	300	380
	831	130	$CClF_3$	300	330
NO	300	160	CCl_2F_2	300	400
O_2	300	160	$CHClF_2$	300	410
CO_2	300	280	$CHCl_2F$	300	460
	870	240	$CHCl_3$	300	480
N_2O	300	230	CHF_3	300	370
H_2O	300	480	CH_2Cl_2	300	460
SF_6	300	400	CH_3Br	300	440
	851	250	CH_3Cl	300	390
CH_4	300	260	CH_4	300	260
	825	200	c-C_3H_6	300	500
C_2H_6	300	380	*i*-C_4H_{10}	300	590
C_3H_8	300	520	*neo*-C_5H_{12}	300	650
	856	420	c-C_6H_{12}	300	750
C_4H_{10}	300	640	Me-c-C_6H_{12}	300	780
C_5H_{12}	300	740	2,2,4-$Me_3C_5H_{12}$	300	930
C_6H_{14}	300	840	C_2H_4	300	400
	815	640	C_3H_6	300	480
C_7H_{16}	300	930	1-C_4H_8	300	590
	864	620	*cis*-2-C_4H_8	300	620
C_8H_{18}	300	990	C_2H_2	300	410
	845	660	C_6H_6	300	610
C_9H_{20}	300	1150	C_7H_8 (toluene)	300	770
$C_{10}H_{22}$	300	1300		848	500
$C_{11}H_{24}$	300	1340			

Cycloheptatriene (Reference 87)

bath molecule	$-\langle\Delta E\rangle_{all}$ temp, K	$-\langle\Delta E\rangle_{all}$ excitation energy 40 000 cm^{-1}	bath molecule	$-\langle\Delta E\rangle_{all}$ temp, K	$-\langle\Delta E\rangle_{all}$ excitation energy 40 000 cm^{-1}
He	300	61	N_2O	300	243
	373	59		573	120
	473	65	SF_6	300	309
	573	73		573	246
Ar	300	133	CH_4	300	290
	373	127		573	212
	473	122	C_4H_8	300	455
	573	135		373	399
	673	126		473	336
N_2	300	111		573	424
	373	125	*n*-C_6H_{14}	300	1058
	473	109		573	768
	573	123	*n*-C_8H_{18}	300	1696
CO	300	179		573	887
	473	158	CF_4	300	395
	573	128		573	201
CO_2	300	321	C_3F_8	300	707
	373	240		373	457
	473	216		473	433
	573	209		573	414

Chung and Carr[148] have photolyzed 1,1,1-trichloroethane at 228.8 nm and observed the pressure dependence of the CH_2CCl_2 yields (resulting from HCl elimination); it is postulated that this product is formed from an excited state, perhaps a triplet state, not the ground state. Their analysis using the stepladder model gave $\langle\Delta E\rangle_d = 17 \pm 5$ and 16 ± 6 kcal/mol for deactivation by the precursor and CF_4, respectively. These values are in qualitative agreement with others.[1]

2. Complex Reactions

Avila et al.[149] produced vibrationally excited vinyl chloride (VC) by the photodecomposition of 3-chloro-3-methyldiazirine. The deactivation of VC by N_2, Ar, He, and CO_2 was experimentally determined by measuring the yield of VC and acetylene formed from HCl

TABLE VI. $\langle\Delta E\rangle_{all}$ for Various Molecules at Various Internal Energies

excited molecule	excitation energy, cm^{-1}	temp, K	bath molecule	$-\langle\Delta E\rangle_{all}$	ref
azulene	29700	298	CO_2	520	56
azulene	29700	298	CO_2	[c]	85
azulene-d_8	29700	298	CO_2	[c]	85
benzene	52270	294	benzene	2060	100
			i-C_5H_{12}	1640	
			C_3H_8	1170	
			O_2	66	
			N_2	58	
			Ar	45	
C_6F_6	51800	298	C_6F_6	1238[a] (945)[b]	102
			Ar	360 (942)	
			N_2	293 (234)	
			O_2	343 (242)	
CF_3I	5000	300[d]	Ar	10	99
			C_3H_8	110	
			C_8H_{18}	280	
CF_3I	10000	300[d]	Ar	40	99
			C_3H_8	210	
			C_8H_{18}	570	
CF_3I	15000	300[d]	Ar	70	99
			C_3H_8	320	
			C_8H_{18}	880	
SF_6	4000–19000	300[d]	Ar	8[e]	106b
SF_6	>4000	300[d]	C_6H_6	90[f]	113
			C_6F_6	70[f]	
			$C_6H_5CH_3$	80[f]	
			C_6H_5F	270[f]	
C_6F_5H	188–6430	300[d]	C_6F_5H	54–175	111
H_2C=CHCl	30400	300[d]	He	<88	149
			Ar	<210	
			N_2	<210	
			CO_2	<270	

[a] Energy-dependent model of $\langle\Delta E\rangle_{all}$. [b] Energy-independent model of $\langle\Delta E\rangle_{all}$. [c] See section VI.A.2 for details. [d] Not explicitly stated but implied from the type of experiment done. [e] At 19000 cm^{-1}. [f] At 1000 cm^{-1}

elimination. Since VC is formed from a fragmentation process, its internal energy distribution is not precisely known and was estimated by a deconvolution procedure; it is bimodal with peaks at ~85 and 105 kcal/mol. The thermokinetic parameters are not well-known for this reaction. The $\langle\Delta E\rangle_d$ results of 0.25, 0.6, 0.6, and 0.75 kcal/mol for He, N_2, Ar, and CO_2 are low compared with simple external activation systems and more in agreement with the magnitudes for $\langle\Delta E\rangle_d$ determined by UVA and IRF techniques.

Jung et al.[150] produced vibrationally excited ethylene by the photoactivation of ethyl bromide at 121.6 nm and 298 K. The ethylene can be stabilized (S) by He, CF_4, CO_2, and C_2H_5Br or undergo unimolecular decomposition to acetylene (D). $\langle\Delta E\rangle_d$ values were obtained by comparing S/D vs pressure plots with those from stepladder model calculations; step sizes increased from 2.0 kcal/mol for He to 4.9 kcal/mol for CF_4 and CO_2 and 18.6 kcal/mol for C_2H_5Br. Knowledge of the energy distribution function for ethylene is crucial; it is estimated that 16% has energies in excess of 80 kcal/mol, the threshold energy for formation of acetylene, and the most probable energy for C_2H_4 is 66 kcal/mol.

Nogar and Spicer[151] have formed vibrationally excited cyclobutane-t (CBT) by the nuclear recoil reaction of T atoms with cyclobutane; CBT can be stabilized by He, Ne, Ar, Kr, and Xe or can decompose to ethylene. They observe that the efficiency for stabilization increases with increasing mass of the deactivator. This is consistent with results from other activation systems except for the TFE system cited above. The average energy of CBT is ~120 kcal/mol; however, the distribution of energy is not known. They have modeled the results in terms of a collision of the inert gas involving at least half of the atoms in CBT; this delocalized collision model gives energy step sizes of 0.5, 1.4, 1.8, 2.0, and 2.1 kcal/mol for the series He to Xe. This model gives values of $\langle\Delta E\rangle_d$ comparable to those observed in other systems.[1]

E. Energy Exchange with Surfaces: Variable-Encounter Method

This review does not cover explicitly gas–surface interactions. Two methods bear directly on the experiments discussed in this review; VLPP was mentioned before, and the variable-encounter method developed by Rabinovitch[129–133] will be briefly discussed now. VEM has provided fundamental information on the dynamics of heterogeneous vibrational energy transfer, i.e., between a gas molecule and a surface. VEM is a technique in which an ensemble of molecules at a low temperature acquires energy via a known and controlled number of successive collisions with a surface at a different but known temperature.[129] The experimental apparatus is simple and provides product integration for enhanced signal; a spherical bulb maintained at temperature T_1 has an attached heated "reaction finger" at T_2. Gas molecules enter the finger and exit after a controlled number of collisions with the wall as determined by the geometry of the finger; during this exposure to the walls at T_2 the reagent can react if sufficient internal energy is available. After exiting the finger, the reagent undergoes thermalizing collisions with the wall at T_1 and the encounter cycle with the finger is reinitiated; the number of encounter cycles per unit time is determined by the entrance area of the finger and the total surface area of the reservoir. This recycling of molecules from T_1 to T_2 is continued until a sufficient yield of products is obtained for analysis by GC but short enough so that secondary reactions are not significant. Thus, the population above the reaction threshold is directly probed by the amount of reaction product formed.[130a,b] Information on the total probability matrix can be obtained by varying the average number of collisions per encounter and the initial temperature T_1.[130] On the order of 15 collisions with the surface are necessary for a steady-state population distribution at T_2 to be achieved;[130] this quantity is directly related to first passage and induction times and consistent with VLPP experiments.[128]

One of the strengths of VEM is that $\langle\Delta E\rangle_d$ can be determined without knowing collision cross sections and/or the necessary vibrational frequencies for master equation calculations. Some of the interesting VEM results are of particular interest for gas–gas collisional energy transfer since in the limiting case where the deactivator contains many atoms the substrate–deactivator collision approaches that of a gas–surface collision. Both the isomerization of cyclopropane and cyclobutene exhibit strong collisions ($\langle\Delta E\rangle_d \approx 28.9$ kcal/mol) with silica walls up to approximately 400 K

at which point $\langle\Delta E\rangle_d$ begins to decrease.[131] For the cyclopropane system $\langle\Delta E\rangle_d$ decreases rapidly to 5.8 kcal/mol at 1000 K and then to ~4.9 kcal/mol at 1300 K; this leveling off is similar to that observed for the gas-phase cyclopropane isomerization. These observations are in accord with the trend predicted by the quasi-statistical accomodation model and the fact that the interaction time on the surface decreases with an increase in temperature so that less time is available for the transfer. The statistical model is also suggested by the fact that as the density of states of the substrate increases, via either isotopic substitution or increasing the number of vibrational modes, $\langle\Delta E\rangle_d$ decreases.[132]

The specific nature of the surface and substrate is also important.[133] Various surfaces, including metals (solid gold and tin and liquid gallium and tin) and glasses with various preparations (seasoned), have different values of $\langle\Delta E\rangle_d$, but all exhibit strong-collider behavior at low temperatures, with $\langle\Delta E\rangle_d$ decreasing with an increase in temperature. The importance of the gas–surface interaction was demonstrated for polar molecules; iodopropane has a larger $\langle\Delta E\rangle_d$ than does cyclobutane at 800 K (8.7 vs 6 kcal/mol). This increase may simply be due to the increased interaction time between the gas and the surface.

VII. Some Outstanding Questions in Intermolecular Energy Transfer between Large Excited Polyatomic and Bath Molecules

The purpose of this section is to summarize the outstanding questions, some of which were already discussed in this review and additional topics not discussed due to constraints and limitations of space and format. At this stage it is not possible to discuss the fundamental principles (unknown!) which tie the database together. The choice of outstanding problems is in the eyes of the beholder, and they reflect our point of view. Needless to say, new experimental or theoretical breakthroughs could open new areas in energy transfer not explored before and not discussed in this section. The subjects are not presented in any hierarchical order, nor are they discussed in great depth. A specific problem may have been discussed in greater depth in the body of the review.

A. Energy Dependence of $\langle\Delta E\rangle_d$ and $\langle\Delta E\rangle_{all}$

One of the major questions in intermolecular energy transfer in collisions between highly excited polyatomic molecules and inert bath molecules is the dependence of $\langle\Delta E\rangle_d$ and $\langle\Delta E\rangle_{all}$ on the internal energy of the excited polyatomic molecule. First, it should be recalled that there is a basic difference between the two quantities $\langle\Delta E\rangle_d$, the average energy in a down collision, and $\langle\Delta E\rangle_{all}$, average over all activating and deactivating collisions (eq 2-13). In many cases $\langle\Delta E\rangle_{all}$ is designated as $\langle\Delta E\rangle$; however, this might cause confusion with $\langle\Delta E\rangle_d$ and the subscript "all" is to be preferred. The dependence of $\langle\Delta E\rangle_{all}$ on E has been discussed by several people.[5,79,82,106b,108b,152-157,163] Bulk averages $\langle\langle E\rangle\rangle$ and $\langle\langle\Delta E\rangle\rangle$ were defined before (eq 2-13). It should be pointed out that $\langle\langle E\rangle\rangle = \langle E\rangle$ namely

$$\langle E\rangle_t = \int_0^\infty E\, f(E,t)\, dE$$

(the population evolves in time). The decay of the internal energy as a function of the bulk averaged $\langle\Delta E\rangle_{all}$ is given by[82,106,152,154]

$$\frac{d\langle E\rangle}{dt} = \omega\langle\langle\Delta E\rangle\rangle_{all} \tag{7-1}$$

For a δ function of excitation such as internal conversion, at $t = 0$ the bulk average is simply the average since the population at $t = 0$ is unity; i.e., $\langle\langle\Delta E\rangle\rangle_{all}{}^0 = \langle\Delta E\rangle_{all}{}^0$, where the superscript indicates $t = 0$. Equation 7-1 thus becomes

$$\left[\frac{d\langle E\rangle}{dt}\right]_{t\to 0} = \omega\langle\langle\Delta E\rangle\rangle_{all}{}^0 \tag{7-2}$$

In such a case the macroscopic decay rate of the internal energy yields directly the microscopic $\langle\Delta E\rangle_{all}$. The sum rule

$$\langle\Delta E\rangle_{all} = a + bE \tag{7-3}$$

must be satisfied.[158] The bulk average of eq 7-3 is

$$\langle\langle\Delta E\rangle\rangle_{all} = a + b\langle E\rangle \tag{7-4}$$

The linear decay given in eq 7-4 is a general conclusion for any transition probability and any initial distribution provided $\langle\Delta E\rangle_{all}$ is constant; in such a case, it can be taken out of the integral of eq 2-13 and it follows that[156,157] $\langle\langle\Delta E\rangle\rangle_{all} = \langle\Delta E\rangle_{all}$.

At equilibrium the average energy exchanged between up and down collisions is zero ($\langle\langle\Delta E\rangle\rangle_{all} = 0$), and we have from 7-4

$$a = -b\langle E\rangle_{eq} \tag{7-5}$$

which yields upon substitution in eq 7-4

$$\langle\langle\Delta E\rangle\rangle_{all} = b\,(\langle E\rangle - \langle E\rangle_{eq}) \tag{7-6}$$

When $b = -1/(\omega\tau)$ eq 7-6 becomes

$$\langle\langle\Delta E\rangle\rangle_{all} = \frac{-(\langle E\rangle - \langle E\rangle_{eq})}{\omega\tau} \tag{7-7}$$

Substituting eq 7-7 into eq 7-1 and integrating, we obtain

$$\langle E\rangle - \langle E\rangle_{eq} = (\langle E\rangle_0 - \langle E\rangle_{eq})e^{-t/\tau} \tag{7-8}$$

where τ is defined as the relaxation time such that $\ln[(\langle E\rangle_\tau - \langle E\rangle_{eq})/(\langle E\rangle_0 - \langle E\rangle_{eq})] = -1$. Combining eqs 7-7 and 7-8

$$\langle\langle E\rangle\rangle_{all} = \langle\langle E\rangle\rangle_{all}{}^0\, e^{-t/\tau} \tag{7-9}$$

For the relaxation time τ, Forst and Barker suggest[163] the Lambert–Salter[22b] expression for collision number

$$Z_{10} = \omega\tau(1 - e^{-h\nu_{min}/kT}) \tag{7-10}$$

where ν_{min} is the lowest frequency of the excited molecule. In IRF and UVA experiments τ is found, and from it the dependence of $\langle\langle\Delta E\rangle\rangle_{all}$ on $\langle E\rangle$ is found from eq 7-7. The bimolecular rate coefficient for deactivation is given[82] as $k = (\tau N)^{-1}$, where N is the number density of the collider.

The dependence of ΔE on E varies with the size of the molecule and level of excitation. For small molecules at low energies (except NO_2, which shows a more complex behavior[159]), $\langle\langle\Delta E\rangle\rangle_{all}$ depends on $\langle E\rangle^2$. For large molecules (azulene) at intermediate levels of excitation,[82-84,98] ~16 000 cm^{-1}, $\langle\langle\Delta E\rangle\rangle_{all}$ is proportional to $\langle E\rangle$. For large molecules at high levels of excitation, Barker[82] finds that for azulene the linear dependence

TABLE VII. $\langle\Delta E\rangle_d$[a] for Various Molecules

excited molecule	excitation energy, cm^{-1}	temp, K	bath molecule	$-\langle\Delta E\rangle_d$, cm^{-1}	ref
SF_6	1000	300	Ar		106a
ethyl acetate	1000	300	Ar		106a
azulene	16700	314	Ar		106a
SF_6	2000–6000	300	Ar		108
C_6F_5H		300	Ar		108
SF_6	3000–14000	300	Ar		112a
SF_6	300–1000	298	SF_6		112b
	1500–5000				
C_6F_5H	550–5500	300	Ar		114
azulene	16700	370	Kr		104
cyclohexene	footnote c, Table III	1200–2000	Kr	550	122
					125
cyclopropane-d_2,t	footnote c, Table III	823–1123	He	380–210	118
cyclopropane-d_2,t	footnote c, Table III	823–933	Kr	780–520	72
		823–973	CO_2	1220–800	
$H_2C{=}CH_2$	28000	298	He	700	150
			CF_4	1700	
			CO_2	1700	
			C_2H_5Br	6500	
cyclohexadiene	29000	528	SF_6	590	147
			CO_2	420	
			N_2	340	
			He	170	
cyclobutane-t	42000	300	He	175	151
			Ne	490	
			Ar	630	
			Kr	700	
			Xe	740	
7-ethylcyclohepta-1,3,5-triene	43200	300	self	1360	144
	39000		self	670	
	37200		self	440	
	35100		self	330	
methylcyclobutane	38600	300	self	1400–2100 SL[b]	141
ethylcyclobutane	36800	300	self	530–1400 SL	142
methylcyclopropane	35800	300	self	1050–2800 SL	143
ethylcyclopropane	35800	300	self	1050–4200 SL	143
1,1,2,2-tetrafluorocyclopropane	30600	300	He	740 exp[c]	146
			Ar	1400 exp	
			CO_2	1750 SL	
			CF_4	2800 SL	
			C_2F_6	3500 SL	
CCl_3CH_3	30800	338	self	5900 SL	148
			CF_4	5600 SL	
CH_3CF_3	35800	195	H_2, N_2	350 exp	139
			CO_2	700 exp	
			C_2F_6	1750 SL	
			SF_6	2100 SL	
		300	He, Ne, Ar, Kr, Xe	350 exp	
			H_2, D_2, N_2	525 exp	
			CO_2	700 exp	
			CH_4	1050 exp	
			CF_4	1750 SL	
			SF_6	2100 SL	
			C_2F_6	2100 SL	
			C_4F_8	3500 SL	
CH_2FCH_2F	32400	300	He	350 exp	145
			N_2	1050 SL	
			CO_2	880 SL	
			SF_6	1750 SL	
CH_3CH_2F	31900	300	He	350 exp	145
			N_2	1050 SL	
			CO_2	700 SL	
			SF_6	1750 SL	
H_2DCCH_2Cl	footnote c, Table III	1049–1130	He	700	134b
			Ne, Kr	600	
CD_3CH_2Cl	footnote c, Table III	975–1213	CO_2	1040	134c
HCD_2CD_2Br	footnote c, Table III	1000–1070	Ne	250	135
			CO_2	600	
			C_2H_4	850	
			C_6H_6	1200	
CH_3CO_2Et	footnote c, Table III	837	He	300	134d
			Ne	400	
			Ar	550	
			Kr	500	
			N_2	500	
			C_2H_4	600	

TABLE VII (Continued)

excited molecule	excitation energy, cm^{-1}	temp, K	bath molecule	$-\langle\Delta E\rangle_d$, cm^{-1}	ref
C_3H_7Br	footnote c, Table III	870	Ne	490	136
			Xe	540	
			C_2H_4	820	
			C_2D_4	740	
C_3D_7Br		870	Ne	440	136
			Xe	570	
			C_2H_4	730	
			C_2D_4	810	
C_4H_9Cl	footnote c, Table III	760	Kr	255	137
			N_2	265	
			CO_2	440	
			C_2H_4	585	
C_4D_9Cl	footnote c, Table III	760	N_2	245	137
			CO_2	370	
			C_2H_4	540	
chlorocyclobutane	footnote c, Table III	970	C_2H_4	1600	134e
1,1,2,2-tetrafluoro-cyclobutane	footnote c, Table III	1105	C_2H_4	965	138b
			CO_2	1740	
1,1,2,2-tetrafluoro-3-chlorocyclobutane	footnote c, Table III	1048	Ne	445	138a
			CH_4	665	
			C_2H_4	920	
			CH_2CF_2	1190	
			CF_4	1370	
			CO_2	735	

[a] The values of $\langle\Delta E\rangle_d$ depend on the collision cross sections used and can, in most cases, be found in the original papers. Without this information the values of $\langle\Delta E\rangle_d$ are of little use. [b] SL = strong collider. [c] Exponential model.

TABLE VIII. Probabilities for Energy Transfer

method	excited molecule	bath molecule	$\langle E\rangle$, cm^{-1}	prob[a]	ref
thermal sensitizn	azulene	quadricyclane	30600	10^{-3}	41
thermal sensitizn	hexafluorobenzene	cyclobutene	38600	3×10^{-3}	42
jet	1,3,5-trimethyl-1,1,3,5,5-pentaphenyltrisiloxane	cyclohexadiene	25000–46000	5×10^{-7}	43

[a] For $E \geq E_0$ in units of mol/kcal.

holds up to ~30000 cm^{-1} while Troe finds for azulene[57,83,84,98] and toluene[86,87] a leveling-off effect above 20000 cm^{-1} whereby $\langle\langle\Delta E\rangle\rangle_{all}$ is almost independent of $\langle E\rangle$[83,84,98] up to $\langle E\rangle$ = 66000 cm^{-1} [84] (Figure 23). At the latter energy there is competition between deactivation and chemical reaction that is taken into consideration. Nakashima et al.[100] and Ichimura et al.[101,102] find energy dependence for benzene derivatives.

Unlike internal conversion experiments discussed above, infrared multiphoton excitation prepares excited molecules in an unknown distribution. Since the only experimental measured parameter is $\langle n\rangle$, the average number of photons absorbed per pulse, the distribution can take any functional shape or form, even a bimodal one.[80,99] Barker et al.[80b] have done additional measurements such as reaction yield, IRF intensity, and decay rate, all as a function of laser fluence and pressure. These observations combined with master equation calculations can provide information on the population distribution function and the energy and temperature dependence for the average energy transferred. Troe et al.[99] have measured the $\langle\langle\Delta E\rangle\rangle_{all}$ dependence on $\langle E\rangle$ for IRMPE CF_3I, an intermediate-size molecule. It was found by UVA that $\langle\langle\Delta E\rangle\rangle_{all}$ is proportional to $\langle E\rangle^m$ where $m \approx 1.5$ as if CF_3I is an intermediate between the small- and large-molecule limits. IRMPE optoacoustic studies of SF_6 deactivation by argon performed by Gordon et al.[108] show a linear dependence of $\langle\langle\Delta E\rangle\rangle_{all}$ on the average energy in the range 4000–19000 cm^{-1}. IRMPE Hg tracer studies of pentafluorobenzene by Braun et al.[111] show a linear dependence of $\langle\langle\Delta E\rangle\rangle_{all}$ on the internal energy below 5000 cm^{-1}. Not discussed in this review are results of experiments at very low levels of excitation where $\langle\langle\Delta E\rangle\rangle_{all}$ shows a nontrivial dependence on $\langle E\rangle$. The dependence of $\langle\langle\Delta E\rangle\rangle_{all}$ on $\langle E\rangle$ remains to be settled experimentally and theoretically.

B. Temperature Dependence of β

As discussed earlier the collisional efficiency is the factor relating the strong-collision rate coefficient to that of the weak collider. Specifically, β' is defined as

$$\beta' = \frac{\Delta k^{wc}}{\Delta k^{sc}} = \left[\frac{\Delta k_{ss}{}^{wc}}{\Delta k_{eq}{}^{wc}}\right]\left[\frac{\Delta k_{eq}{}^{wc}}{\Delta k_{ss}{}^{sc}}\right] = \gamma(N)\ \gamma(K) \quad (7\text{-}11)$$

where wc and sc correspond to the weak and strong colliders and ss and eq relate to the steady-state and equilibrium population distributions. The $\gamma(N)$ term relates to population deficiency while $\gamma(K)$ relates to the transport of molecules above E_0; in the high-pressure limit the γ terms are unity. As the pressure decreases for a weak collider, these factors decrease monotonically. Thus, it is apparent that β' is dependent upon the population distribution, which in turn is determined by the probability model. In general, as the temperature increases, β' decreases. This is readily seen to be the case by considering the operational definition of collisional efficiency; collisions are strong when $\langle\Delta E\rangle_d \approx 5\langle E^+\rangle$ (the average excess energy of molecules above E_0). Quantitatively the exact temperature dependence of β' is difficult to predict; however, for weak collisions ($\beta' < 0.05$) β' is proportional to[1] $\langle\Delta E\rangle_d{}^2$ and $\langle E^+\rangle^{-2}$.

These factors will be discussed in the following paragraphs. In nonreactive (physical) systems, effectiveness can be used instead of efficiency.

The temperature dependence of $\langle \Delta E \rangle_d$ is also complex since the average vibrational energy of the substrate increases as well as the relative translational energy of the collision pair. As discussed in the energy dependence section, it is observed that $\langle \Delta E \rangle_d$ increases with excitation energy (see Table IV); this increase is also in accord with a statistical model and trajectory calculations. The effect of translational energy is dependent on the type of interaction: For an attractive potential an increase in the relative translational energy will decrease $\langle \Delta E \rangle_d$ while for a repulsive potential (in the Landau–Teller regime[23]) an increase in $\langle \Delta E \rangle_d$ is predicted. Thus, depending on the particular system and temperature region, $\langle \Delta E \rangle_d$ may increase, remain constant, or decrease with an increase in temperature. It is important that these factors have been quantitatively determined in order to predict temperature dependences. The inverse, finding the factors from the temperature dependence, may not be unique.

It has been determined[14] that $\langle E^+ \rangle$ increases linearly with temperature at low temperature and more rapidly as the temperature increase; the increase is larger for more complex substrates and/or lower E_0. However, for large molecules at relatively high temperatures, i.e., cyclohexene[123] at 1500 K, the most probable energy is comparable to E_0 (62.5 kcal/mol) and $\langle E^+ \rangle$ loses its significance as an operational parameter in determining β' since most collisions will be "activating" collisions. In fact, the meaning of a rate coefficient for these conditions must be further elucidated.

The problems associated with calculating β' from transition probability models must also be considered. For example Troe at al.[66b] reported that β' increases with temperature above ~1300 K for the thermal unimolecular reaction of cycloheptatriene with $\langle \Delta E \rangle_d$ = 500 and 2000 cm^{-1}. However, numerical problems might have been the cause of the reported turnup in β' with temperature.[160] The construction of the transition probability matrix at high temperatures should be scrutinized so that detailed balance and completeness are rigorously obeyed with physically realistic probabilities.

Experimental determination of the temperature dependence for both β' and $\langle \Delta E \rangle_d$ has been reported for the isomerization of cyclopropane[72,118] and the decomposition of ethyl acetate.[134d] The cyclopropane study made use of multichannel paths for the cyclopropane-1-t_1,2,2-d_2 substrate over the 823–1123 K temperature range in a conventional homogeneous reaction in the second-order region. For helium as the deactivator, $\langle \Delta E \rangle_d$ decreased as T^{-1} while β' decreased as $T^{-5.6}$; the β' dependence was in agreement with that predicted by ref 1. The ethyl acetate results, determined by the VLPP technique at 837 K and multiphoton decomposition at 340 K, for $\langle \Delta E \rangle_d$ were $T^{-(0.1-0.3)}$ for helium and neon and $T^{-(0.3-0.5)}$ for argon, krypton, and nitrogen, similar to that determined by the UVA technique. The collisional efficiency decreased by a factor of 10 over this temperature range, so that $\beta' \approx T^{-2.6}$. It is not clear whether cyclopropane and ethyl acetate behave differently or the difference is due to large experimental errors.

The physical methods utilizing UVA for cycloheptatrienes and toluene and IRF for azulene and 1,1,2-trifluoroethane have also provided information on the temperature dependence of $\langle \Delta E \rangle_{all}$. For these systems the temperature dependence falls in the range $T^{0\pm0.5}$; this is in sharp contrast to that observed for chemical (nonphysical) techniques.

The knowledge of the temperature dependence of β' is necessary so that the extent of falloff is known; a decrease in β' shifts the degree of falloff to higher pressure.

C. High Temperatures

The issue of reliability of various master equation calculations at high temperatures was raised in previous sections. There is a question whether a system at high temperature achieves a steady-state population distribution. Calculations by Tzidoni and Oref[161] indicate that at high temperatures the system never obtains a steady state. That is to say, the solution of the master equation yields an ensemble of eigenvalues (rate coefficients) producing a nonexponential decay of the populations. Figure 24 shows the dependence of the overall rate coefficient on time for a system of substrate and bath molecules of 10 normal modes at 600, 1500, and 2500 K at three pressures. As can be seen, k is constant at the high-pressure limit but changes with time at lower pressures and high temperatures. At 600 K, the system is well behaved, k is constant with time, and the system attains a steady state. The fact that systems do not achieve a steady state can be proven analytically for the specific case of a strong collider. Shi and Barker[125,162] have run detailed master equation calculations on cyclohexene decomposition at high temperatures. They find that their system obtains a steady state before it reaches 15% total decomposition. As mentioned before, completeness and detailed balance must be obeyed. This is done in a manner described in section I.B. At high temperatures extra care must be taken to make sure that the two constraints are obeyed. Specifically, the recursion equation (1-28) fails, and the normalization coefficients $C(E)$ obtain unphysical values; certain mathematical skills are required to obtain meaningful results.

D. Shape of the Transition Probability Function

A major bottleneck in solving the master equation for weak collisions in a specific system is the lack of detailed knowledge of the form of the transition probability function. Various mathematical models and constructs are reported in the literature and were discussed in sections II.B and II.D. Most experiments yield average quantities such as $\langle \Delta E \rangle_d$ and $\langle \Delta E \rangle_{all}$ from which it is impossible to deconvolute the "true" functional form of the transition probability. Experiments determining $P(E',E)$ as a function of $\Delta E_E = E' - E$ (of which Oref's[41-43] and Luther's[44,45] are examples) are needed to provide the data for basic understanding of energy-transfer processes.

E. Intermediate Levels of Excitation

Most energy-transfer experiments have been done at two extreme energy limits. At low levels of excitation, polyatomic colliders vibrational–vibrational energy

transfer can efficiently take place and the monatomic bath where energy-transfer probability is very low. At high levels of excitation, above the threshold energy for reaction (decomposition or isomerization), where both energy-transfer probabilities and step sizes are larger than for the low levels of excitation, vibrational to translational and/or rotational energy transfer are much more dominant. In this review the high-energy case was discussed. Very little is known about energy-transfer processes at intermediate levels of excitation, that is to say where the internal energy is in the range $E_0/2 < E < E_0$. Information in this region is difficult to obtain with conventional methods since it is hard to excite and probe this region as no chemical changes take place that can be monitored. Excitation can be obtained by intracavity overtone absorption or IR multiphoton excitation, each with its advantages and drawbacks. With the development of new physical detection methods such as IRF, UVA, MPI, TROA, and others, the prospects of charting this unknown region are improving.

F. Theoretical Computations

Theoretical modeling and calculations can contribute to better understanding of energy-transfer processes in various ways. These are mentioned briefly below.

The number of trajectory calculations on energy transfer in large polyatomic molecules is very limited and is reported in this review. There is a clear need to widen the scope of these studies. A great deal of work is being done now on surface processes; however, they do not correlate directly with experiments such as VEM or VLPP. Bringing together theoretically detailed studies on energy exchange at a well-defined surface with that of a "fuzzy" surface as used in VEM and VLPP can contribute to the understanding of the accommodation processes at the surface. A third approach not explored in full is treating a large polyatomic molecule as a surface with which an atom or a diatom encounters a collision. The ergodic behavior of such a molecule[25,164,165] and its size compared with the small bath give credence to such an approach.

XIII. Acknowledgment

This work is supported by the U.S.–Israel Binational Science Foundation, by the German–Israeli Foundation for Scientific Research and Development, by the Fund for Promotion of Research at the Technion, and by the Division of Chemical Sciences, U.S. Department of Energy (Grant No. DE-FG02-87ER13700). We thank Prof. B. S. Rabinovitch for his hospitality and many interesting discussions. We also thank Professors J. R. Barker, W. C. Gardiner, Jr., R. G. Gilbert, and J. Troe for useful comments on the manuscript.

IX. References

(1) Tardy, D. C.; Rabinovitch, B. S. *Chem. Rev.* **1977**, *77*, 369.
(2) Quack, M.; Troe, J. *Gas Kinetics and Energy Transfer*; The Chemical Society: London, 1977; Vol. 2.
(3) Flynn, G. W. *Acc. Chem. Res.* **1981**, *14*, 334.
(4) Krajnovich, D. J.; Parmenter, C. S.; Catlett, D. L., Jr. *Chem. Rev.* **1987**, *87*, 237.
(5) Hippler, H.; Troe, J. Recent Direct Studies of Collisional Energy Transfer in Vibrationally Highly Excited Molecules in the Ground Electronic State. *Bimolecular Collisions*; Baggott, J. E., Ashfold, M. N., Eds.; The Royal Society of Chemistry: London, 1989; in press.
(6) (a) Marcus, R. A.; Rice, O. K. *J. Phys. Colloid Chem.* **1951**, *55*, 894. (b) Marcus, R. A. *J. Chem. Phys.* **1952**, *20*, 359.
(7) Robinson, P. J.; Holbrook, K. A. *Unimolecular Reactions*; Wiley: New York, 1972.
(8) Forst, W. *Theory of Unimolecular Reactions*; Academic Press: New York, 1973.
(9) (a) Waage, E. V.; Rabinovitch, B. S. *Chem. Rev.* **1970**, *70*, 377. (b) Troe, J. Fifth International Symposium on Combustion, Tokyo, 1979.
(10) (a) Gillespie, D. T. *J. Comp. Phys.* **1976**, *22*, 403; *J. Comp. Phys.* **1978**, *28*, 395; *J. Phys. Chem.* **1977**, *81*, 2340. (b) Barker, J. R. *Chem. Phys.* **1983**, *77*, 301.
(11) Montroll, E. W.; Shuler, K. E. *Adv. Chem. Phys.* **1958**, *1*, 361.
(12) (a) Oref, I.; Tardy, D. C. *J. Chem. Phys.* **1989**, *91*, 205. (b) Nordholm, S.; Schranz, H. W. *Chem. Phys.* **1981**, *62*, 459.
(13) Gilbert, R. G.; King, K. D. *Chem. Phys.* **1980**, *49*, 367.
(14) Tardy, D. C.; Rabinovitch, B. S. *J. Chem. Phys.* **1968**, *48*, 1282.
(15) Tzidoni, E.; Oref, I. *Chem. Phys.* **1984**, *84*, 403.
(16) (a) This subject merits a special review. See Forst's work[58b] and Troe's work[66] as well as Gilbert's work listed below. (b) Smith, S. C.; Gilbert, R. G. *Int. J. Chem. Kinet.* **1988**, *20*, 307. (c) *Ibid.*, in press.
(17) Eliason, M. A.; Hirschfelder, J. O. *J. Chem. Phys.* **1959**, *30*, 1426.
(18) Levine, R. D.; Bernstein, R. B. *Molecular Reaction Dynamics and Chemical Reactivity*; Oxford University Press: New York, 1987.
(19) Miller, W. H. *Dynamics of Molecular Collisions*; Plenum: New York, 1976.
(20) (a) Bunker, D. L. *Math. Comput. Phys.* **1971**, *10*, 287. (b) Grinchak, M. B.; Levitsky, A. A.; Polak, L. S.; Umanskii, S. Ya. *Chem. Phys.* **1984**, *88*, 365. (c) Muckerman, J. T. CLASTR programs. *QCPE 229*. Chapman, S.; et al. *QCPE 273*. *QCPE 316*. Hase, W. L. MERCURY program. *QCPE 453*. (d) Bunker, D. L.; Hase, W. L. *J. Chem. Phys.* **1973**, *59*, 4621. (e) Hase, W. L.; Wolf, R. J.; Sloane, C. S. *J. Chem. Phys.* **1979**, *71*, 2911. (f) Wolf, R. J.; Hase, W. L. *J. Chem. Phys.* **1980**, *72*, 316.
(21) Yardley, J. T. *Introduction to Molecular Energy Transfer*; Academic Press: New York, 1980.
(22) (a) See for example: Tang, K. Y.; Parmenter, C. S. *J. Chem. Phys.* **1983**, *78*, 3922. (b) Lambert, J. D. *Vibrational and Rotational Relaxation in Gases*; Clarendon Press: Oxford, U.K., 1977.
(23) Schwartz, R. N.; Slawsky, Z. I.; Herzfeld, K. F. *J. Chem. Phys.* **1952**, *20*, 5091.
(24) Tanczos, F. I. *J. Chem. Phys.* **1956**, *25*, 439.
(25) Oref, I.; Rabinovitch, B. S. *Acc. Chem. Res.* **1979**, *12*, 166.
(26) Glass, J. V. S.; Hinshelwood, C. N. *J. Chem. Soc.* **1929**, 1804, 1815.
(27) (a) Light, J. C. *J. Chem. Phys.* **1964**, *40*, 322. (b) Oref, I.; Rabinovitch, B. S. *Chem. Phys.* **1977**, *26*, 385. (c) Forst, W.; Bhattacharjee, R. C. *Chem. Phys.* **1979**, *37*, 343.
(28) (a) Serauskas, R. V.; Schlag, E. W. *J. Chem. Phys.* **1965**, *42*, 3009. (b) Serauskas, R. V.; Schlag, E. W. *J. Chem. Phys.* **1965**, *43*, 898. (c) Serauskas, R. V.; Schlag, E. W. *J. Chem. Phys.* **1966**, *45*, 3706.
(29) Lin, Y. N.; Rabinovitch, B. S. *J. Phys. Chem.* **1970**, *74*, 3151.
(30) Bhattacharjee, R. C.; Forst, W. *Chem. Phys.* **1978**, *30*, 217.
(31) (a) Oref, I. *Int. J. Chem. Kinet.* **1977**, *9*, 751. (b) Oref, I. *J. Chem. Phys.* **1981**, *75*, 131. (c) Oref, I. *J. Chem. Phys.* **1982**, *77*, 1253. (d) Herscovitz, O.; Tzidoni, E.; Oref, I. *Chem. Phys.* **1982**, *71*, 221.
(32) Troe, J. *Ber. Bunsen-Ges. Phys. Chem.* **1973**, *77*, 665.
(33) (a) Nordholm, S.; Freasier, B. C.; Jolly, D. L. *Chem. Phys.* **1977**, *25*, 433. (b) Freasier, B. C.; Jolly, D. L.; Nordholm, S. *Chem. Phys.* **1978**, *32*, 161, 169.
(34) Schranz, H. W.; Nordholm, S. *Int. J. Chem. Kinet.* **1981**, *13*, 1051.
(35) (a) Brown, N. J.; Miller, J. A. *J. Chem. Phys.* **1984**, *80*, 5568. (b) Hippler, H.; Schranz, H. W.; Troe, J. *J. Phys. Chem.* **1986**, *90*, 6158. (c) Stace, A. J.; Murrell, J. N. *J. Chem. Phys.* **1978**, *68*, 3028. (d) Novak, M. M.; Balint-Kurti, G. G.; Clary, D. C. *Chem. Phys.* **1987**, *114*, 221.
(36) Bruehl, M.; Schatz, G. C. *J. Chem. Phys.* **1988**, *89*, 770. Bruehl, M.; Schatz, G. C. *J. Phys. Chem.* **1988**, *92*, 7223.
(37) Bunker, D. L.; Jayich, S. A. *Chem. Phys.* **1976**, *13*, 129.
(38) Hynes, R. G.; Sceats, M. G. *J. Chem. Phys.* **1989**, *91*, 6804. Sceats, M. G. *J. Chem. Phys.* **1989**, *91*, 6795.
(39) (a) Date, N.; Hase, W. L.; Gilbert, R. G. *J. Phys. Chem.* **1984**, *88*, 5135. (b) Miller, W. H.; Hase, W. L.; Darling, C. L. *J. Chem. Phys.* **1989**, *91*, 2863. (c) Bowman, J. M.; Gazdy, B.; Sun, Q. *J. Chem. Phys.* **1989**, *91*, 2859.
(40) (a) Lim, K. F.; Gilbert, R. G. *J. Chem. Phys.* **1986**, *84*, 6129. (b) Lim, K. F.; Gilbert, R. G. *J. Phys. Chem.* **1990**, *94*, 77. (c) Lim, K. F.; Gilbert, R. G. *J. Chem. Phys.* **1990**, *92*, 1819.
(41) Hassoon, S.; Oref, I.; Steel, C. *J. Chem. Phys.* **1988**, *89*, 1743.
(42) Morgulis, I. M.; Sapers, S. S.; Steel, C.; Oref, I. *J. Chem. Phys.* **1989**, *90*, 923.

(43) Pashutzki, A.; Oref, I. *J. Phys. Chem.* **1988**, *92*, 178.
(44) Lohmannsroben, H. G.; Luther, K. *Chem. Phys. Lett.* **1988**, *144*, 473.
(45) Luther, K.; Reihs, K. *Ber. Bunsen-Ges. Phys. Chem.* **1988**, *92*, 442.
(46) Polanyi, J. C. *Acc. Chem. Res.* **1972**, *5*, 161.
(47) Hu, X.; Hase, W. L. *J. Phys. Chem.* **1988**, *92*, 4040.
(48) Whyte, A. R.; Lim, K. F.; Gilbert, R. G.; Hase, W. L. *Chem. Phys. Lett.* **1988**, *52*, 377.
(49) Lin, Y. N.; Chan, S. C.; Rabinovitch, B. S. *J. Phys. Chem.* **1968**, *72*, 1932.
(50) Spicer, L. D.; Rabinovitch, B. S. *J. Phys. Chem.* **1970**, *74*, 2445.
(51) Pavlou, S. P.; Rabinovitch, B. S. *J. Phys. Chem.* **1971**, *75*, 2171.
(52) Durant, J. L.; Kaufman, F. *Chem. Phys. Lett.* **1987**, *142*, 246.
(53) (a) Hirschfelder, J. O.; Curtiss, C. F.; Bird, R. B. *Molecular Theory of Gases and Liquids*; Wiley: New York, 1954. (b) Kohlmaier, G.; Rabinovitch, B. S. *J. Chem. Phys.* **1963**, *38*, 1692, 1709. (c) Reid, R. C.; Sherwood, T. K. *The Properties of Gases and Liquids*, 2nd ed.; McGraw-Hill: New York, 1966. (d) Troe, J. *J. Chem. Phys.* **1977**, *66*, 4758.
(54) Lim, K. F. Ph.D. Thesis, University of Sydney, NSW, Australia, 1988.
(55) Barker, J. R.; Golden, R. E. *J. Phys. Chem.* **1984**, *88*, 1012.
(56) Barker, J. R. *J. Phys. Chem.* **1984**, *88*, 11.
(57) Hippler, H.; Lindemann, L.; Troe, J. *J. Chem. Phys.* **1985**, *83*, 3906.
(58) (a) Penner, A. P.; Forst, W. *J. Chem. Phys.* **1977**, *67*, 5296. (b) Penner, A. P.; Forst, W. *Chem. Phys.* **1975**, *11*, 243.
(59) (a) Tardy, D. C.; Rabinovitch, B. S. *J. Phys. Chem.* **1985**, *89*, 2442. (b) Tardy, D. C.; Rabinovitch, B. S. *J. Phys. Chem.* **1986**, *90*, 1187.
(60) Snider, N. *J. Phys. Chem.* **1986**, *90*, 4366.
(61) Gilbert, R. G. *Chem. Phys. Lett.* **1983**, *96*, 259.
(62) Swamy, K. N.; Hase, W. L. *J. Am. Chem. Soc.* **1984**, *106*, 4071.
(63) Wang, F. M.; Rabinovitch, B. S. *J. Phys. Chem.* **1974**, *78*, 863.
(64) Keck, J. C. *J. Chem. Phys.* **1967**, *46*, 4211.
(65) Keck, J. C.; Carrier, G. *J. Chem. Phys.* **1964**, *43*, 2284.
(66) (a) Troe, J. *J. Chem. Phys.* **1977**, *66*, 4745, 4758. (b) Gilbert, R. G.; Luther, K.; Troe, J. *Ber. Bunsen-Ges. Phys. Chem.* **1983**, *87*, 169.
(67) Troe, J. *J. Phys. Chem.* **1979**, *83*, 114.
(68) (a) Oref, I. *J. Phys. Chem.* **1989**, *93*, 3465. (b) Pawlowska, Z.; Oref, I. *J. Phys. Chem.* **1990**, *94*, 567.
(69) (a) Gardiner, W. C., Jr. Proceedings of the 12th IMACS World Congress on Scientific Computations, Paris, 1988. (b) Gardiner, W. C., Jr.; Oref, I. In preparation.
(70) Troe, J. *Ber. Bunsen-Ges. Phys. Chem.* **1983**, *87*, 161.
(71) Forst, W. *J. Phys. Chem.* **1986**, *90*, 456.
(72) Krongauz, V. V.; Rabinovitch, B. S. *J. Chem. Phys.* **1983**, *78*, 3872.
(73) Krongauz, V. V.; Rabinovitch, B. S.; Linkaityte-Weiss, E. *J. Chem. Phys.* **1983**, *78*, 5643.
(74) Endo, H.; Glanzer, K.; Troe, J. *J. Phys. Chem.* **1979**, *83*, 2083.
(75) Larson, C. W.; Patrick, R.; Golden, D. M. *Combust. Flame* **1984**, *58*, 229.
(76) Churchill, S. W.; Usagi, R. *AIChE J.* **1972**, *18*, 1121.
(77) (a) Malins, R. J.; Tardy, D. C. *Int. J. Chem. Kinet.* **1979**, *11*, 1007. (b) Dove, J. E.; Troe, J. *Chem. Phys.* **1978**, *3*, 1.
(78) Rossi, M. J.; Barker, J. R. *Chem. Phys. Lett.* **1982**, *85*, 21.
(79) Rossi, M. J.; Pladziewicz, J. R.; Barker, J. R. *J. Chem. Phys.* **1983**, *78*, 6695.
(80) (a) Zellweger, J. M.; Brown, T. C.; Barker, J. R. *J. Phys. Chem.* **1986**, *90*, 461. (b) Zellweger, J. M.; Brown, T. C.; Barker, J. R. *J. Chem. Phys.* **1985**, *83*, 6251, 6261.
(81) Shi, J.; Bernfeld, D.; Barker, J. R. *J. Chem. Phys.* **1988**, *88*, 6211.
(82) Shi, J.; Barker, J. R. *J. Chem. Phys.* **1988**, *88*, 6219.
(83) Otto, B. Ph.D. dissertation quoted in ref 5.
(84) Hippler, H.; Otto, B.; Troe, J. *Ber. Bunsen-Ges. Phys. Chem.* **1989**, *93*, 428.
(85) Jalenak, W.; Weston, R. E., Jr.; Sears, T. J.; Flynn, G. W. *J. Chem. Phys.* **1988**, *89*, 2015.
(86) (a) Hippler, H.; Troe, J.; Wendelken, H. J. *Chem. Phys. Lett.* **1981**, *84*, 257. (b) Hippler, H.; Troe, J.; Wendelken, H. J. *J. Chem. Phys.* **1983**, *78*, 5351, 6709, 6718.
(87) Heymann, M.; Hippler, H.; Troe, J. *J. Chem. Phys.* **1984**, *80*, 1853.
(88) Hippler, H. *Ber. Bunsen-Ges. Phys. Chem.* **1985**, *89*, 303.
(89) Dove, J. E.; Hippler, H.; Troe, J. *J. Chem. Phys.* **1985**, *82*, 1907.
(90) Cobos, C. J.; Hippler, H.; Troe, J. *J. Phys. Chem.* **1985**, *89*, 1778.
(91) Brouwer, L.; Hippler, H.; Lindemann, L.; Troe, J. *J. Phys. Chem.* **1985**, *89*, 4608.
(92) Dove, J. E.; Hippler, H.; Plach, J.; Troe, J. *J. Chem. Phys.* **1984**, *81*, 1209.
(93) Herzog, B.; Hippler, H.; Kang, L.; Troe, J. *Chem. Phys. Lett.* **1985**, *120*, 124.
(94) Durana, J. F.; McDonald, J. D. *J. Chem. Phys.* **1976**, *64*, 2518.
(95) Barker, J. R. *Chem. Phys.* **1983**, *77*, 301.
(96) Oref, I.; Rabinovitch, B. S. *J. Chem. Soc., Faraday Trans.* **1984**, *80*, 769.
(97) Bogan, D. J.; Setser, D. W. *J. Chem. Phys.* **1976**, *64*, 586.
(98) Damm, M.; Hippler, H.; Troe, J. *J. Chem. Phys.* **1988**, *88*, 3564.
(99) Able, B.; Herzog, B.; Hippler, H.; Troe, J. *J. Chem. Phys.* **1989**, *91*, 890, 900.
(100) Nakashima, N.; Yoshihara, Y. *J. Chem. Phys.* **1983**, *79*, 2727.
(101) Ichimura, T.; Mori, Y.; Nakashima, N.; Yoshihara, Y. *J. Chem. Phys.* **1985**, *83*, 117.
(102) Ichimura, T.; Takahashi, M.; Mori, Y. *Chem. Phys.* **1987**, *114*, 111.
(103) (a) Barker, J. R.; Rothem, T. *Chem. Phys.* **1982**, *68*, 331. (b) Jacobs, S. J. *Chem. Phys.* **1989**, *132*, 71.
(104) Barker, J. R.; Toselli, B. M. Photothermal Studies of Energy Transfer and Reaction Rates. In *Photothermal Investigations of Solids and Fluids*; Sell, J. A., Ed.; Academic Press: New York, 1989; p 155.
(105) Bailey, R. T.; Cruickshank, F. R.; Guthrie, R.; Pugh, D.; Weir, I. J. M. *Mol. Phys.* **1983**, *48*, 81.
(106) (a) Beck, K. M.; Ringwelski, A.; Gordon, R. J. *Chem. Phys. Lett.* **1985**, *121*, 529. (b) Beck, K. M.; Gordon, R. J. *J. Chem. Phys.* **1987**, *87*, 5681.
(107) Rosencwaig, A. *Photoacoustics and Photoacoustic Spectroscopy*; Wiley: New York, 1980.
(108) (a) Beck, K. M.; Gordon, R. J. *J. Chem. Phys.* **1988**, *89*, 5560. Gordon, R. J. *Comments At. Mol. Phys.* **1988**, *21*, 123.
(109) Braun, W.; Price, I.; Cadoff, B. C.; Peterson, N. C. *Int. J. Chem. Kinet.* **1989**, *21*, 1029.
(110) Trevor, P. L.; Rothem, T.; Barker, J. R. *Chem. Phys.* **1982**, *68*, 341.
(111) Wallington, T. J.; Scheer, M. D.; Braun, W. *Chem. Phys. Lett.* **1987**, *138*, 538.
(112) (a) Wallington, T. J.; Braun, W.; Beck, K. M.; Gordon, R. J. *J. Phys. Chem.* **1988**, *92*, 3839. (b) Braun, W.; Scheer, M. D.; Cvetanovic, R. J. *J. Chem. Phys.* **1988**, *88*, 3715.
(113) Dagaut, P.; Wallington, T. J.; Braun, W. *J. Photochem. Photobiol., A* **1988**, *45*, 151.
(114) Braun, W.; Wallington, T. J. *Chem. Phys. Lett.* **1987**, *140*, 441.
(115) Chow, N.; Wilson, D. J. *J. Phys. Chem.* **1962**, *66*, 342.
(116) Tardy, D. C.; Larson, C. W.; Rabinovitch, B. S. *Can. J. Chem.* **1968**, *46*, 341.
(117) (a) Klein, I. E.; Rabinovitch, B. S.; Jung, K. H. *J. Chem. Phys.* **1977**, *67*, 3833. (b) Klein, I. E.; Rabinovitch, B. S. *Chem. Phys.* **1978**, *35*, 439.
(118) Krongauz, V. V.; Rabinovitch, B. S. *Chem. Phys.* **1982**, *67*, 201.
(119) *Combustion Chemistry*; Gardiner, W. C., Jr., Ed.; Springer-Verlag, New York, 1984.
(120) See various volumes of the *International Symposium on Combustion*.
(121) Hucknall, D. J. *Chemistry of Hydrocarbon Combustion*; Chapman and Hall: London, 1985.
(122) Kiefer, J. H.; Shah, J. N. *J. Phys. Chem.* **1987**, *91*, 3024.
(123) Tardy, D. C.; Rabinovitch, B. S. *J. Phys. Chem.* **1990**, *94*, 1876.
(124) Master equation calculations on cyclohexene: Tardy, D. C. Unpublished work.
(125) Shi, J.; Barker, J. D. Paper presented at Second International Conference on Chemical Kinetics, July 24–27, Gaithersburg, MD, 1989.
(126) Gilbert, R. G.; Smith, S. C. *QCPE 460*.
(127) Smith, S. C.; Gilbert, R. G. *Theory of Unimolecular and Recombination Reactions*; Blackwell Scientific Publications: Oxford, England, 1990.
(128) Golden, D. M.; Spokes, G. N.; Benson, S. W. *Angew. Chem., Int. Ed. Engl.* **1973**, *85*, 602.
(129) (a) Kelley, D. F.; Zalotai, L.; Rabinovitch, B. S. *Chem. Phys.* **1980**, *46*, 379. (b) Kelley, D. F.; Barton, B. D.; Zalotai, L.; Rabinovitch, B. S. *J. Chem. Phys.* **1979**, *71*, 538.
(130) (a) Barton, B. D.; Kelley, D. F.; Rabinovitch, B. S. *J. Phys. Chem.* **1980**, *84*, 1299. (b) Kelley, D. F.; Kasai, T.; Rabinovitch, B. S. *J. Chem. Phys.* **1980**, *73*, 5611. (c) Arakawa, R.; Kelley, D. F.; Rabinovitch, B. S. *J. Chem. Phys.* **1982**, *76*, 2384.
(131) (a) Flowers, M. C.; Wolters, F. C.; Kelley, D. F.; Rabinovitch, B. S. *Chem. Phys. Lett.* **1980**, *69*, 543. (b) Kelley, D. F.; Kasai, T.; Rabinovitch, B. S. *J. Phys. Chem.* **1981**, *85*, 1100. (c) Kasai, T.; Kelley, D. F.; Rabinovitch, B. S. *Chem. Phys. Lett.* **1981**, *81*, 126.
(132) (a) Yuan, W.; Tosa, R.; Chao, K. J.; Rabinovitch, B. S. *Chem. Phys. Lett.* **1982**, *85*, 27. (b) Flowers, M. C.; Wolters, F. C.; Kelley, D. F.; Rabinovitch, B. S. *J. Phys. Chem.* **1981**, *85*, 849.

(133) (a) Yuan, W.; Rabinovitch, B. S.; Tosa, R. *J. Phys. Chem.* **1982**, *86*, 2796. (b) Yuan, W.; Rabinovitch, B. S. *J. Phys. Chem.* **1983**, *87*, 2167. (c) Nilsson, W. B.; Rabinovitch, B. S. *Langmuir* **1985**, *1*, 71. (d) Oswald, D. A.; Nilsson, W. B.; Rabinovitch, B. S. *J. Phys. Chem.* **1986**, *90*, 3541. (e) Wolters, F. C.; Chao, K. J.; Rabinovitch, B. S. *Int. J. Chem. Kinet.* **1981**, *13*, 1289.
(134) (a) Gilbert, R. G.; Gaynor, B. J.; King, K. D. *Int. J. Chem. Kinet.* **1979**, *11*, 317. (b) King, K. D.; Nguyen, T. T.; Gilbert, R. G. *Chem. Phys.* **1981**, *61*, 221. (c) Francisco, J. S.; Steinfeld, J. I.; King, K. D.; Gilbert, R. G. *J. Phys. Chem.* **1981**, *85*, 4106. (d) Brown, T. C.; Taylor, J. A.; King, K. D.; Gilbert, R. G. *J. Phys. Chem.* **1983**, *87*, 5214. (e) Gilbert, R. B.; King, K. D. *Chem. Phys.* **1980**, *49*, 367.
(135) Nguyen, T. T.; King, K. D.; Gilbert, R. G. *J. Phys. Chem.* **1983**, *87*, 494.
(136) Brown, T. C.; King, K. D.; Gilbert, R. G. *Int. J. Chem. Kinet.* **1987**, *19*, 851.
(137) Brown, T. C.; King, K. D.; Gilbert, R. G. *Int. J. Chem. Kinet.* **1984**, *16*, 1455.
(138) (a) Staker, W. S.; King, K. D. *J. Phys. Chem.* **1989**, *93*, 1805. (b) Brown, T. C. Ph.D. Thesis, University of Adelaide, Adelaide, Australia, 1988.
(139) Marcoux, P. J.; Setser, D. W. *J. Phys. Chem.* **1978**, *82*, 97.
(140) Pettijohn, R. R.; Mutch, G. W.; Root, J. W. *J. Phys. Chem.* **1975**, *79*, 1747, 2077.
(141) McCluskey, R. J.; Carr, R. W. *J. Phys. Chem.* **1976**, *80*, 1393.
(142) McCluskey, R. J.; Carr, R. W. *J. Phys. Chem.* **1977**, *81*, 2045.
(143) McCluskey, R. J.; Carr, R. W. *J. Phys. Chem.* **1978**, *82*, 2637.
(144) Chung, G. Y.; Carr, R. W. *J. Phys. Chem.* **1987**, *91*, 2831.
(145) (a) Richmond, G.; Setser, D. W. *J. Phys. Chem.* **1980**, *84*, 2699. (b) Setser, D. W.; Siefert, E. E. *J. Chem. Phys.* **1972**, *57*, 3613.
(146) Arbilla, G.; Ferrero, J. C.; Staricco, E. H. *J. Phys. Chem.* **1984**, *88*, 5221.
(147) Orchard, S. W.; Ramsden, J. *Int. J. Chem. Kinet.* **1982**, *14*, 43.
(148) Chung, G. Y.; Carr, R. W. *J. Photochem. Photobiol., A* **1989**, *48*, 199.
(149) Avila, J. J.; Figuera, J. M.; Rodriguez, J. C. *Chem. Phys.* **1987**, *113*, 231.
(150) Jung, K. H.; Oh, D. K.; Kwon, O. S. *J. Photochem. Photobiol., A* **1988**, *42*, 39.
(151) Nogar, N. S.; Spicer, L. D. *J. Phys. Chem.* **1976**, *80*, 1736.
(152) Forst, W. *J. Chem. Phys.* **1984**, *80*, 2504.
(153) Procaccia, I.; Levine, R. D. *Chem. Phys. Lett.* **1975**, *33*, 5.
(154) Procaccia, I.; Shimoni, Y.; Levine, R. D. *J. Chem. Phys.* **1976**, *65*, 3284.
(155) Troe, J. *J. Chem. Phys.* **1982**, *77*, 3485.
(156) Lim, K. F. *J. Chem. Phys.* **1988**, *89*, 5964.
(157) Forst, W. *J. Chem. Phys.* **1988**, *89*, 5965.
(158) Shuler, K. E.; Weiss, G. H.; Andersen, K. *J. Math. Phys.* **1962**, *3*, 550.
(159) Barker, J. R. Private communication.
(160) Troe, J. Private communication.
(161) Tzidoni, E.; Oref, I. Unpublished calculations.
(162) Shi, J.; Barker, J. R. *Int. J. Chem. Kinet.* **1990**, *22*, 187.
(163) Forst, W.; Barker, J. R. *J. Chem. Phys.* **1985**, *83*, 124.
(164) Gordon, N.; Oref, I. *J. Phys. Chem.* **1978**, *82*, 2035.
(165) Park, J.; Bersohn, R.; Oref, I. Submitted for publication.